Near Infrared Spectroscopy and Photometry of Novae

A THESIS

Submitted for the Award of Ph.D. degree of

MOHANLAL SUKHADIA UNIVERSITY

In the

Faculty of Science

by

Ashish Raj

Under the Supervision of

Prof. Ashok Ambastha
Physical Research Laboratory, Ahmedabad

Department of Physics

MOHANLAL SUKHADIA UNIVERSITY

UDAIPUR

2012

To

my parents and beloved wife

DECLARATION

I, **Mr. Ashish Raj**, S/o Sri Vijay Kumar Srivastava, resident of A-5, PRL residences, Navrangpura, Ahmedabad 380009, hereby declare that the research work incorporated in the present thesis entitled, **"Near Infrared Spectroscopy and Photometry of Novae"** is my own work and is original. This work (in part or in full) has not been submitted to any University for the award of a Degree or a Diploma. I have properly acknowledged the material collected from secondary sources wherever required. I solely own the responsibility for the originality of the entire content.

Date:

Ashish Raj

(Author)

CERTIFICATE

I feel great pleasure in certifying that the research work presenred in the thesis entitled, **"Near Infrared Spectroscopy and Photometry of Novae"** by Mr. Ashish Raj was done under my guidance. He has completed the following requirements as per Ph.D regulations of the University.

(a) Course work as per the university rules.

(b) Residential requirements of the university.

(c) Regularly submitted six monthly progress reports.

(d) Presented his work in the departmental committee.

(e) Published minimum of one research papers in a referred research journal.

I recommend the submission of thesis.

Date:

Prof. Ashok Ambastha
(Thesis Supervisor)
Professor
Physical Research Laboratory,
Ahmedabad - 380 009.

Countersigned by
Head of the Department

Acknowledgements

My sincere thanks are due to the Physical Research Laboratory and the Department of Space, Govt. of India for funding my research and extending me all necessary facilities for carrying out my research work.

I take this opportunity to offer my profound gratitude to Prof. Ashok Ambastha for providing guidence to me throughout the period of this research work. I acknowledge all the help he has provided me time and again whenever I asked for it.

I express my sincere and deepest gratitude to Prof. N. M. Ashok, for valuable discussion and help in carrying out the research work reported in this thesis. His deep insight in the subject and vast experience helped me immensely in learning the subject. Discussion with him was a great pleasure as he always gave importance to my views and was always patient with me. It was a great experience to work with him and I consider myself fortunate to have him as my supervisor.

I greatly acknowledge the assistance I got from my other collaborator, Prof. D. P. K. Banerjee. It was a pleasing experience to work with him and the discussions we had during my Ph. D. tenure, helped me in clearing many doubts.

I thank Prof. J. N. Goswami, the Director, Prof. A. K. Singhvi and Prof. Anjan Joshipura, former Deans, and Prof. Utpal Sarkar, Dean of PRL for providing necessary facilities and encouragements to carry out research work.

I pay my tribute to other faculty members: Prof. B. G. Anandarao, Prof. T. Chandrasekhar, Prof. U. C. Joshi, Prof. P. Janardhan, Prof. K. S. Baliyan, Prof. H. O. Vats, Dr. A. Singhal, Dr. A. Chakraborty and Dr.S. Naik, who always encouraged me during this period.

I take this opportunity to thank to all other scientists and staff members of Astronomy and Astrophysics division for their co-operation and support.

I would also like to express my heartfelt thanks to all the staff members at the Mount Abu Observatory who always were co-operative and extended their hands for all kinds of helps. I am grateful to Mr. Jinesh K. Jain, Mr. G.

S. Rajpurohit and Mr. Nafees Ahmed who were with me handle the instruments with utmost care and to take observations. I am very much thankful to Mr. Rajesh Shah for his continuous and unconditional efforts to keep the telescope and related softwares free from any trouble to make successful and smooth observations.

I thank all the staff members of PRL computer center for providing excellent computational and internet facilities. I must express my appreciation for the co-operation and help extended ever-willingly by the library and its staff members.

I specially thank R. K. Das, Blesson, Tapas, Vishal, Ketan, Sunil, Arun, Susanta, Bhaswar, Anjali, Priyanka, Tanmoy, Gaurav, Sandeep, Suman, Anand, Rohit, Vimal, Neeraj, Arvind, Pankaj, Sudhanwa and others for their unconditional support and many memorable experiences with them.

The support I got from my parents, my wife (Shikha) and all my family member is something beyond acknowledgement. Shikha always motivated me to finish my thesis in time and pointed out my mistakes in the thesis as well. They were always with me and the encouragement I received from them will never fade away.

Ashish

Abstract

Classical Novae(CNe) outbursts are violent thermonuclear explosions arising on the surface of white dwarfs in close binary systems and are contributors to the chemical evolution of the interstellar medium through the production and ejection of copious amounts of metal rich material. Observations and modeling of CNe eruptions illuminate numerous fundamental processes of astrophysical interest, including non-equilibrium thermonuclear runaway, radiative processes in dynamic nebular environments, binary star interaction, mass loss from red dwarfs, molecule formation, dust condensation and dust growth.

This thesis concentrates on studying the novae near their optical maximum brightness, the temporal evolution of the early decline phase and investigating the physical properties of the underlying binary system. The results that emerged from the extensive studies of three novae, viz., V5579 Sagittarii, V496 Scuti and KT Eridani are presented. Of these three novae, V5579 Sgr and V496 Sct are of Fe II class while the third nova KT Eri is of He/N class. The system parameters like the distance to the nova, absolute magnitude, expansion velocity of the ejecta, mass of the ejecta and gas to dust ratio are calculated.

The nova V5579 Sgr showed pre-maximum rise lasting for about 5 days it was possible to obtain near infrared observations near its optical maximum. The spectra near peak brightness show strong P Cygni signatures. The blackbody fit to the spectral energy distribution of the optical and near infrared data during the fireball phase near optical maximum is consistent with the A - F spectral type pseudo-photosphere usually displayed by novae at outburst. The optical light curve showed a sharp fall about 15 days after the optical maximum indicating the onset of dust formation. The formation of dust in V5579 Sgr is consistent with the presence of emission lines of elements with low ionization potentials like Na and Mg in their early spectra. The early presence of such low ionization potential lines has been suggested as likely indicators of dust formation in the expanding nova ejecta at later times. With $t_2 = 8$ days, V5579 Sgr is one of the few fast Fe II classes of novae that formed dust.

The highlight of our study of V496 Sct is the detection of the rarely observed CO first overtone emission bands of CO. The formation of molecules in nova ejecta is expected to begin before the dust formation epoch. Though the dust formation has been observed in several Fe II class novae the CO detection has been done in very few novae. The CO bands have been modeled, assuming the CO gas to be in thermal equilibrium, to estimate the mass of the CO gas in the ejecta and the temperature of this emitting gas. In addition the $^{12}C/^{13}C$ ratio was estimated and compared with the model predicted values. The subsequent observations have detected the formation of dust in V496 Sct. In addition the evolution of optical spectra has also been studied using the data by Italian group made available as part of the collaborative efforts to study novae.

The He/N class nova KT Eri, which has been proposed as a possible recurrent nova on the basis of its similarity with the observed properties of RS Oph, was observed during the first 100 days following its discovery and evidence for high velocity bi-polar flow is presented. With its location at galactic latitude of -32 deg, KT Eri is one of the very few novae discovered at such high galactic latitudes. The nature of progenitor of KT Eri has been studied using the pre-discovery optical and near-infrared photometric data. The spectral energy distribution shows a power law dependence with a spectral index of 1/3 suggesting an accretion disk as the source of this continuum radiation. The evolution of post-outburst continuum radiation over an extended infrared spectral range using the WISE data was done and it shows a departure from the expected free-free phase following its fast decline.

The research work presented in this thesis is based on the photometric and spectroscopic observations of selected novae discovered during the period 2008 to 2010. The near-infrared observations were obtained from the 1.2m telescope at Mt. Abu Infrared Observatory of Physical Research Laboratory, Ahmedabad using the near-infrared camera/spectrograph (PRLNIC). The optical photometric data from the archives of American Association of Variable Star Observers (AAVSO) were used to generate the light curves of the novae.

LIST OF PUBLICATIONS

A. Publications related to the thesis work

1. **“Nova V5579 Sgr 2008: near-infrared studies during maximum and the early decline phase”**
   Ashish Raj, N. M. Ashok, D. P. K. Banerjee
   2011, Mon. Not. R. Astron. Soc., **415**, 3455

2. **“V496 Scuti: an Fe II nova with dust shell accompanied by CO emission”**
   Ashish Raj, N. M. Ashok, D. P. K. Banerjee, U. Munari, P. Valisa and S. Dallaporta
   2012, Mon. Not. R. Astron. Soc., **425**, 2576

B. Conference Proceedings

1. **“Near-infrared study of fast nova KT Eridani”**
   Ashish Raj, N. M. Ashok, D. P. K. Banerjee
   2011, BASI, 3, 113

C. CBETs and ATels

1. **Ashish Raj**, N. M. Ashok, D. P. K. Banerjee, 2009, CBET, 2002

2. **Ashish Raj**, N. M. Ashok, D. P. K. Banerjee, 2009, CBET, 2069

3. **Ashish Raj**, N. M. Ashok, D. P. K. Banerjee and V. Venkata Raman, 2012, ATel, 4027

4. **Ashish Raj**, N. M. Ashok, D. P. K. Banerjee and V. Venkata Raman, 2012, ATel, 4093

5. **Ashish Raj**, V. Venkata Raman, N. M. Ashok and D. P. K. Banerjee, 2012, ATel, 4107

6. **Ashish Raj**, N. M. Ashok, D. P. K. Banerjee, 2012, ATel, 4169

7. **Ashish Raj**, N. M. Ashok, D. P. K. Banerjee, 2012, ATel, 4211

Contents

List of Tables

List of Figures

Chapter 1

Introduction

The name nova comes from the Latin words *"stella nova"* which means *"new star"*. All novae are members of close binary systems containing white dwarfs (WDs) as the primary stars and late type main sequence (MS) stars or giants as the secondaries or companions. A close binary may be detached, semi-detached, or a contact system depending on whether the companion star fills its Roche lobe (Figure 1.1). In a nova the sudden increase in the brightness is the result of a thermonuclear explosion on the surface of a white dwarf (WD) in a close binary system. The explosion ejects material from the WD surface into the surrounding interstellar medium (ISM) at velocities ranging from a few hundred to a few thousand km s^{-1}. The majority of the ejected material is hydrogen (H), but there are also substantial quantities of metals produced by explosive nucleosynthesis and dredged up material from the underlying WD and mixed into the ejecta. Hence, the ejecta of classical novae may have a considerable impact on the local chemical evolution of the ISM. In a nova explosion, the energy produced amounts to about 10^{45} erg. All novae are Cataclysmic Variables (semi-detached binary) - a name first suggested by Gaposchkin (Payne-Gaposchkin 1977). Cataclysmic variables (CVs) are binary star systems in which one component of the system, a low mass red dwarf, is transferring matter onto the second component, a degenerate white dwarf. The mass transfer results in the formation of an accretion disc around the white dwarf. Instabilities in the accretion disk like sudden transfer of

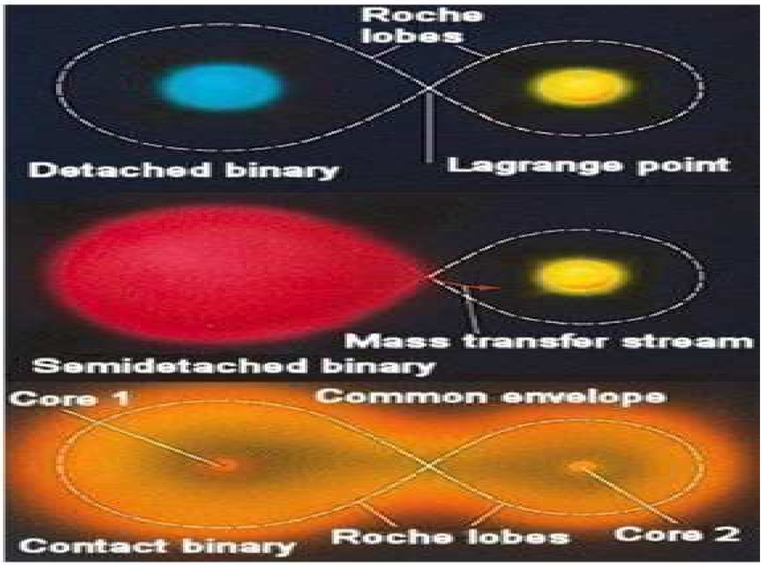

Figure 1.1: *Diagram for three types of close binary systems; detached, semi-detached and contact, depending upon whether the companion fills its Roche lobe.*

matter to the white dwarf or runaway thermonuclear reactions on the white dwarf surface give rise to the cataclysmic outburst, the sudden brightening, observed in these systems. The novae are interacting binary star systems containing a Roche-lobe filling secondary, on or near main sequence which is losing hydrogen-rich material through the inner Lagrangian point to the white dwarf primary.

1.1 Classical Novae

The classical novae (CNe), one of the subclasses of CVs, are close binary systems with a late-type main sequence star (the secondary) transferring material via Roche lobe overflow to a companion star (the primary; Crawford & Kraft 1956). The white dwarf primary is a compact object in the case of CNe (Gallagher & Starrfield 1978). Novae brighten by 10 - 12 magnitudes in a few hours and subsequently fade back to the original faint level over a period lasting several months to years. Novae provide a unique opportunity to study the

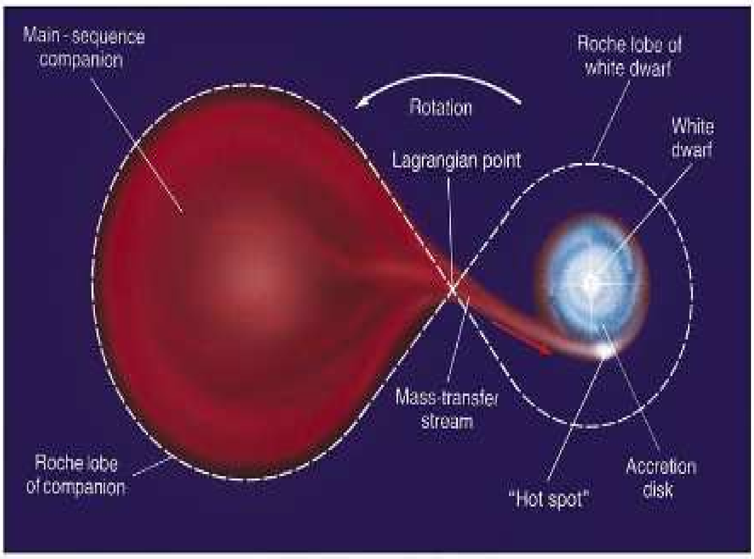

Figure 1.2: *The schematic diagram showing the semi-detached binary, the primary, companion, Lagrangian point, mass stream, hot spot and accretion disk.*

interaction of changing radiation field with expanding ejecta spanning a wide range of physical parameters like electron number density and temperature. The WD composition is determined by the initial mass of the primary star, which determines the amount of nuclear processing that will be completed before depletion of the star's fuel reserves. The mass of the secondary in systems such as these, with a short orbital period P_{orb} and a Roche lobe-filling main sequence secondary, can be approximated as follows

$$M_s/M_\odot \simeq 0.065(P_{orb})^{1.25}(hours), \quad (1.1)$$

where M_s is the mass of the secondary and $M_\odot$ the mass of the Sun (Warner 1995b). The primary can have a wide range of mass up to the Chandrasekhar limit, and usually it is found to be above ~ 0.5 $M_\odot$. The binarity is evident through the eclipsing nature when the viewing geometry is favorable or its imprint on the ejecta, due to the bipolar wind and/or anisotropic irradiation of the outburst material (Warner 2008).

The CNe binary system is generally accepted to contain a carbon-oxygen (CO) or oxygen-neon (ONe) WD primary and a low mass secondary. The material starts to flow through the inner Lagrangian point into the primary's lobe when the secondary fills its Roche lobe. From Figure 1.2 it is evident that a thin disc is formed around the WD due to the high angular momentum of the transferred material. Hydrodynamic studies show that this accretion from the secondary results in a growing layer of hydrogen-rich gas on the WD surface (Starrfield et al. 2008). The mass accretion rate for these systems are from 10^{-9} to 10^{-10} $M_\odot$ yr^{-1} (Cassisi et al. 1998). The mixing of the matter can occur between the outer layers of the WD and the accreted hydrogen-rich envelope, allowing enrichment of CO or ONe nuclei to be included in the envelope. As more material is accreted on to the WD surface, the pressure and temperature of the material at the base of the envelope increases and when the pressure reaches a critical value $\sim 2 \times 10^{19}$ dynes cm^{-2} consistent with numerical hydrostatic models of nova explosion, the thermonuclear runaway (TNR) starts. This explosive burning of hydrogen is commonly termed as a 'nova explosion'. After explosion the CNe can eject some or all of the accreted envelope, including material that has been dredged up from the surface layers of WD. All CNe have only one recorded outburst but they are thought to recur on timescales of tens of thousands of years (Yaron et al. 2005).

1.2 Recurrent Novae

The previously recognized classical novae that are found to repeat their eruptions on the time scale of a decade or few decade are called as recurrent novae. Till date, about 10 have been recognized as Galactic recurrent novae with a few others considered as potential candidates. They group themselves in three subgroups (Warner 2008):

The T CrB type: These systems have orbital periods of several hundred days, and contain a red giant secondary, similar to symbiotic novae (Anupama 2002). The systems in this group have very similar behaviour, both in outburst and at quiescence. They have a high frequency of eruption attributed to the high rate of mass transfer $\dot{M}$ associated with the giant secondary (Warner

2008). Due to high mass transfer rate they erupt more frequently. The definite members of this class are T CrB, V745 Sco, V3890 Sgr and RS Oph.

The U Sco type: They consist of an evolved main sequence or subgiant secondary and are similar to the CNe systems. The subgroup includes U Sco, V394 CrA, CI Aql and LMC-RN. They are among the fastest novae observed. Unlike normal novae, in quiescence, their spectra are dominated by He lines. The outburst and quiescent properties of U Sco and V394 CrA are very similar. U Sco and CI Aql with their periods $\sim$1 d are typical of the class.

The T Pyx type: T Pyx is the only recurrent nova that is known to have a Roche-lobe filling main sequence secondary. It has an orbital period of 0.0762 days (Patterson et al. 1998; Uthas, Knigge & Steeghs 2010). The light curve and the spectral development are very similar to the slow classical novae. The spectral development of the 1966 outburst indicates T Pyx also belongs to the class of 'hybrid' novae. Theoretical models to explain the outburst light curve indicate a white dwarf mass of 1.2 $M_{\odot}$ (Hachisu, 2002). T Pyx is the only recurrent nova that shows a discernable shell. The structure of the shell is similar to that of GK Per, and is composed of thousands of unresolved knots, some of which are variable, typically on a time scale of months (Shara et al. 1997). The observations support the model in which the rapidly moving, initial ejecta from a nova eruption catches up and collides with the slow moving ejecta from a previous eruption (Shara et al. 1997, Contini & Prialnik, 1997). This collision produces the observed clumping, observed emission lines and the knot variability. T Pyx has an extremely large quiescent luminosity and it has been suggested that it is in a rapid and possibly terminal phase of evolution. It will end up either with an evaporation of the secondary or as a Type Ia SN if the WD reaches the Chandrasekhar mass (Knigge et al. 2000). The outburst properties of T Pyx, CI Aql and IM Nor are similar (Anupama 2002).

The much shorter inter-outburst period for RNe compared to CNe is predicted to be due to a combination of high WD mass and a high accretion rate (Starrfield et al. 1985; Yaron et al. 2005). The theoretical models for RNe lead to the ejection of smaller amounts of material at higher velocities than those for CNe (typically 10^{-8} to 10^{-6} $M_\odot$ and several thousand km s^{-1}, respectively, for RNe).

1.3 Dwarf Novae

The dwarf novae erupt frequently ranging from few days to few years. They have a well define time scale for each object where amplitude of outburst is typically of 2-5 magnitudes and in rare cases it can go upto 8 magnitude. The dwarf nova outburst is well understood. On the basis of light curve dwarf novae are classified into 3 distinct subtype viz. Z Cam stars, SU UMa stars and U Gem stars.

1.4 Nova like variables (NLs)

Nova like variables include all of the 'non-eruptive' CVs. Their spectra indicate that they are possibly novae that are either in a pre-or post-outburst stage and perhaps Z Cam and UX UMa stars. The period between outburst is too long to have been seen by modern observations. Most NLs have emission line spectra, but a subgroup called UX UMa stars show additional absorption lines.

1.5 Magnetic CVs

They have an intense magnetic field that is strong enough to disrupt the accretion disk either partially or totally. The two main subclasses are:

(a)**Polars:** They have the strongest magnetic field (B $\geq 10^7$ G). The field lines connect to the inter-star stream and prevent the formation of any accretion disc.

(b)**Intermediate Polars (IPs):** They have relatively weaker fields ($10^6 \leq$ B $\leq 10^7$ G), e.g., DQ Her. In case of IPs, a disc forms but the inner parts are truncated where the primary's magnetosphere controls the flow of the material on the surface of the white dwarf.

1.6 Symbiotic Novae

Symbiotic novae are a subclass of Symbiotic stars. The symbiotic stars are interacting binaries containing an evolved giant transferring matter to a hot and compact companion, usually a white dwarf. A typical symbiotic binary is embedded in a circumstellar nebula which is mainly formed from material lost in the red giant, while the hot component (WD) is responsible for its ionization. The orbital separation at which the interaction of the material from the secondary with the ionizing radiation from the white dwarf occurs is determined by the nature of the giant. Two types of symbiotic stars are there; S-type (stellar), which has normal M giants, and D-type (dusty) which has heavily dust-reddened Mira variables (Warner 1995a). The S-type and D-type have $M_{wind} \sim 10^{-8}$ - 10^{-7} $M_{\odot}$ yr^{-1} and 10^{-6} - 10^{-5} $M_{\odot}$ yr^{-1}, respectively (Kenyon 1988). The binary must have enough room for the red giant as in the case of D-types for its dust shell and yet allow it to transfer sufficient mass to its companion. The orbital periods for the S - types are of about 1 - 15 years, and more than 20 years for the D - types, which are the longest orbital periods among interacting binaries. Symbiotic stars are a very attractive laboratory to study various aspects of interactions and evolution in binary systems and important tracers of late phases of stellar evolution. The presence of both the accreting white dwarf and the red giant (with its degenerate core) makes symbiotic stars also a promising “factory” of Type Ia supernovae (SN Ia). The path to Type Ia supernovae (SN Ia) can be either a thermonuclear explosion of CO white dwarf upon crossing the Chandrasekhar limit (the single degenerate (SD) scenario) or by merging of a double CO white dwarf system (the double degenerate (DD) scenario). Symbiotic novae form a small subclass of cataclysmic variables in which the outburst is caused by thermonuclear runaway. The typical separation between the components is $\sim 10^{9}$ - 10^{10} km.

1.7 Nova light curves

The first systematic studies of CNe were limited to the characterization of their optical light curves, i.e., the changing observed brightness with time. Observations of this photometric development revealed a surprising diversity in light curve evolution (Gaposchkin 1957).

In the initial rise phase where the nova increases in brightness up to 9 magnitude (see Figure 1.3), the detailed observations are rare due to the unpredictable nature of nova outbursts. This initial rise can take from 1 - 2 days in the fast CNe to several weeks in the slowest CNe. The instruments like the Solar Mass Ejection Imager (SMEI) on board the Coriolis satellite, which scans most of the sky every 102 minute orbit (Hick et al. 2007) have made possible to observe the rising part of the novae outburst with high cadence. The detection and detailed observations of the initial rise for a sample of three CNe, KT Eri, V598 Pup and V1280 Sco, and one RNe, RS Oph using SMEI have been made by Hounsell et al. (2010).

After the initial rise, some CNe show a pause in the light curve, about 2 magnitudes below maximum (e.g., HR Del). This pause can be of a few hours in the fast CNe to a few days in the slowest CNe. The fast CNe take 1 - 2 days and it takes several weeks for the slower CNe to reach the maximum brightness. The fast novae will remain at or around maximum brightness for only a few hours and slow CNe will remain for few days. Hounsell et al. (2010) have sampled well the region of the pre-maximum halt for a few novae determining the duration of the halt. The initial decline from maximum brightness is often smooth but there are some exceptions like V705 Cas, DQ Her and GK Per which show a transition where a large dip is seen in their brightness. Subsequently these novae slowly recover their brightness to reach a level that closely matches the level expected from the extrapolation of the light curve prior to the sudden dip. As discussed later this sudden fading is due to dust formation in the nova ejecta. Sometimes the slow CNe exhibit variations in the brightness on time scales of 1 - 20 days with amplitudes of up

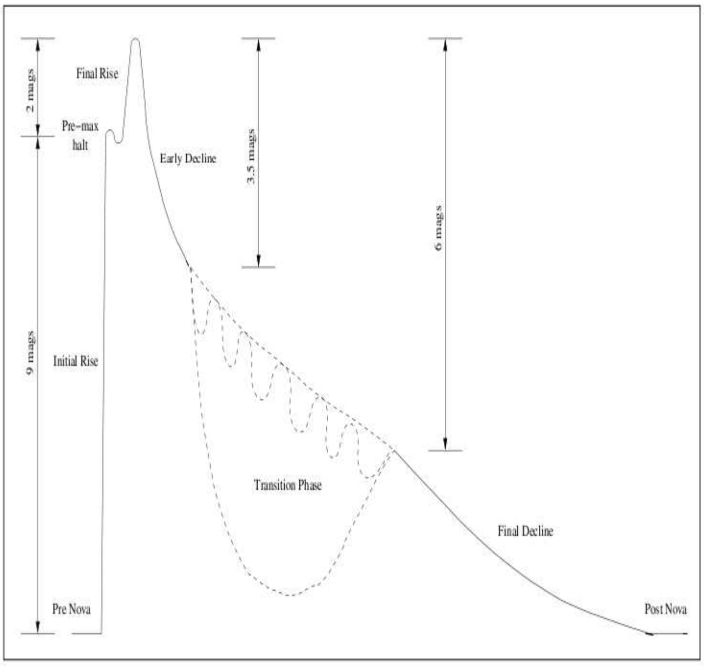

Figure 1.3: *A typical light curve of a nova (taken from Bode & Evans 2008).*

to two magnitudes. The CNe light curve shows a steady decline in brightness with small fluctuations after the transition phase. Strope et al. (2010) have studied the characteristics of 93 nova light curves and classify them on the basis of the shape of the light curve and the time of decline by 3 magnitudes (t_3). They classify the light curves in 7 categories namely S, P, D, C, O, F and J class.

1.8 Post-outburst development of novae

In the initial phase of development in novae about 10% - 50% of the hydrogen layer is ejected in the nova explosion and the rest of the accreted matter settles down on the surface of the white dwarf. During hydrostatic equilibrium stage, which is most important for slow novae, energy is produced at constant bolometric luminosity which is related to the Eddington luminosity defined as the maximum luminosity which a star of a given mass can have before the

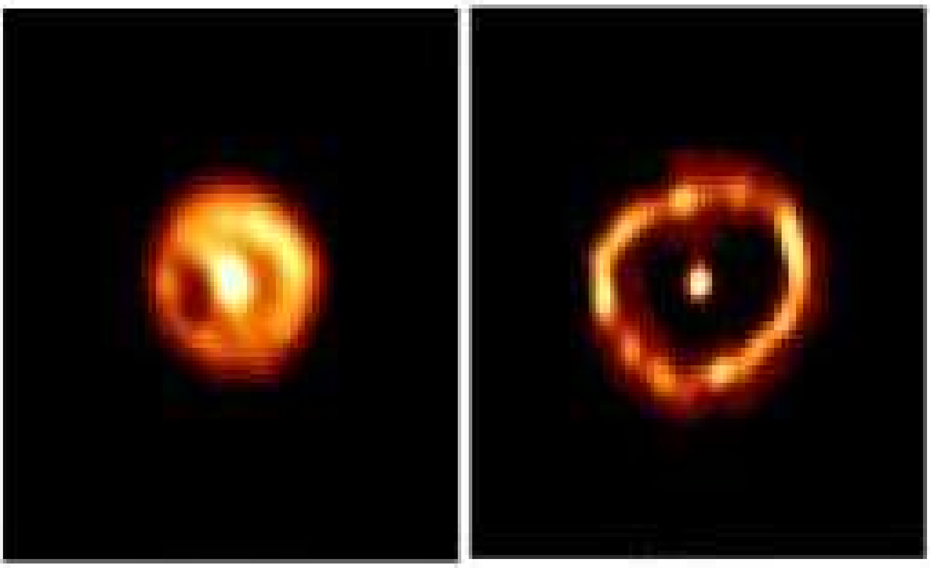

Figure 1.4: *In a classical nova, the unburnt hydrogen is ejected as a shell of rapidly-expanding material. The images of Nova Gygni 1992 taken by Hubble Space Telescope (HST) are shown. The time difference between the left and right image is 7 months. The left image was taken before the optical aberation of the HST was rectified. The right image was taken after the corrective optics were installed. Credit: F. Paresce, R. Jedrzejewski, NASA/STScI/ESA*

outward radiation pressure exceeds the inward gravitational force. It is given by the equation-

$$L_{Edd} = 4\pi G c M_{WD}/\kappa_T \tag{1.2}$$

where c = 2.9979×10^{10} cm s^{-1}, κ_T is the Thomson opacity for scattering by free electrons and equal to 0.3975 cm^2 g^{-1} for hydrogen (Gehrz 1998).

Gehrz (1998) has identified three phases in the post-outburst development of novae from the studies of infrared temporal evolution of a large number of classical novae. These three different phases after the nova explosion are as follows.

Fireball phase: This is the initial phase of the nova explosion. In this phase the ejecta is optically thick and behaves like a fireball, which radiates as a hot blackbody of temperature 6,000 - 10,000 K. The observed light originates

Table 1.1: Typical parameters for novae outburst.

Parameter		Value
Outburst energy (L_O)	=	10^{45} ergs
Bolometric luminosity	=	$2 \times 10^4 L_\odot$ (constant)
Outburst amplitude	=	6-15 magnitudes
t_2	=	7-250 days
t_3	=	5-1000 days
Dust formation time (t_d)	=	7-100 days
Dust temperature (T_d)	=	1000-1700 K
Grain size (a)	=	0.1 to 3 micron
Velocity of the ejecta (V_{ej})	=	few 100 to few 1000 km s^{-1}
Absolute magnitude (M_V)	=	-7 to -9
Mass of the ejected gas (M_{ej})	=	10^{-6} - 10^{-4} $M_\odot$
Ejecta particle density	=	5×10^{11} cm^{-3} (at t=5 days)
Composition	=	Metals (C, N, O, Fe, Na, Mg etc.) enhanced over cosmic abundances by 10-100 times, grains, molecules, radioactive nuclei

in this "pseudo photosphere" of the expanding fireball. At this point the spectrum of the nova resembles an A to F spectral type.

Optically thin expansion phase: After a few days of the nova explosion the optically thin expansion phase starts. At this point the nova shell of gas expands, becomes less dense and transparent. The energy distribution will no longer appear as blackbody in optically thin expansion phase. When the fireball has become optically thin, the continuum distribution beyond 2 μm is dominated by thermal bremsstrahlung or free-free emission (Gehrz 1988). The central white dwarf, swollen by its hydrostatic burning phase, now has the appearance of a blue horizontal-branch object located just blueward of the RR Lyrae stars on the HR diagram. There may be substantial fluctuations in the brightness in some novae because of the irregular burning of the white dwarf envelope.

Dust formation phase: After a few months or days the temperature of the expanding ejecta falls down to about $\sim$ 1200 K (see Table 1.1), which is suitable for the carbon and other heavy elements in the ejecta for the condensation of dust. In roughly 50% of all dust forming novae the dust shell becomes optically thick. This can be seen by the sudden fall of the V band light curve of the nova. Now the energy from the white dwarf is absorbed and re-emitted by the dust grains. Novae with a carbon-oxygen core white dwarf generally tend to form dust and about 25% - 30% of all novae pass through dust formation phase. The region in the ejecta where carbon is in ionized state, the formation of nucleation sites for dust is suppressed. The reason for the suppression is that the most efficient chemical pathways for molecular formation of basic molecules (e.g., CO, CH, C_2), which precede the formation of more complex hydrocarbons, involve reactions with H_2, which is easily photo dissociated in the carbon-ionized zone (Evans & Rawlings 2008). Due to neutral exchange reactions, the presence of oxygen in the ejecta is believed to inhibit the formation of nucleation sites. The recent models by Pontefract & Rawlings (2004) have been relatively successful at generating sufficient nucleation sites to allow grain growth even in the presence of oxygen in gas phase. These models have also successfully reproduced the observed CO abundances in novae ejecta. The characteristics of the dust observed in CNe show the complexity of the dust condensation process. The classical novae have been observed to produce both carbon rich and oxygen rich dust species in the same eruption (e.g., Gehrz et al. 1992) which is unlike most astronomical sources of dust. The chemical dichotomy observed in CNe may be explained by incomplete carbon monoxide formation in the ejecta (Evans & Rawlings 2008 and Pontefract & Rawlings 2004). If the formation of CO does not reach the saturation, then carbon and oxygen both will be available for dust production. The abundance gradients in the ejecta or a globally inhomogeneous abundance distribution could result in the production of different dust species. The optically thin ejecta is ionized and excited by the hot central remnant and shows nebular and coronal lines in the novae which do not form dust.

1.9 Spectral Evolution

The changing radiation field and the physical conditions in the nova ejecta result in significant changes in their spectra as they evolve after their outburst. An evolutionary sequence for the nova spectra has been described by McLaughlin (1960).

1.9.1 Pre-Maximum Spectrum

These spectra are seen on the rising branch of the light curve and they are dominated by broad, blue-shifted absorption lines, resembling those of early type stars. The spectral lines generally display P Cygni absorption features. The pre-maximum spectra are characteristic of a uniformly expanding optically thick envelope.

1.9.2 The Principal Spectrum

The principal spectrum shows stronger and more blueshifted absorption lines than those of the pre-maximum spectrum and appears at visual maximum. The strength of the spectral lines resembles an A or F supergiant spectrum with enhanced CNO lines (Warner 1995a). The mean velocity of the absorption lines is related to the speed class (which is based on t_2 and t_3, the time decline by 2 and 3 magnitude, Table 1.2). McLaughlin (1960) found that these can be represented by

$$log\ v_{prin}(km\ s^{-1}) = 3.70 - 0.5\ log\ t_3(d) = 3.57 - 0.5\ log\ t_2(d) \tag{1.3}$$

The P Cygni profiles that develop at or immediately after maximum brightness, with H I, Ca II, Na I and Fe II in the optical spectrum follow the above equation (Warner 1995a). The emission lines have complex profiles in general which is indicative of non-uniformity of the ejected gas.

1.9.3 The Diffuse enhanced spectrum

In the diffuse enhanced phase, the lines are broader than the principal spectrum and the peaks are blueshifted by about twice that of the principal spectrum. The expansion velocities derived here are also related to the speed classes (McLaughlin 1960)

$$log\ v_{denh}(km\ s^{-1}) = 3.81 - 0.41\ log\ t_3(d) = 3.71 - 0.4\ log\ t_2(d) \qquad (1.4)$$

The P Cygni profiles are common here too but wider than in the principal spectrum. The broad absorptions often show multiple narrow structures in the later stages.

1.9.4 The Orion spectrum

The orion spectrum starts appearing below 1 - 2 mag from maximum light, displaced blueward by at least as much as the diffuse enhanced system and at first consists predominantly of He I, C II, [N II] and [O II], then with [N III] and [N V] emissions, reaching its maximum strength at about the same time as the diffuse enhanced spectrum disappears (McLaughlin 1960). It is called as Orion spectrum because of its similarity to the stellar wind lines in luminous OB stars which appears after the novae have declined by one to two magnitudes from maximum. Its absorption lines are usually single, diffuse and blue-shifted by at least as much as the diffuse enhanced system, from -2700 to -1000 km s^{-1}. These velocities become steadily larger until the Orion spectrum disappears which is about 2 mag down from maximum for slow novae and 4 mag down for fast novae.

1.9.5 The Nebular Spectrum

The final recognized distinctive stage of the nova spectra is similar to the planetary nabula, where the spectrum is an entirely emission spectrum having radiative temperature less than 10^5 K. Here the [O I] and [N II] components of the principal spectrum are retained and then producing [O III] and [Ne III], strengthening relative to the H I, He I, He II, [N II], [N III] emission lines, evolving towards the spectrum of a planetary nebula. It should be emphasized that the spectrum can be complex indeed. Several of these stages may be present simultaneously and each stage may have multiple components.

1.10 Spectral Classification

The characteristic features of novae are the presence of strong Balmer H I lines seen in their optical spectra soon after their discovery. Consequently, Williams (1992) devised a classification system based on the strength of non-Balmer emission lines. On the basis of a large number of early post-outburst optical spectra of novae Williams (1992) divided them in to two classes, namely, Fe II type nova and He/N type nova.

The "Fe II" class novae frequently show the prominent P Cygni absorption features in the Balmer and Fe II emission lines. The spectral development is slow, over timescales of weeks, and the emission lines tend to be narrower than in "He/N" novae. The velocity of the ejecta is also less compared to "He/N" novae. These novae show low ionization transitions in the earliest phases of the spectral evolution (Figure 1.2, Williams 1992). The first forbidden lines to appear are those of auroral transitions and low ionization lines (Williams 1992). In the "He/N" spectral class novae the strongest non-Balmer emission lines are almost always either He II 4686 Å, He I 5876 Å, N II 5679 Å or 5001 Å, or N III 4640 Å. The HWZI is beyond 5000 km s^{-1}, the excitation levels are higher than the "Fe II" novae and the line profiles are usually broader. Generally, the line intensity of He II 4686 Å becomes stronger than Hβ (Figure 1.3, Williams 1992). There are a few novae that present a hybrid character in which the spectrum early after outburst evolves from a "Fe II" class to a "He/N" class before forbidden lines appear. However, some of the novae also show simultaneous emission from both classes (Figure 1.4, Williams 1992).

Williams (1992) proposed that the Fe II type spectrum is formed in a continuous wind, while the He/N type spectrum is formed in a discrete shell. Following the outburst, the emitted spectrum of novae is dictated by the evolution of the photosphere, wind, and surface nuclear reactions, which are all related. Therefore the excitation level of novae is low initially, then increasing to the point where coronal emission lines can be observed, and then decreasing to low levels again (Williams 1990). However in a recent work, Williams (2012) has put forward alternative explanations for the difference between the He/N and Fe II type spectra.

1.11 General properties of novae obtained from light curves and spectra

During eruption, it is true that no two novae show exactly the same kind of lightcurves (see Figure 1.3) or spectra. It is possible to obtain several common properties to most of the novae from systematic studies of light curves and spectra. Here we discuss some general properties with necessary mathematical relations and some of these properties are of immense value in other areas also.

1.11.1 Distribution and frequency of novae in the Galaxy

Most of the novae are concentrated towards the Galactic plane and bulge (Warner 2008). Therefore, some of their global properties have only been revealed recently from studies of novae in nearby galaxies. Novae are generally associated with an older stellar population in galaxies. The more massive ONe novae are concentrated towards the Galactic plane than the lower mass CO novae (della Valle et al. 1992). There are so many factors that lead to incompleteness in nova searches like seasonal, weather, biasing of sky coverage

Table 1.2: Speed classification of novae.

Author	Speed class	t_2 (in days)	t_3 (in days)
McLaughlin (1945)	Very fast	<7	<15
	Fast	8-24	15-45
	Average	25-49	50-84
	Slow	50-250	85-449
	RT Ser	≥300	≥500
Payne-Gaposchkin (1957)	Very fast	<10	<20
	Fast	11-25	21-49
	Moderately fast	26-80	50-140
	Slow	81-150	141-264
	Very slow	151-250	265-440

towards the Galactic bulge and missed fast novae. Considering all of them, selection effects and interstellar extinction produces estimates for a total Galactic nova rate of 73 ± 24 yr^{-1} (Liller & Mayer 1987), 29 ± 17 yr^{-1} (Ciardullo et al. 1990), 30 ± 10 yr^{-1} (Shafter 2002) and 34^{15}_{12} yr^{-1} (Darnley et al. 2006).

1.11.2 Maximum magnitude-rate of decline relationship

Novae in outburst are effective distance indicators since they radiate almost at constant bolometric luminosity during their outburst. By studying CNe in M31, Hubble (1929) noticed that the brighter CNe (at maximum light) fade faster. The pioneering studies of Zwicky (1936) and McLaughlin (1939) showed that the absolute magnitude of novae at maximum correlates with their rate of decline. This correlation was later confirmed by McLaughlin (1945), who used absolute magnitudes derived from expansion parallaxes, interstellar line strengths and Galactic rotation, for Galactic CNe. This correlation which he referred as 'life-luminosity relation', is presently known as Maximum Magnitude-Rate of Decline (MMRD). This relation can also be used as a distance indicator. On the basis of the observations for 11 Galactic novae Schmidt (1957) got a relation between M_V and log t_3. After that Pfau (1976), Cohen (1985), Capaccioli et al. (1990) and Livio (1992) have tried to improve the MMRD relation for novae on the basis of the observation for Galactic and extra-Galactic novae. The importance of the maximum magnitude-rate of decline (MMRD) relationship as an extragalactic distance indicator is immense and has resulted in continued discussion and updating. The observational MMRD results given by della Valle and Livio (1995) are considered to be the most comprehensive to date. Generally, the linear MMRD relationship is usually expressed in the form:

$$M_\lambda = b_n \; log \; t_n + a_n, \tag{1.5}$$

where M_λ is the absolute magnitude at a given waveband (e.g., M_V for visual), and t_n is the time taken for the nova to decline by n magnitudes from maximum, typically n = 2 or 3. Typical values of a_n and b_n are given in Table 1.3. The MMRD relation given by della Valle & Livio (1995) is:

$$M_V = -7.92 - 0.81 \; arctan \; (1.32 - log \; t_2)/0.23 \tag{1.6}$$

where M_V is the absolute magnitude of the nova.

Downes & Duerbeck (2000) showed that a linear relationship suffices to model the Galactic MMRD. They also derived a scatter of $\sim$ 0.6 mags.

1.12 Determination of physical parameters

The physical parameters of the nova system can be determined by the photometric and spectroscopic observations. From the analysis of the optical/infrared spectral energy distribution (SED) the physical parameters of the nova ejecta are derived. Several authors (Gehrz 2008 and references therein) have discussed about the physical parameters of several novae and a brief discussion

Table 1.3: Typical values of MMRD constants (Warner 2008).

M_λ	n	a_n	b_n	References
pg	3	-11.3	2.4	de Vaucouleurs (1978)
B	3	-10.67 ($\pm$ 0.30)	1.80 ($\pm$ 0.20)	Pfau (1976)
V	2	-10.70 ($\pm$ 0.30)	2.41 ($\pm$ 0.23)	Cohen (1985)
V	2	-11.32 ($\pm$ 0.44)	2.55 ($\pm$ 0.32)	Downes & Duerbeck (2000)
V	3	-11.99 ($\pm$ 0.56)	2.54 ($\pm$ 0.35)	Downes & Duerbeck (2000)

of these results is given below.

1.12.1 Angular radius and distance to the nova

In the fireball phase, nova ejecta behave like hot blackbodies (6000 - 10000 K). The temperature of the blackbody (T_{BB}) can be determined by the SED fitting. The bolometric apparent flux is expressed by the relation:

$$F = \sigma T_{BB}^4 = 1.3586(\lambda f_\lambda)_{max} \tag{1.7}$$

where $(\lambda f \lambda)_{max}$ is peak apparent flux density of the spectral energy distribution in W cm^{-2} and $\sigma = 5.6696 \times 10^5$ erg s^{-1} cm^{-2} K^{-4} is the Stefan-Boltzmann constant (see Gehrz & Ney 1992). Using the above relation, the angular diameter θ_{BB} (in milliarcsecond) can be calculated from the equation:

$$\theta_{BB} = 2.0 \times 10^{14} (\lambda f_\lambda)_{max}^{1/2} (T_{bb})^{-2} \tag{1.8}$$

Considering the ejecta expanding at constant velocity, the angular size of the fireball can give us the exact time of starting of ejection by back extrapolation of θ_{BB} versus time t plot to $\theta_{BB} = 0$. The same technique can be used to determine the angular size and expansion rate (dθ/dt) of a optically thick dust shell around a nova (see Ennis et al. 1977).

The angular expansion rate combined with the Doppler expansion velocities can be used to determine the distance D (in kiloparsec) to the nova through the following equation (Gehrz 2008):

$$D = 1.15 \times 10^{-3} V_{ej}/(d\theta/dt) = 5.69 \times 10^{-18} (T_{BB})^2 V_{ej} t/(\lambda f_\lambda)^{1/2}_{max} \tag{1.9}$$

The expansion velocity V_{ej} (in km s^{-1}) can be determined from optical/infrared spectral lines, the expansion rate $d\theta_{BB}/dt$ (in milliarcsec day^{-1}) can be obtained from the blackbody fits of blackbody energy distribution (see Ney & Hatfield 1978; Gehrz et al. 1980).

1.12.2 Velocity and geometry of the ejecta

The expansion velocity is measured from the width of the spectral lines using the Doppler shift relation:

$$V_{ej}/c = HWHM/\lambda \tag{1.10}$$

where, c is the velocity of light = $3\times\ 10^{10}$ cm s^{-1}, HWHM is the half width at half maxima of the spectral line at wavelength λ. However, the velocity is not uniform everywhere in the ejecta and generally the ejecta is non-spherical. The geometry of the ejecta may be interpreted by studying the multiple absorption and emission features, width and shapes of the spectral lines. Few examples related to the present work may be presented here to explain this. The trace of the absorption feature, which is due to P Cygni profile, on the wings of the Paβ in V5579 Sgr (see Chapter 3) confirmed that mass ejection is a sustained process. The presence of wings on the spectral lines of KT Eri were due to the non-spherical shape of the ejecta in the form of high velocity polar blobs.

1.12.3 Mass of the ejected gas

The mass of the ejected gas (M_{gas}) can be estimated by the Infrared observations of novae. It is a crucial parameter for constraining the TNR models and to calculate the abundance in the ejecta. When the expanding photosphere of nova starts to deviate from blackbody energy distribution and becomes optically thin at infrared wavelengths, the gas temperature T is still high enough that Thomson scattering dominates, and the envelope mass is given by (Gehrz 2008):

$$M_{env}/M_{\odot} = \pi(R_{env})^2/\kappa_T = 3.3 \times 10^{-13}(V_{ej}t_T)^2 \tag{1.11}$$

where, κ_T is the Thomson's scattering opacity, R_{env} is the radius of the gas envelope, V_{ej} is the expansion velocity in km s^{-1} and t_T is the time when the SED starts to deviate from blackbody energy distribution and becomes optically thin at infrared wavelengths.

1.12.4 Ejecta abundances

To get the abundance in the nova ejecta many different techniques are used at different stages of the nova outburst. Different techniques of the abundance analysis have been discussed by several authors viz. Boyarchuk & Antipova (1990), Snijders (1990), Andrea (1994). By modeling the ultraviolet, optical, and infrared spectra observed in the early phase and/or nebular and coronal phase, the compositions and the physical conditions of the nova ejecta can be estimated. There are several computer codes are available such as PHOENIX and CLOUDY to model the spectra. Abundances may also be derived from spatially resolved nova shells. All the derivations show that the novae ejecta are highly abundant in metals about 10 - 100 times the cosmic abundances (Jose & Hernanz 1998).

1.13 Observations of novae in different bands

To understand the nova phenomena completely it is required to observe them at all wavelengths from γ-rays to radio by using all modern techniques. It is seen that the novae radiate significantly in different bands viz. γ-rays, UV, X-rays, IR, and radio. With the help of modern technique like digital detectors on satellites in space along with the data from ground-based observatories, we can understand the novae in a better way.

1.13.1 γ-ray observations

The prime reason for the γ-rays emission in novae is electron-positron annihilation; positrons come from the decay of ^{13}N, ^{14}O, ^{15}O, ^{22}Na, ^{14}O and ^{22}Na (Clayton & Hoyle 1974) and transformation of ^{7}Be (through an electron capture) to an excited state of ^{7}Li (Clayton 1981). The European Space Agency has launch the satellite INTEGRAL (INTErnational Gamma-Ray Astrophysics Laboratory) in 2002, which has opened new perspectives for the detection of the γ-rays, the most energetic (> 10 kev) photons in the whole electromagnetic spectrum, from nuclear radioactivity in explosive events like novae and supernovae. During the nova explosions, γ-rays are capable to give a direct insight into the nucleosynthesis and also into the global properties, like the density, temperature, chemical composition and velocity profiles of the expanding ejecta. Gamma ray observations can directly trace isotopes and thus should trace the Galactic distribution of classical novae. However, more sophisticated calculations show that possibility of the production of γ-rays from the above reaction is very less. Interestingly three novae, at the time of writing, have been detected in γ-rays viz. a symbiotic binary V407 Cygni (V407 Cyg) by Abdo et al. (2010), Nova Sco 2012 by Cheung et al. (2012a) and Nova Mon 2012 by Cheung et al. (2012b).

1.13.2 UV and X-ray Observations

The excitation of the ejecta is due to illumination by the hot pseudo photosphere throughout the early development of classical novae (CNe). The hotter layers are revealed until the photospheric surface approaches that of the WD as the pseudo photosphere shrinks. Because of this recession we see a transition of the peak emission into the UV and X-ray regimes. The UV data are particularly useful to determine the chemical abundances in the nova ejecta (see e.g., Stickland et al. 1981; Williams et al. 1985; Snijders et al. 1987). As the white dwarf radiates most of the energy in UV so the UV observations can tell about the nature of the white dwarf. In addition, the UV observations provide effective means to determine the value of the reddening from the strength of the 2200 Ådust feature or from the emission line ratios. The major achievements of UV observations are the determination of the bolometric light of Nova Serpentis (1970), the discovery of a new class of novae, the ONe novae (Starrfield, Sparks and Truran 1986), in which very large overabundance of intermediate mass nuclei like Ne, Mg, O and Al have been found (see Snijders et al. 1984, 1987 for V1370 Aql 1982 and Williams et al. 1985 for V693 CrA 1981). The recent observations of CNe have confirmed that most of the classical novae undergo an extended period of super-soft source (SSS) X-ray emission (Ness et al. 2007). The steady accretion of H-rich material onto the WD surface is not responsible for this emission, as in other SSSs (Kahabka & van den Heuvel 1997). The SSS emission arises from nuclear burning of the material left over from the mass ejection event. The duration of the SSS stage tells about the mass of the H-rich material left behind on the WD surface after the mass ejection event. Therefore, it is related to the mass of the WD progenitor as well as the mass accretion rate and WD temperature (Yaron et al. 2005). The duration of the SSS phase can be predicted based on the amount of material predicted to be left behind after the CNe eruption and it can be $> 10^3$ years (Hernanz & Sala 2002). But ROSAT observations show that most novae turn off within 10 years after outburst (Orio et al. 2001) and more recent observations indicate that the duration of the SSS phase in

Galactic CNe is typically rather short, of order 2 - 3 years (Ness et al. 2007). This very large discrepancy between theoretical and observed turnoff times likely indicates higher than expected mass loss during the eruption though the theoretical explanation for this high mass loss is not yet understood (Hernanz & Sala 2010). In the SSS phase, the ejecta are subjected to an intense flux of high photons (0.5 - 10 keV) it can have a significant impact on the observed spectroscopic characteristics of the emission lines and the dust. It is possible to determine the connection between X-ray, optical and IR observational characteristics of novae by coordinating observations using the Swift telescope with optical monitoring efforts. It may associate a class of optical spectral features with a general state of X-ray emission. As we can say the optical signature of [Fe X] 6375 Åmay be a good indicator that a CNe is in a SSS state.

1.13.3 IR observations

During the evolution, the novae radiate a significant amount of energy in infrared band. The prime sources for the infrared emission are optically thick ejecta in the fireball phase, thermal bremsstrahlung in the free expansion phase, dust formed in the ejecta. The isothermal dust phase has been observed in a number of novae and analysis of this phase has provided valuable information, especially on the properties of the emitting dust, emission from X-ray heated grains, fine-structure line emission from a cold phase of the nova nebula and cooling of grains heated by the shocked gas at the interface between the nova ejecta and the interstellar medium. The infrared spectroscopic and photometric observations of novae are very useful to determine the metal abundances in the nova ejecta and the phenomena of dust formation. The derivations of formulae for evaluating specific physical parameters from the analysis of the infrared data, and summaries of results on recent bright novae is given in detail by a number of authors (Gehrz 1988, 1998, 2002; Gehrz, Truran & Williams, 1993 and references therein).

On the basis of infrared observations, novae can be divided into two groups which depends on the type of the white dwarf:

CO novae: The nova explosion which occurs on the low-mass carbon-oxygen (CO) white dwarfs is called as CO novae. They generally show P Cygni profiles in their spectra and slow post-outburst evolution with low expansion velocity. They are known to generally form dust, either optically thick or thin. They also show enhanced CNO abundances but not generally heavier elements and the He/H ratio is near the solar abundance.

ONe novae: The nova explosion which occurs on the high mass oxygen-neon (ONe) ($M_{WD} \geq 1.2$) white dwarf is called ONe novae. They evolve fast with a high expansion velocity and generally do not form dust. The infrared spectra generally show the early emission of [Ne II] 12.8 micron in greater strength, which is responsible for their classification as 'neon novae'. They usually show some evidence of carbon depletion relative to solar, with associated enhancements of oxygen and neon.

1.13.4 Radio observations

The prime reason behind radio emission from novae is thermal bremsstrahlung. As there is no internal and/or external extinction by the dust for the radio emission so they have the benefit over the observations in the other wavelength regions. The radio observations are very useful for resolved images from which we can estimate the optically thick radio surface brightness and hence the electron temperature. By comparing the angular expansion rates derived from the radio with the absorption line velocities, the distance to the nova can be determined. As the separation of CVs is of the order of 10^{11} cm and the radio observations provides a mean to probe the large scale structure of the binaries on the scale of $\geq 10^{11}$ cm so the radio observations are very important for knowing the separation of the binary system. Radio observations provide important information on the ejected mass and geometry, often not well-determined using other methods. Standard models predict free-free radio emission from the expanding nova ejecta. Although in some novae we also expect non-thermal radio emission from shock interactions. In the initial phase the flux density is optically thick and increases as the source expands but then turns over as it becomes optically thin. This timescales depends on the ejecta mass and velocity. The first detection of classical novae were made by Hjellming and Wade (1970) by using the three-element interferometer of the National Radio Astronomy Observatory (NRAO) at 2.7 and 8.1 GHz. These novae were HR Del and FH Ser. The early studies of novae at radio wavelength are summarized by Hjellming (1974). There are some observatories all over the world who are doing radio observations but most of the radio observations have been made with a three-element interferometer at Green Bank, West Virginia, the Westerbork Synthesis Radio Telescope (WSRT), the Very Large Array (VLA) in New Mexico, or the MERLIN network of telescopes (Seaquist & Bode 2008) and GMRT in India. As the modern telescopes have a high resolving power so it has been possible to resolve the expanding shell in many novae and recurrent novae and to detect a few dwarf novae and magnetic CVs.

1.14 Significance of IR observations of novae

The IR observations are important for the novae because they tell about the properties of low temperature zones. In that way they will be helpful to get the information about the phenomena related to low temperature. Novae are known to produce prolific amount of dust and every known type of astrophysical grain. IR observations become the sole instrument to study all physical and chemical properties related to the dust and associated dust grains. From IR photometry at longer wavelengths we can use to distinguish between the temporal development of extreme CO and ONe novae. It also can be used for determining the occurrence rate and the global influence of novae in the near by galaxies. As very less near-IR observations are available but the combination of optical and near-IR data can provide quantitative measurements at primary physical parameters that characterized the outburst and the nature of the ejecta. The IR observations can be of more help to tell about the cooler components of the novae system like atmosphere of the secondary and the cool outer region of the accretion disk at quiescent state. Apart from that the infrared observations are the best tracers of the true fireball stage since the principal opacity source at these long wavelengths is due to thermal bremsstrahlung which depends only on the change in the column density.

1.15 Motivation and scope of the present work

Astrophysical observations in the near IR picked up momentum with the development of sensitive single element detectors in the 1970s and two dimensional arrays in 1980s. Since then, infrared observations of novae using ground based observatories and satellites in space have made significant contributions in understanding the novae outbursts and their temporal evolution. There are still many unsolved problems and intriguing puzzles which need to be addresed and understood by obtaining additional infrared observations. The unpredictable nature of the nova outbursts and often unexpected changes in their temporal behaviour demand continued observations. The prime objectives of the present investigation are to study and understand the infrared characteristics of novae in details. We are interested in several aspects viz. understanding the process of dust formation in these objects, studying the evolution of novae spectra in the IR in details, identifying and understanding the different lines that are seen in the near-IR spectra like their strengths, temporal variations, excitation mechanisms through modeling. It was noticed that only in limited number the detailed studies of novae has been done and there is a need for dedicated observational programme to monitor the infrared temporal evolution of novae. The advantage of having a captive home telescope is that the accessibility to telescope time becomes easier and flexibility in scheduling is possible for targets of opportunity such as novae. We realize that bright novae can be extensively observed over a large number of epochs hence giving a good coverage of their temporal evolution. It was noted that such extensive observations documenting the infrared evolution of novae had rarely been done. This realization thus served as one of the motivational drivers of the present work. Observations from Mt. Abu were made of more than ten novae (a list of the observed novae is presented in Chapter 2), out of which a few were observed relatively more extensively than the others. I have concentrated in the present thesis on three of the more extensively observed objects viz. V5579 Sagittarii, V496 Scuti and KT Eri - a brief description of these novae is given below:

V5579 Sagittarii (V5579 Sgr): Nova V5579 Sgr was discovered on 2008 April 18.784 UT. It reached the maximum brightness very quickly on 2008 April 23.541 UT. V5579 Sgr belongs to the class of 'classical nova' of Fe II type. This nova formed thick dust in the later stages. Following the outburst the near IR observations commenced on 2008 April 23.949 UT while the nova was around maximum brightness and continued till 2008 May 14.919 UT.

V496 Scuti (V496 Sct): Nova V496 Sct was discovered on 2009 November 8.370 UT. The nova brightened quickly to its maximum in visual light on 2009 November 18.716 UT. V496 Sct belongs to the class of 'classical nova' of Fe II type. The highlight of the observations was the rare detection of the first-overtone CO emission (2.29 - 2.4 μm) in the nova - similar emission has been recorded previously only in a few novae. It also formed dust in the later stages. Following the outburst the near IR observations commenced on 2009 November 19.57 UT and continued till 2011 April 22.96 UT.

KT Eridani (KT Eri): Classical nova KT Eri was discovered on 2009 November 25.536 UT. The near-IR observations of KT Eri, presented in the thesis, were started on 2009 November 28.854 UT. The nova was followed till 2010 March 3.734 UT. KT Eri belongs to the class of 'classical nova' of He/N type.

Chapter 2

Observations and Data Analysis

The near-infrared spectroscopic and photometric observations of novae, presented in this thesis, were made using the 1.2m telescope at the Mount Abu Infrared Observatory shown in Figure 2.1 (latitude: 24^0 $39'$ $10''$N, longitude: 72^0 $46'$ $47''$ E, altitude 1680 m), Mount Abu, Rajasthan, India. The observatory is operated by the Physical Research Laboratory (PRL), Ahmedabad, India.

In this chapter, we present the details of the Mt. Abu Infrared Observatory and the focal plane instruments for the 1.2m telescope. The observing season starts from October after the withdrawal of the Indian monsoon and continues till May of the following year when the dust content starts increasing leading to the onset of the monsoon in early July. The low amount of precipitable water vapour in the winter months, 2 - 3 mm, at Mt. Abu makes it a good site for IR observations. This is followed by a detailed description of the observation procedures and data analysis techniques. The optical photometric and spectroscopic data of one nova (V496 Sct), presented in this thesis was obtained from Asiago (Italy).

Figure 2.1: *Front view of the Mt. Abu Infrared Observatory, Mount Abu, Rajasthan, India.*

2.1 1.2m telescope at Mt. Abu Infrared Observatory

The Mount Abu Infrared Observatory is the first major facility for infrared astronomical observations in India. This is specially designed for the ground based observations in the near-Infrared region (J, H and K bands) with an equatorial mount. The optical system of the telescope consists of a 1.2m paraboloid primary mirror having focal ratio of f/3 and a hyperboloid secondary mirror with a focal ratio of f/3.5. The Cassegrain configuration has an effective focal ratio of f/13. The details of the optical parameters of the telescope system are given in Banerjee et al. (1997). The f/13 beam, emerging through the Cassegrain focus is directed to the NICMOS3 detector (Figure 2.2) by a gold coated mirror by folding the beam at 45 deg. The schematic diagram of the camera along with the unit that couples it to the telescope is shown in the Figure 2.3. The peak to valley surface accuracy of the telescope mirrors is one tenth lambda ($\lambda/10$) at 589 nm so that the telescope can be effectively used for imaging in visible as well as in infrared region.

Table 2.1: Description of broad-band filters.

Band	Central Wavelength (μm)	Bandwidth (μm)	Lower cut-off (μm)	Upper cut-off (μm)	Transmission at peak wavelength (%)
J	1.253	0.296	1.105	1.401	93.23
H	1.659	0.288	1.514	1.803	91.96
K	2.185	0.408	1.981	2.389	85.39
K'	2.120	0.360	1.940	2.300	> 80

Presently, five instruments are used with the telescope for different kind of observations:

I. PRL Near Infrared Camera cum Grating Spectrometer (PRLNICS)

II. High Speed Two Channel IR Photometer

III. Optical Polarimeter

IV. CCD imager

V. PARAS (PRL Advanced Radial Velocity All Sky Search)

In the present work, the required spectroscopic and photometric observations of novae have been made using the PRLNICS. The basic design of the PRLNICS system is described in the next section.

2.2 PRL Near Infrared Camera cum Grating Spectrometer

PRL Near Infrared Camera/Spectrometer is India's first operational infrared camera cum grating spectrometer. Its design is based on the Near-Infrared Camera and Multi-Object Spectrograph (NICMOS3) array (256 × 256 HgCdTe detector) cooled to liquid nitrogen temperature (77 K). It was fabricated for

Table 2.2: Description of narrow-band filters.

Band	Central Wavelength (μm)	Bandwidth (μm)	Lower cut-off (μm)	Upper cut-off (μm)	Transmission at peak wavelength (%)
$[FeII]$	1.645	0.0375	1.6262	1.6638	> 80
H_2S(1)	2.1175	0.0429	2.0961	2.1390	74.1
Narrow band 1	2.1352	0.0428	2.1138	2.1566	78.0
Br γ	2.164	0.0443	2.1427	2.1870	59.1
CO band	2.3726	0.1013	2.3220	2.4232	83.0
Narrow band 2	2.2169	0.0831	2.1754	2.2585	74.0

PRL by Infrared Labs Inc., USA.

The f/13 beam, which is reflected by the gold coated mirror at 45 deg, enters the 50 mm entrance aperture of the camera. This beam can be compressed by a focal reducer lens that changes the focal ratio to f/6.5 beam. The focal reducer also changes the camera field of view (FOV) from $2' \times 2'$ to $4' \times 4'$. Correspondingly, the plate scale changes from $0.5'$/pixel to $1'$/pixel for the two FOVs respectively.

The focal reducer lens is a cooled plano convex doublet that has BaF_2 and Fused Silica components. The beam then passes through the filter wheels and the system has two circular filter wheels: the first one contains broad band filters ($JHKK'$) and the second one contains narrow band filters. The descriptions of these filters are presented in Tables 2.1 and 2.2, respectively.

The PRLNIC cum Spectrograph follows Ebert-Fastie configuration. An entrance aperture/slit, which is placed at the focal plane of the telescope, a collimating mirror to make the optical beam from the telescope parallel, a mirror and dispersing element (grating) mounted back to back, and a camera

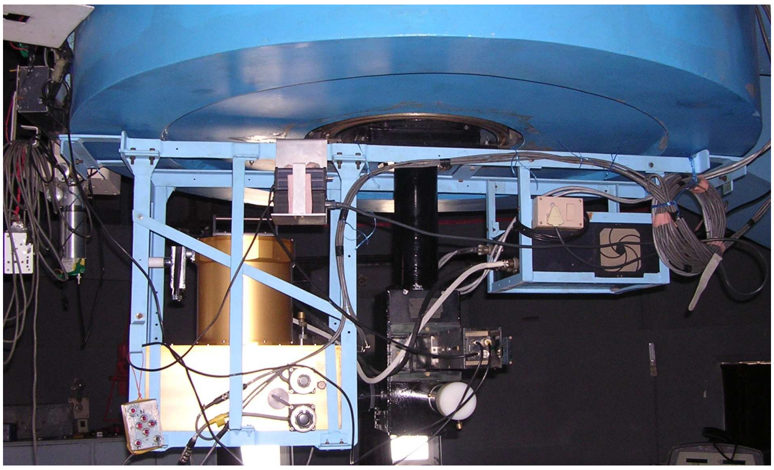

Figure 2.2: *Close-up view of the PRLNICS system (golden colored dewar on the left side) attached to the cassegrain focus of the 1.2m telescope.*

mirror that is used to image the stellar field or spectrum on to the NICMOS3 array. The instrument can be quickly changed from the imaging mode to spectrograph mode by rotating the platform on which the mirror and grating are mounted. The required wavelength range is chosen by rotating the grating about its axis to change the angle of reflection. As the grating equation can be satisfied for several different wavelength values and order for a given diffraction angle, different orders can overlap and lead to contamination of the spectra. A blocking filter, known as order sorting filter is placed in the beam to remove such unwanted contamination. The broad band filters used for the photometric observations are used as order sorting filters. The converging beam then falls on the NICMOS3 array after 45 degree reflection by a plane mirror. Remote control operations for moving the mirror/grating, platform and selecting the filters using stepper motors are available from the control room. The change over from the imaging aperture to the slit is done manually. In addition, a facility for centering the star on the slit, using a combination of a beam splitter that reflects the optical wavelengths at 45 degree and a fast read out CCD to display the stellar field prior to the beam entering NICMOS3 dewar is available. The characteristics of the optical elements of the spectrometer and the detector are given in Table 2.3 and 2.4, respectively. A schematic diagram

Table 2.3: Specifications of the near-infrared Spectrometer.

Element	Specification
Collimator Mirror	-508 CCV, 63.4mm $\times$ 44.8mm, 40 deg off-axis
Camera Mirror	-508 CCV, 84.2mm $\times$ 64mm, 40 deg off-axis
Grating	Flat, 73.8mm $\times$ 44mm, 6.95 deg blaze and 149.1 lines/mm
Slit width	76 μm
Dispersion	9.5 Å/pixel

of this multimode instrument is shown in Figure 2.4.

2.3 Observation and Data Reduction

To get the true or intrinsic image we have to do some task, like removing the unwanted background emission from the telescope and the atmosphere, a number of instrumental effects such as bad pixels, different kinds of noise, effects of cosmic rays and other things from the raw observed image. In addition to that we have to deal with the infrared radiation from the source, on its way to the observer, which suffers scattering and absorption by both the inter stellar medium and the Earth's atmosphere; the atmospheric transmission is not uniform and varies with wavelengths. All these effects must be eliminated from the acquired image to get the proper image or the spectrum of the source. In order to achieve this, certain procedures are followed during observations that aid in the reduction and analysis of the data.

2.3.1 Spectroscopic observations

1. A set of at least two spectra of the nova are taken each time with the object dithered to two positions (offset by 20 - 30 arcseconds) along the slit;

Table 2.4: Characteristics of the detector array.

Detector	256 × 256 HgCdTe
Pixel size	40 μm
Readnoise	53 e-
Darknoise	$\leq$0.7 e-/s
ADC	32 bit
Bad Pixels	$\sim$ 200
Total yield (Usable Pixels)	99.7 %
System Quantum Efficiencies	
J band	32.75 %
H band	18.30 %
K band	28.91 %

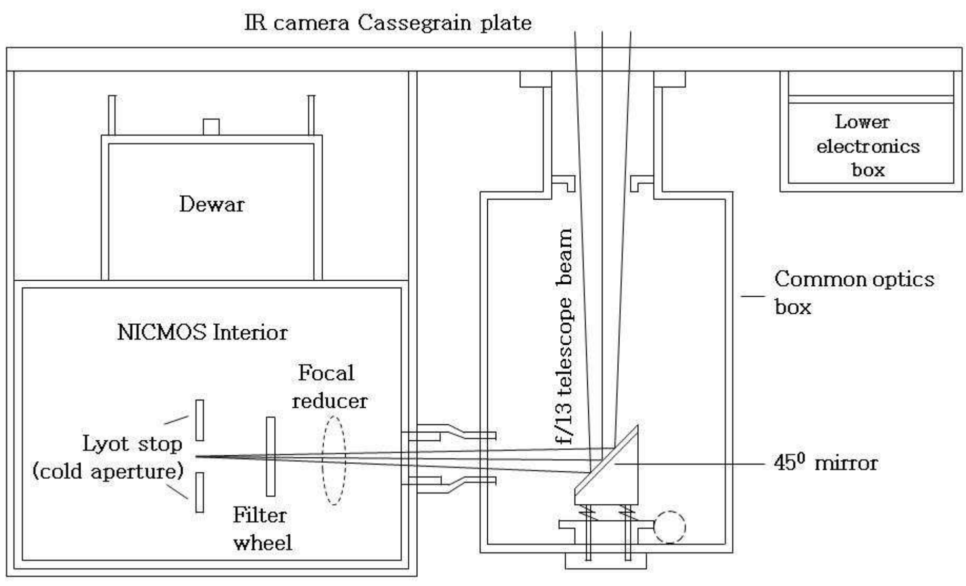

Figure 2.3: *Schematic diagram of the PRLNICS optical system coupled with the 1.2m telescope at Mt. Abu Observatory.*

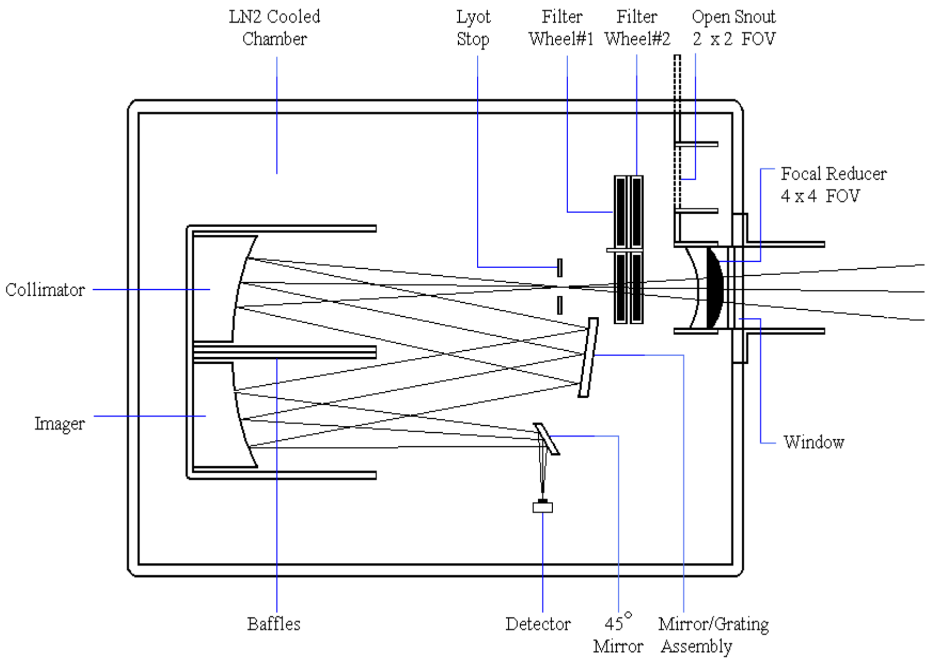

Figure 2.4: *The optical layout of the PRLNICS camera system.*

the exposure time is same for both the spectra. The purpose of taking two spectra at two different locations is to remove the background contribution (sky + dark counts) by subtracting the images from each other.

2. Following the same procedure mentioned above, two spectra of a standard star are obtained along with the nova spectra. The spectra of the standard star are used to correct the effects of atmospheric transmissions, reflectivity of the telescope optics and the spectral response of the spectrometer. Since the intensity of the atmospheric transmission varies with the airmass, we have always tried to choose a standard star near the nova so that the airmasses do not differ too much. Generally a standard star of spectral type A was chosen because the spectra of A type stars have a featureless continuum except for the presence of prominent absorption lines of H I which can be easily identified and removed.

3. The dispersion in each of the JHK bands exceeds the array size. Hence, the spectra were observed, in each band, in two parts. The initial part of the wavelength region is positioned on the detector by rotating the grating/mirror

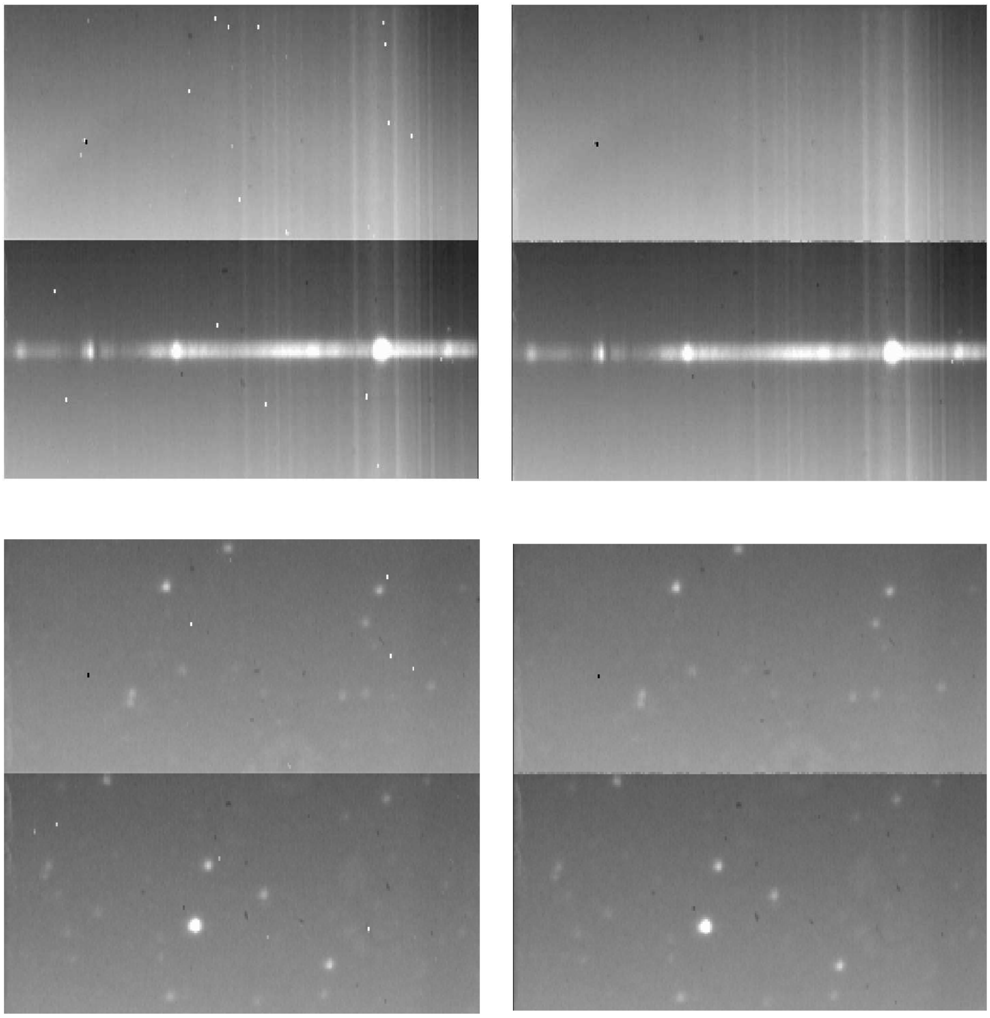

Figure 2.5: *The effect of cosmic rays on the observed spectra and the images is shown in left panels on top and bottom. The randomly located white spots are due to the cosmic ray hits. In the right panels on top and bottom, the effect of high counts on individual pixels caused by cosmic rays has been removed.*

assembly by a known amount and then the later part of the spectra is brought on the detector by additional small amount of rotation of the grating/mirror assembly. In both the spectral images the middle part of the spectra was kept common, so that the intensities of the spectral features in the middle part could be matched and the two parts could be spliced together to form the complete spectra.

2.3.2 Photometric observations

1. In each of the JHK bands, generally images of the nova were obtained at five dithered positions, offset typically by 20 arcsec. At each position, a large number of frames of short integration time were obtained depending on the brightness of the nova.

2. Following the same method, several frames of a standard star were acquired at five dithered locations either before or soon after the nova observations. The standard star was chosen in such a way that it is located close to the nova in the sky, has spectral class close to A0V and the difference between the magnitudes of the target nova and the standard star is small (generally $\sim$ 2 - 3 magnitudes).

3. The detector array is a combination of four individual quadrants. Since, the response of these parts are not same, the dithered images of the nova during photometry, were preferably taken in the same (first) quadrant of the array. The reason for choosing the first quadrant is that, it contains less number of bad pixels relative to the others.

2.4 Data Reduction

Spectroscopic observations of novae were made using the grating spectrometer based on HgCdTe 256 $\times$ 256 focal plane array (resolving power $\lambda/\triangle\lambda \sim 1000$; dispersion of $\sim$ 9.5 Angstroms per pixel) whereas photometric observations were performed under photometric sky conditions using the imaging mode of the NICMOS3 array. Observed data were analyzed using several tasks under *IRAF*. *IRAF* (Image Reduction and Analysis Facility) is an image processing and astronomical data analysis software developed at the National Optical Astronomy Observatories (NOAO), USA. The different steps of the data analysis process and the principal tasks used are presented in Table 2.5.

2.4.1 Spectroscopic data reduction

The spectra were extracted using the APEXTRACT task in *IRAF*. The spectral extraction process follows the following steps -

1. We remove the effects of the cosmic rays by using the *IRAF* task *cosmicrays*. Cosmic ray events appear as high count signals randomly scattered over the observed frames (see Figure 2.5) caused by ionizing radiation. The cosmic ray hits are usually confined to one or two pixels.

2. In order to remove the sky background and dark counts, the frames of two spectra, observed in the same wavelength region but with the star shifted along the slit, were subtracted from each other by using the *IRAF* task *imarith* (see Figure 2.6).

3. After the subtraction, an image contains two spectra of the star viz. one spectrum with positive counts and the second one with negative counts. Generally, the full width at zero intensity of the spectrum spreads over about ten pixels. The positive spectrum is converted to a 1D spectra using the task *apall*. The extracted spectrum is a plot of the number of counts against the pixel number.

4. The calibration of the *JHK* spectra (conversion of pixel number to wavelength) is done with the help of OH sky lines and telluric lines that register with the stellar spectra. We select a particular frame where the OH sky lines are prominently seen. We first calibrate this frame with the help of the sky lines and use it as a reference for calibrating the other spectra in the same wavelength region.

5. The hydrogen Paschen and Brackett absorption lines are manually removed from the spectra of the standard star and the telluric absorption feature is removed by dividing the nova spectra from the standard star spectra.

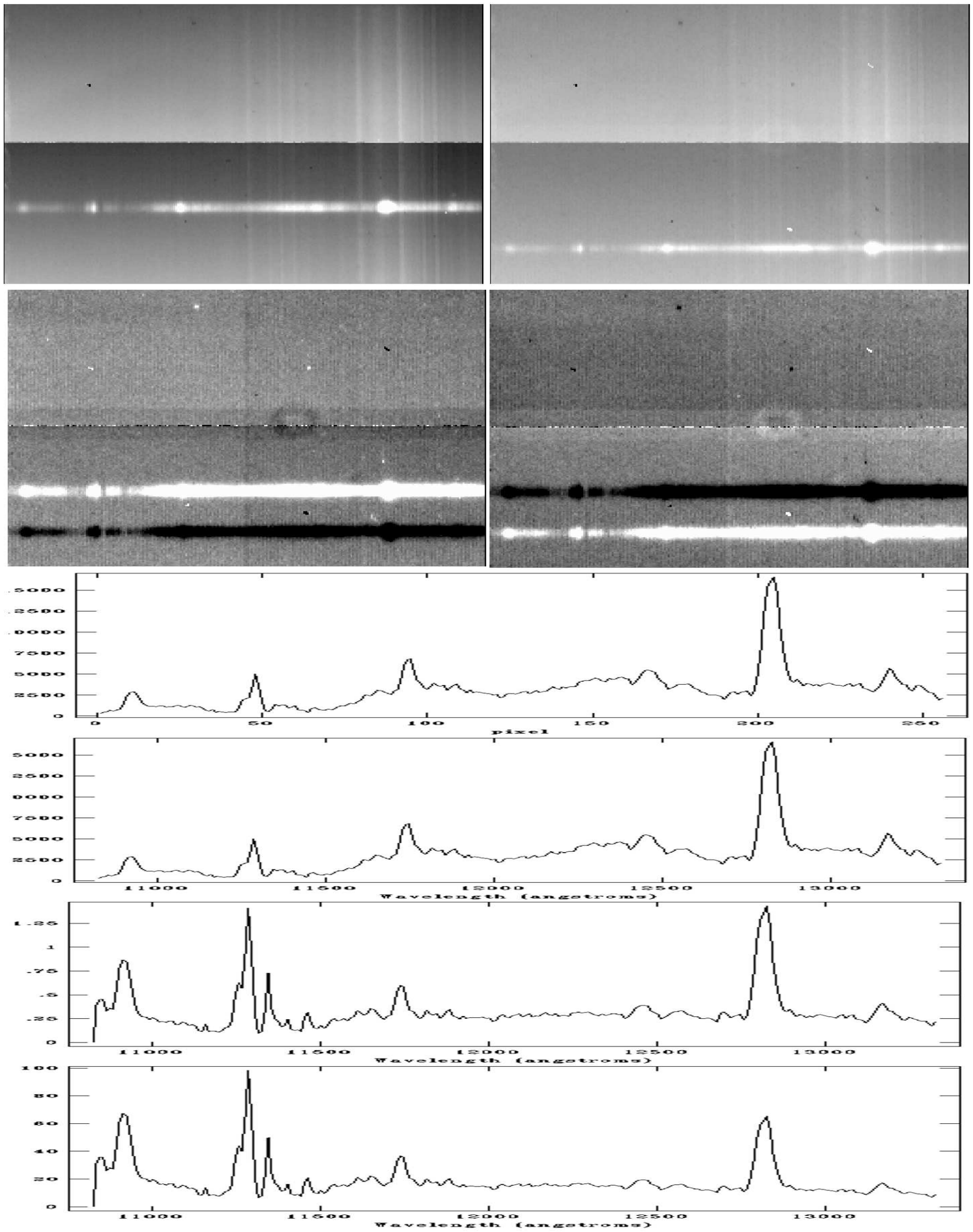

Figure 2.6: *Illustration of the steps involved in the spectral reduction is shown from top to bottom. A set of spectra of the nova (corrected for cosmic rays), at two positions along the slit is followed by the subtracted images that show the removal of the sky background and dark counts. The extracted spectrum shows counts vs pixel plot followed by the wavelength calibrated spectrum. An example of the nova spectrum divided by the standard star spectrum shows the removal of telluric and filter transmission effects from the nova spectrum. The intrinsic nova spectrum shown in the last panel, is obtained by multiplying the ratioed spectra by a black body curve corresponding to the temperature of the standard star (see subsection 2.4.1 for more details).*

6. The intrinsic nova spectrum is recovered by multiplying the ratioed spectra by a black body curve corresponding to the effective temperature of the standard star to correct for the instrument response function.

Table 2.5: List of *IRAF* tasks used for the data reduction.

Steps	*IRAF* tasks
Cosmicrays removal	cosmicrays
Subtraction of images	imarith
Defining the dispersion axis	hedit
Extracting spectra	apall
Wavelength calibration	identify, refspectra and dispcor
Making blackbody curve	mk1dspec
Arithmetic of spectra	sarith
Plotting spectra	splot, specplot
Combining images	imcombine
Aperture photometry	tasks under APPHOT

2.4.2 Photometric data reduction

Photometric data were reduced to derive JHK magnitudes of the nova using the *IRAF* aperture photometry task APPHOT. The photometric data reduction process follows the following steps (see Figure 2.7)-

1. First, we remove the effects of cosmic rays by using the *IRAF* task *cosmicrays.*

2. From each set of the images of star observed at a particular position, an average frame is generated. This process improves the signal to noise ratio in the average frames.

3. A sky frame of equal exposure time devoid of the field stars is generated by median averaging the 5 average frames at 5 dithered positions. The background is removed by subtracting the sky frame from each of the average frames.

4. After the removal of the sky and dark current background, a subtracted frame contains the signal from the star only. From the subtracted images the instrumental magnitude of the nova is obtained using aperture photometry.

Following the same procedure described above, the instrumental magnitude of the observed standard star is also derived.

5. After getting the apparent magnitude we apply the correction for the interstellar extinction in the nova direction. The interstellar extinction refers to the loss of radiation from the star by scattering and absorbtion by the interstellar medium. The necessary corrections are made by using the extinction coefficients for each photometric band. The typical atmospheric extinction coefficients for the Mt. Abu Infrared Observatory site are $E_J = 0.11$, $E_H = 0.07$ and $E_K = 0.09$ magnitude per airmass (Varricattu 1998).

The observing and reduction procedure described above minimized the errors arising out of airmass corrections.

In the present work, we have calculated the interstellar extinction corrections using Koornneef (1983) relations:

$A_V = 3.1 \times E(B\text{-}V)$

$A_J = 0.265 \times A_V$

$A_H = 0.155 \times A_V$

$A_K = 0.09 \times A_V$

where E(B - V) is the color excess and the A_J, A_H and A_K are the extinction coefficients in the respective bands. Hence, the corrected magnitudes will be

$m_C = m_{nova} - A_C$ where $C = J$, H or K.

2.4.3 Flux calibration

The PRLNICS filters are quite similar to the 2MASS filters. We have used the 2MASS magnitudes for the photometric standard stars selected for the

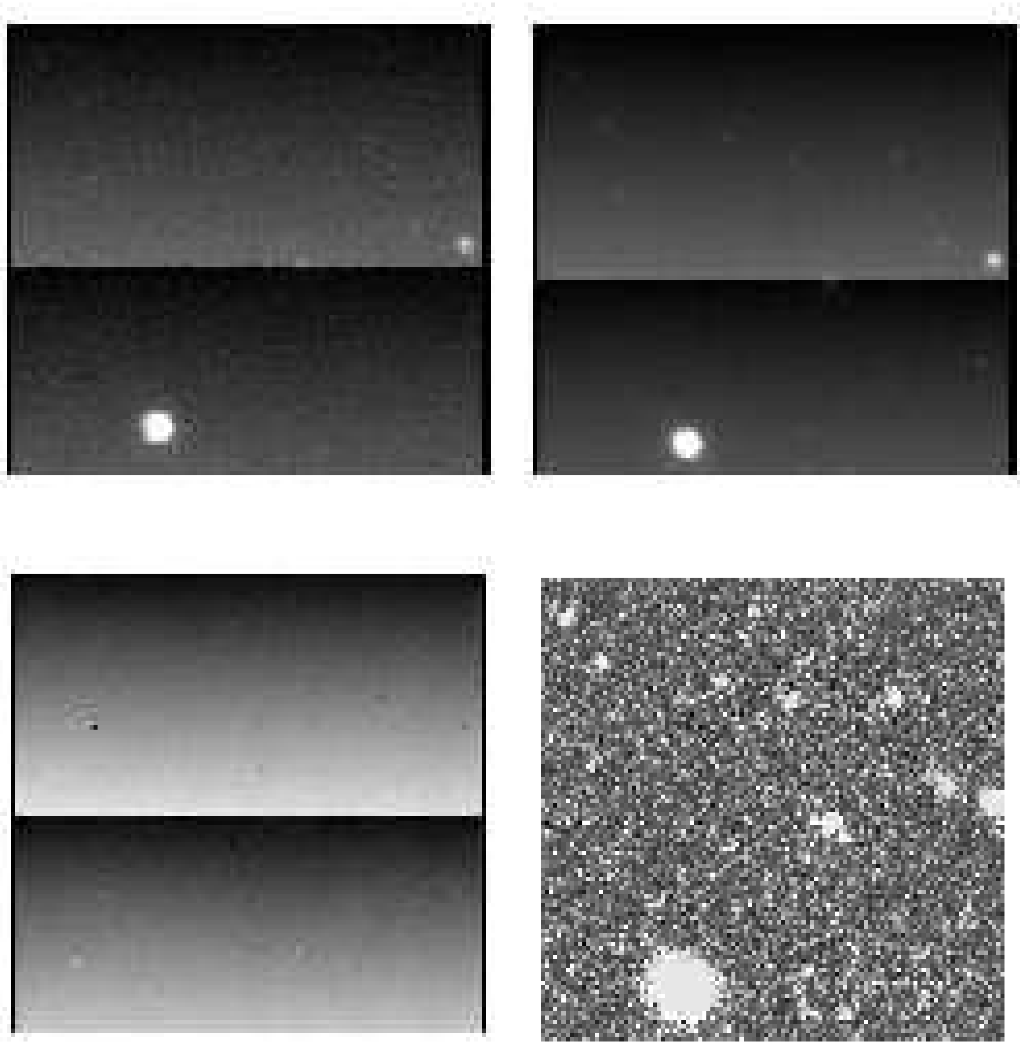

Figure 2.7: *Illustraion of the steps involved in the photometric data reduction is shown in the panels from top left to bottom right. The individual image (corrected for cosmic rays) of nova (top left) observed at one of the five dithered positions followed by the average image at the same position are shown (top right). The sky frame generated from median combining the average images at the five dithered positions is shown next (bottom left). The final panel shows the sky subtracted nova image (bottom right) which clearly shows some of the fainter field stars (see the subsection 2.4.2 for details).*

Table 2.6: The flux densities for a zero-magnitude star (Bessell et al. 1998).

Near-IR bands	λeff (μm)	Fλ W cm^{-2} μm^{-1}	Fν W cm^{-2}Hz^{-1}
J	1.22	3.15×10^{-13}	1.59×10^{-23}
H	1.63	1.14×10^{-13}	1.02×10^{-23}
K	2.19	3.96×10^{-14}	6.40×10^{-24}

nova observations. The flux from the nova at the effective wavelength of near-infrared JHK bands, F_λ, is derived using the basic equation

m_λ = -2.5 log($F_\lambda/F_\lambda(0)$)

where m_λ is the corrected magnitude of the nova, $F_\lambda(0)$ is the flux of a zero magnitude star. In the present work, we have used the flux values for the zero magnitude star in the JHK bands from the work of Bessel, Castelli and Plez (1998) as given in Table 2.6.

2.5 Details of all the observed novae

Apart from the three novae (which are discussed in this thesis) few additional novae are also observed by the author from Mt. Abu during the period of the present thesis to explore the properties of the nova system. The present thesis incorporates results of the three best-observed novae viz. V5579 Sagittarii, V496 Scuti and KT Eridani. Out of these KT Eridani shows some features of a recurrent nova. A list of the all observed novae is given in Table 2.7.

Table 2.7: List of observed novae in the JHK bands.

Observed novae	Discovery date	Spectroscopy Epochs	Photometry Epochs
V2468 Cyg	Mar. 7.801 UT, 2008	6	4
V5579 Sgr	Apr. 18.784 UT, 2008	6	4
V5584 Sgr	Oct. 26.439 UT, 2009	8	10
V496 Sct	Nov. 8.370 UT, 2009	10	5
KT Eri	Nov. 25.536 UT, 2009	10	17
V1722 Aql	Dec. 14.400 UT, 2009	3	4
V2673 Oph	Jan. 15.857 UT, 2010	6	4
V5585 Sgr	Jan. 20.720 UT, 2010	2	2
V1310 Sco	Feb. 20.857 UT, 2010	2	4
V2674 Oph	Feb. 18.845 UT, 2010	2	6
V1311 Sco	Apr. 25.788 UT, 2010	-	1
Nova Oph 2012	Mar. 25.789 UT, 2012	-	15
Nova Sgr 2012	Apr. 21.011 UT, 2012	-	2
Nova Oph 2012 No.2	May. 19.484 UT, 2012	1	10
Nova Sco 2012	May. 22.800 UT, 2012	1	1

Chapter 3

Study of V5579 Sagittarii

3.1 Introduction

Nova Sgr 2008 (V5579 Sgr) was discovered by K. Nishiyama and F. Kabashima at $V = 8.4$ on 2008 April 18.784 UT (Nakano, Nishiyama & Kabashima 2008) on two 30 s unfiltered CCD images. Munari et al. (2008) reported a rapid and steady brightening of about 0.7 mag per day in the initial stages leading to the possibility of V5579 Sgr reaching naked eye visibility if the trend continued. However, the brightening lasted only for 5 days and V5579 Sgr reached a maximum brightness of $V_{max} = 6.65$ on 2008 April 23.541 UT. The early optical spectrum taken during the pre-maximum phase by Fujii (2008) on 2008 April 19.82 UT showed hydrogen Balmer series absorption lines with Hα having a prominent P Cygni profile and also several additional broad absorption lines indicating that V5579 Sgr is a classical nova. The infrared spectra taken by Russell et al. (2008) on 2008 May 9 showed lines of O I, N I, Ca II and exceptionally strong lines of C I. The full width at half maximum (FWHM) of the lines are approximately 1600 km s^{-1}. Even though the Fe II features were weak Russell et al. (2008) classify V5579 Sgr to be a Fe II type nova. The lines of neutral helium had not yet formed and the strongest lines were the O I lines that are fluorescently excited by Lyβ. The infrared continuum showed strong thermal emission from dust at a temperature of 1370 K. Subsequent infrared observations extending to 13.5 μm by Rudy et al. (2008) showed significant spectral changes like substantial decrease in the line strengths and pronounced absorption dip at the line centers. There was an increase in the dust emission and associated cooling of the dust temperature to 1080 K. The formation of dust can also be seen from the light curve. After reaching the maximum, V5579 Sgr followed a smooth and fast decline. This fading was interrupted, about 20 days after discovery, by a sharp decline seen in the AAVSO light curve consistent with the formation of dust in the nova ejecta as reported by Russell et al. (2008). A search in the Digitized Sky Survey (DSS) red image and U.K. Schmidt red plate by Dvorak (2008) did not reveal any object at the position of V5579 Sgr. With the limiting magnitude of these surveys being close to 20 magnitudes, V5579 Sgr is one of the large amplitude ($\triangle V = 13$ magnitudes) novae observed in recent years. A BVR_CI_C photometric sequence around V5579 Sgr was performed by Henden & Munari (2008). They found that the field is extremely crowded, with several very faint field stars lying within 4 arcsec from nova position and not listed in USNO B1 or 2MASS catalogs. The astrometry was also done using SLALIB (Wallace, 1994) linear plate transformation routines in conjunction with the UCAC2 reference catalog. The errors in the coordinates was less then 0.3 arcsec for the nova. The Plate archive photometry was also done by Jurdana-Sepic & Munari (2008) for nova V5579 Sgr. The Asiago Schmidt plate archive was searched for nova V5579 Sgr, and 106 plates were found covering its position. After plate inspection 58 good B and I_C band plates were finally retained. These 58 good plates covered the period 1961 June 16 to 1977 July 24, with an average limiting magnitude $B \sim 18$, $I_C \sim 15.5$. They found that the progenitor was below limiting magnitude on all the plates. The J band images of the nova V5579 Sgr from Mt. Abu after the outburst and a 2MASS image before outburst are shown in Figure 3.1 (left and right panels). The position of the nova is marked in 2MASS image, as circle in the right panel of Figure 3.1.

This chapter discusses the near-infrared photometric and spectroscopic observations in Section 3.2. The results of the analysis of V band light curve,

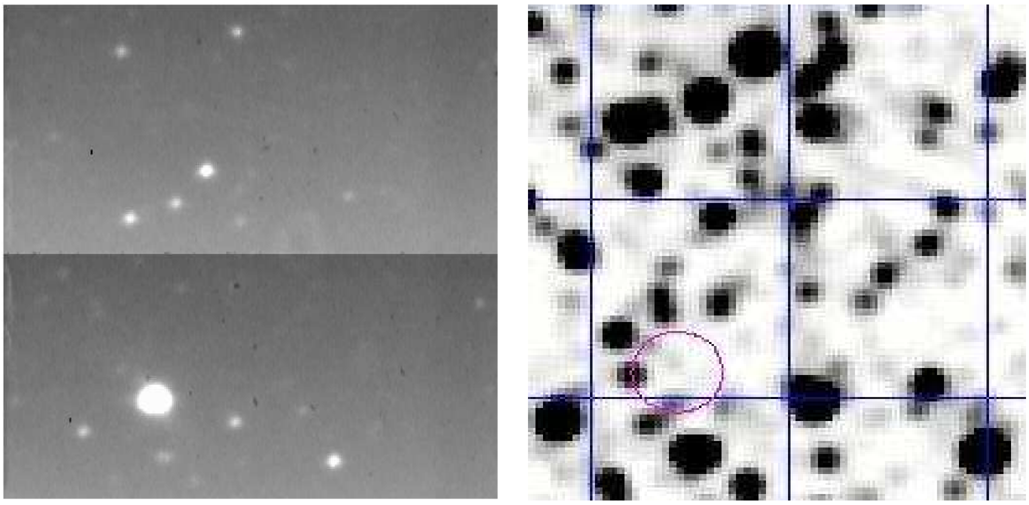

Figure 3.1: *The J band images (2 × 2 arcmin) of V5579 Sgr. The left panel shows the image obtained during the outburst from Mt. Abu and the right panel is 2MASS image with suggested progenitor marked with a circle. North is on the top and East is to the right.*

evolution and general characteristics of the near-infrared spectra, dust formation and ejecta mass estimate are presented in Section 3.3. In Section 3.4 the results are summarized.

3.2 Observations

Near-IR observations were obtained using the 1.2m telescope of Mt. Abu Infrared Observatory from 2008 April 23 to 2008 May 15. The deteriorating sky conditions associated with the pre-monsoon conditions did not allow observations after 2008 May 15. The log of the spectroscopic and photometric observations are given in Table 3.1 and Table 3.2 respectively. The spectra were obtained at a resolution of $\sim$ 1000 using a Near-Infrared Imager/Spectrometer with a 256×256 HgCdTe NICMOS3 array. In each of the JHK bands a set of spectra was taken with the nova off-set to two different positions along the slit. Spectral calibration was done using the OH sky lines that register with the stellar spectra. The spectra of the comparison star SAO 185320 were taken at similar airmass as that of V5579 Sgr to ensure that the ratioing process (nova spectrum divided by the standard star spectrum) removes the telluric features reliably. To avoid artificially generated emission lines in the ratioed spectrum, the H I absorption lines in the spectra of standard star were removed by interpolation before ratioing. The ratioed spectra were then multiplied by a blackbody curve corresponding to the standard star's effective temperature to yield the final spectra. Photometry in the JHK bands was done in clear sky conditions using the NICMOS3 array in the imaging mode. Several frames, in 4 dithered positions, offset by $\sim$ 30 arcsec were obtained in all the bands. The sky frames, which are subtracted from the nova frames, were generated by median combining the dithered frames. The star SAO 185779 located close to the nova was used for photometric calibration; the typical errors in the observed magnitudes are $\pm$0.03. The parameters of the standard stars are given in Table 3.3. The data is reduced and analyzed using the $IRAF$ package. The details of the data analysis procedures are discussed in Chapter 2.

Table 3.1: Log of spectroscopic observations of V5579 Sgr. The date of outburst has been assumed to be its discovery date viz. 2008 Apr 18.784 UT.

Date 2008 (UT)	Days since Outburst	Integration time (s) J	H	K
Apr 23.949	5.165	20	40	40
Apr 26.966	8.182	40	40	20
May 3.947	15.163	30	30	60
May 4.977	16.193	30	30	60
May 8.972	20.188	45	45	60
May 13.914	25.130	200	100	–

Table 3.2: A log of the JHK photometric observations of V5579 Sgr. The date of outburst has been assumed to be its discovery date viz. 2008 Apr 18.784 UT.

Date 2008 (UT)	Days since outburst	Magnitudes J	H	K
Apr 23.988	5.204	4.58	4.47	4.16
May 1.894	13.11	5.58	5.14	4.90
May 8.926	20.142	6.19	5.96	4.69
May 14.919	26.135	6.85	5.47	4.09

Table 3.3: Parameters of the standard stars used for spectral and photometric reduction.

Star	Equatorial and Galactic co-ordinates (2000)	V	J	H	K	Spectral type
SAO 185320	17h 22m 0.58s -24d 59m 58.37s 0.46, 6.55	3.248	3.631	3.656	3.831	B2 IV
SAO 185779	17h 48m 27.84s -26d 58m 29.8s 2.002, 0.48	6.35	5.909	5.848	5.861	B4 IV

3.3 Results

Before presenting the results proper, we estimate some useful parameters for V5579 Sgr. The basic useful parameters for the nova V5579 Sgr, namely the outburst luminosity, the interstellar reddening and the distance, are derived using the V band light curve.

3.3.1 The pre-maximum rise, outburst luminosity, reddening and distance

The light curves based on the V band data of AAVSO and JHK magnitudes from Mt. Abu are presented in Figure 3.2. The date of discovery as given by Nakano, Nishiyama & Kabashima (2008) is 2008 April 18.784 UT. There is a good photometric coverage of the nova's rise to maximum which lasts for almost 5 days culminating in a peak brightness of V_{max} = 6.65 on 2008 April 23.541 UT. The decline rate is calculated from the epoch of peak brightness 2008 April 23.541 UT. We fit a least square regression to the post maximum light curve and estimate the time decline by 2 & 3 magnitudes (t_2 & t_3) about 8 $\pm$ 0.5 d and 14 $\pm$ 0.5 d, respectively. This small observed value of t_2 makes V5579 Sgr as one of the fast Fe II class of novae in recent years. The example of the fast novae of Fe II class in recent years are N Aql 1999 (V1494 Aql, t_2 = 6.6 d), N Sgr 2004 (V5114 Sgr, t_2 = 11 d), N Cyg 2005 (V2361 Cyg, t_2 = 6 d), N Cyg 2006 (V2362 Cyg, t_2 = 10.4 d), N Oph 2006 (V2576 Oph, t_2 = 8 d), N Cyg 2007 (V2467 Cyg, t_2 = 7 d), and N Cyg 2008 (V2468 Cyg, t_2 = 7.8 d). The earlier example of Fe II class nova with fast decline rate is N Aql 1995 (V1425 Aql) with t_2 = 11 d (Kamath et al. 1997). As mentioned earlier V5579 Sgr is also one of the large amplitude novae observed in recent years with $\triangle V$ = 13 magnitudes.

These observed values of the amplitude $\triangle V = 13$ and $t_2 = 8$ days for V5579 Sgr are consistent with its location in the amplitude versus decline rate plot for classical novae presented by Warner (2008) which shows $\triangle V$ = 12 - 15 for t_2 = 8 days.

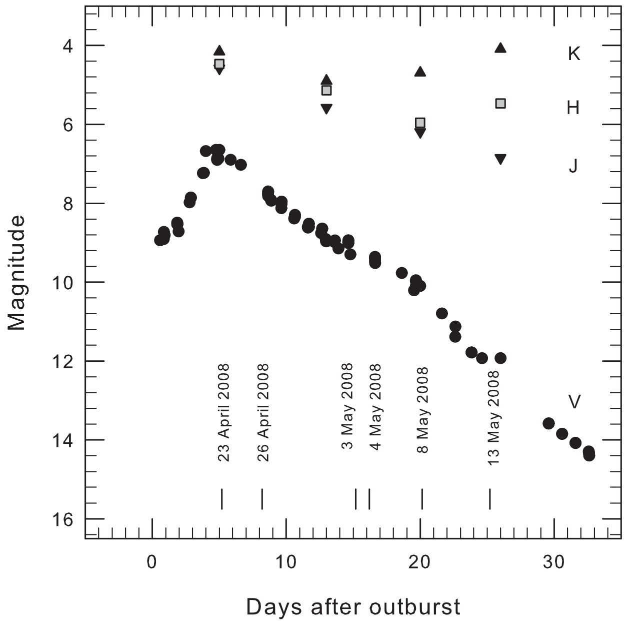

Figure 3.2: *The V band lightcurve of V5579 Sgr from AAVSO data. The days of spectroscopic observations are indicated by dashes below. The Mt Abu JHK photometric data is also shown.*

Using the maximum magnitude versus rate of decline (MMRD) relation of della Valle & Livio (1995), we determine the absolute magnitude of the nova to be M_V = -8.8 ± 0.1 giving a distance modulus of V_{max} - M_V = 15.50.

The reddening is derived using the intrinsic colors of novae at peak brightness, namely (B - V) = 0.23 ± 0.06, as derived by van den Bergh & Younger (1987). We have used the optical photometry data from the AAVSO to calculate E(B - V). The observed (B - V) = 0.95 ± 0.06 results in E(B - V) = 0.72 ± 0.06 and A_V = 2.23 ± 0.08 for R = 3.1. Russell et al. (2008) estimate E(B - V) = 1.2 using the O I lines in the spectra obtained on 2008 May 9 but remark that part of the reddening may be local to the nova as dust had already formed. Our observations, discussed in a later subsection, also clearly show the dust formation in V5579 Sgr by 2008 May 9. In their study of the spatial distribution of the interstellar extinction, Neckel & Klare (1980) have shown that close to the direction of V5579 Sgr, A_V steadily increases to a value of ∼ 1.8 mag around 2 kpc and flattens after that. The moderate value of A_V estimated by us appears reasonable even though the nova is located close to the direction of Galactic Center (Galactic coordinates: 3.73, -3.02 see Table 3.8). The distance to the nova is calculated using the expression for the distance modulus

$$V_{max} - M_V = 5\ log\ d - 5 + A_V \tag{3.1}$$

Based on the above we obtain a value of the distance to the nova $d = 4.4 \pm 0.2$ kpc. The height from the galactic plane is estimated to be $z = 232 \pm 11$ pc to the nova.

We have estimated the white dwarf mass by using the derived value of the absolute magnitude M_V and relation given by Livio (1992); Warner (1995b):

$$M_V = -8.3 - 10\ log\ M_{WD}/M_{\odot} \tag{3.2}$$

The mass of the underlying white dwarf (M_{WD}) in V5579 Sgr is estimated to be $M_{WD} \sim 1.12\ M_{\odot}$. The outburst luminosity of V5579 Sgr as calculated from M_V is $L_O = 2.7 \times 10^5\ L_{\odot}$.

3.3.2 The nature of the light curve

A classification system for the optical light curves for novae on the basis of the shape of the light curve and the time to decline by 3 magnitude (t_3) has been presented (see Chapter 1) by Strope et al. (2010). The shape of the optical light curve of V5579 Sgr presented in Figure 3.2 has all the characteristics of D class of nova which shows a dust dip in the V band light curve after the optical maximum. The early decline of V5579 Sgr following the rise to the maximum is interrupted by fast decline around 15 days after optical maximum and continues further. Thus the classification of the optical light curve for V5579 Sgr is D(14), as the estimated value of t_3 is $\sim$ 14 days for V5579 Sgr. The t_3 value obtained by us using the AAVSO V band light curve is little less with the value obtained by the relation $t_3 = 2.75\ (t_2)^{0.88}$ which gives $t_3 = 17$ days (Warner 1995b).

3.3.3 Line identification, evolution and general characteristics of the JHK spectra

The JHK spectra are presented in Figures 3.3 to 3.5 respectively; line identification in graphical and tabular form are shown in Figure 3.6 and given in Table 3.4 respectively. The infrared observations presented here cover all the phases with the first infrared spectra taken on 2008 April 23 very close to the visual maximum. These spectra near optical maximum are dominated by lines of hydrogen, neutral nitrogen and carbon and display deep P Cygni profiles. The emission components of all these lines have become stronger in the spectra taken on 2008 April 26 and by 2008 May 3 all the lines are seen in emission. The typical FWHM of the H I lines are 1500 km s^{-1}. A noticeable feature of these early spectra is the presence of lines due to Na I and Mg I. In the spectra taken on 2008 May 3 the Na I lines at 1.1381 μm, 1.1404 μm, 2.1452 μm, 2.2056 μm and 2.2084 μm and Mg I lines at 1.1828 μm, 1.5040 μm, 1.5749 μm and 1.7109 μm are clearly seen. In an earlier study of V1280 Sco, Das et al. (2008) had suggested that the presence of spectral lines of low ionization species like Na I and Mg I in the early spectra are indicators of low temperature zones conducive to dust formation in the nova ejecta and this is very well borne out by the present observations in the case of V5579 Sgr. We would like to point out the presence of a large number of strong lines of neutral carbon. These are typical of Fe II type nova as seen in the case of V1280 Sco (Das et al. 2008) and V2615 Oph (Das et al. 2009). The rising continuum is seen in the spectra taken on 2008 May 8 indicating formation of significant amount of dust in the nova ejecta. The dust continuum has started dominating the spectrum on 2008 May 13.

From the K band spectra we do not find CO emission bands in the first overtone. However it is possible that such emission may be weakly present but below detection levels. It is thus useful to try and set an upper limit on the strength of the CO emission and hence on the CO mass. An upper limit can be set by computing a model spectrum for the CO emission and using

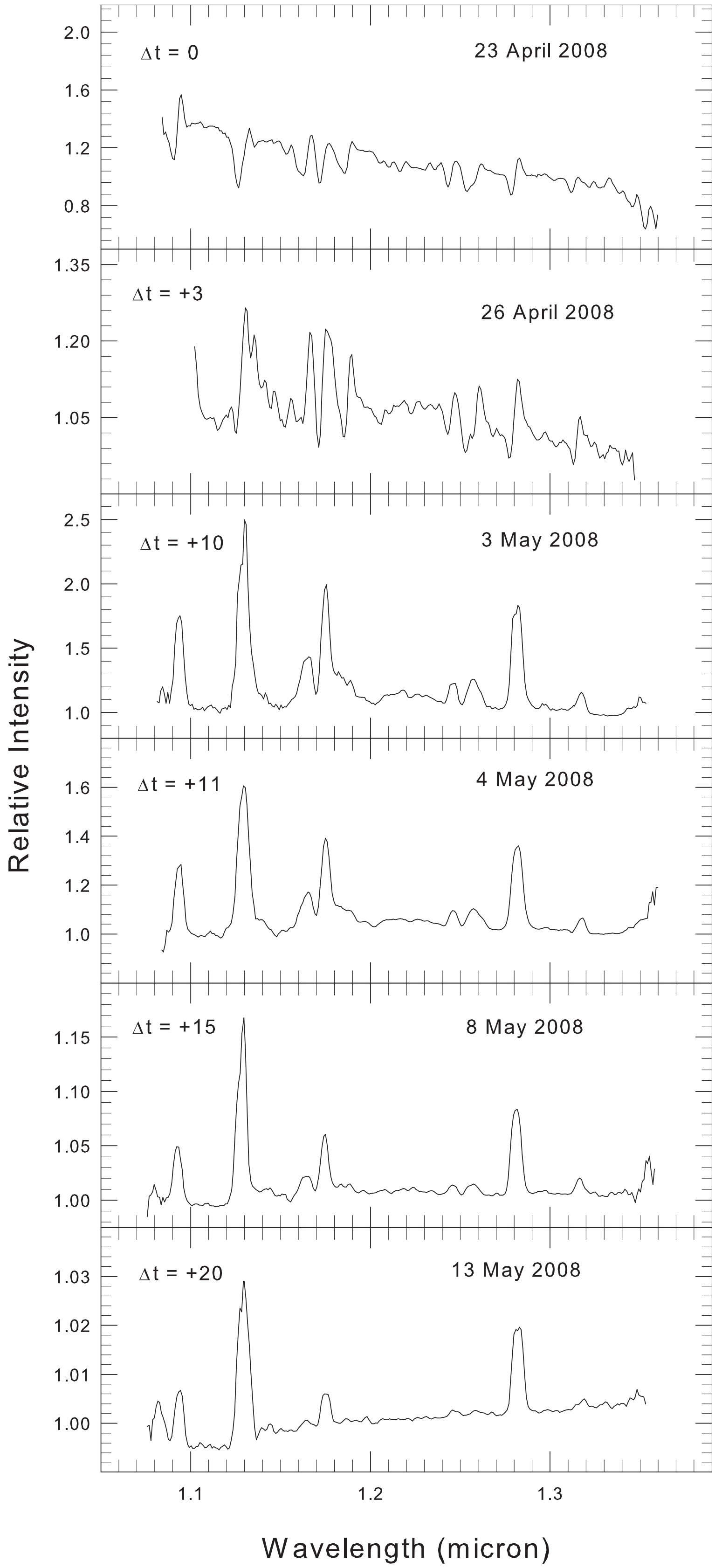

Figure 3.3: *The J band spectra of V5579 Sgr are shown at different epochs. The relative intensity is normalized to unity at 1.25 μm. The time from optical maximum are given for each spectrum.*

the criterion that CO emission should be discernible if the calculated model strengths of the CO bands are atleast 3σ times the value of the continuum noise in the CO band region (2.29 - 2.4 μm). The model CO spectrum has been computed along the same lines as done for the nova V2615 Oph, where CO was strongly detected, and which is described in Das et al. (2009). The details of the model calculations for CO bands are given in Chapter 4 where we report the detection of CO bands in emission for the nova V496 Sct. The model calculations were done for the temperature range of 2500 K to 4200 K corresponding to the observed values in case of novae where CO has been detected and modeled (first overtone detections have been made in V2274 Cyg - Rudy et al. 2003; NQ Vul - Ferland et al. 1979; V842 Cen - Hyland & Mcgregor 1989, Wichmann et al. 1990, 1991; V705 Cas - Evans et al. 1996; V1419 Aql - Lynch et al. 1995; V2615 Oph - Das et al. 2009; V496 Sct - Rudy et al. 2009, Raj et al. 2009). A value of 3 - 5 $\times$ 10^{-9} $M_\odot$ is obtained for the upper limit of M_{CO} using a distance of 4.4 kpc to the nova.

Theoretically, the detailed modeling of Pontefract and Rawlings (2004) for molecule formation and destruction in nova winds, predicts that CO should form early after the outburst, remain constant in strength for $\sim$ 15 days thereafter and then get rapidly destroyed. Fairly consistent with this picture, most of the CO detections outlined above have indeed been reported early after the outburst. Thus, in the present case too, CO emission could have been expected. Its absence indicates that it either is present but below detection levels or that it did not form for reasons which are not clearly understood.

3.3.4 Fireball phase

As noted earlier, V5579 Sgr showed pre-maximum brightening. After its discovery on 2008 April 18.784 UT by Nishiyama & Kabashima (Nakano 2008) at 8.4 mag, it brightened by nearly 1.8 mag over next five days to reach maximum of $V = 6.65$ mag on 2008 April 23.541 UT. This pre-maximum rise is well observed at optical wavebands. Our first near-IR photometric observations are available for 2008 April 23.988 UT close to the optical maximum. We have

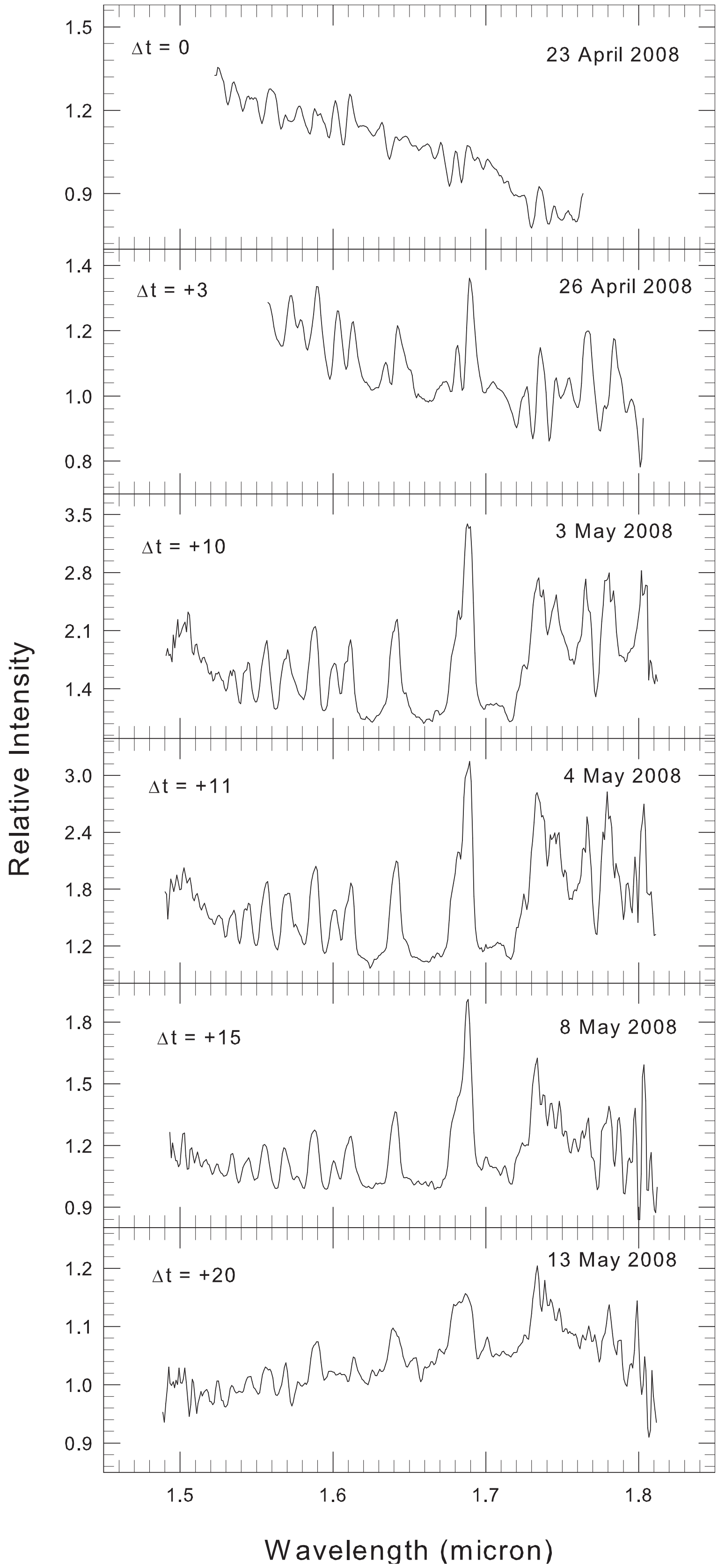

Figure 3.4: *The H band spectra of V5579 Sgr are shown at different epochs. The relative intensity is normalized to unity at 1.65 μm. The time from optical maximum are given for each spectrum.*

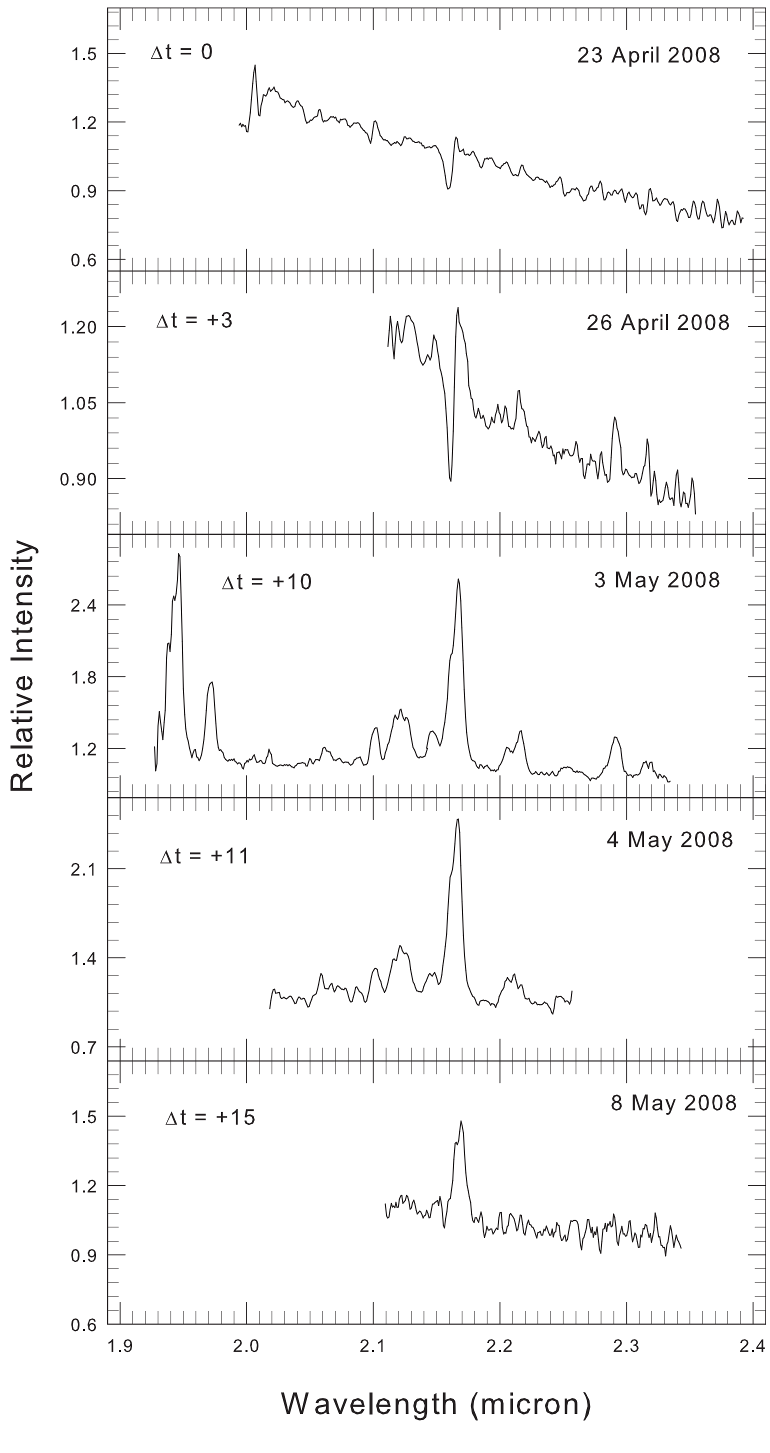

Figure 3.5: *The K band spectra of V5579 Sgr are shown at different epochs. The relative intensity is normalized to unity at 2.2 μm. The time from optical maximum are given for each spectrum.*

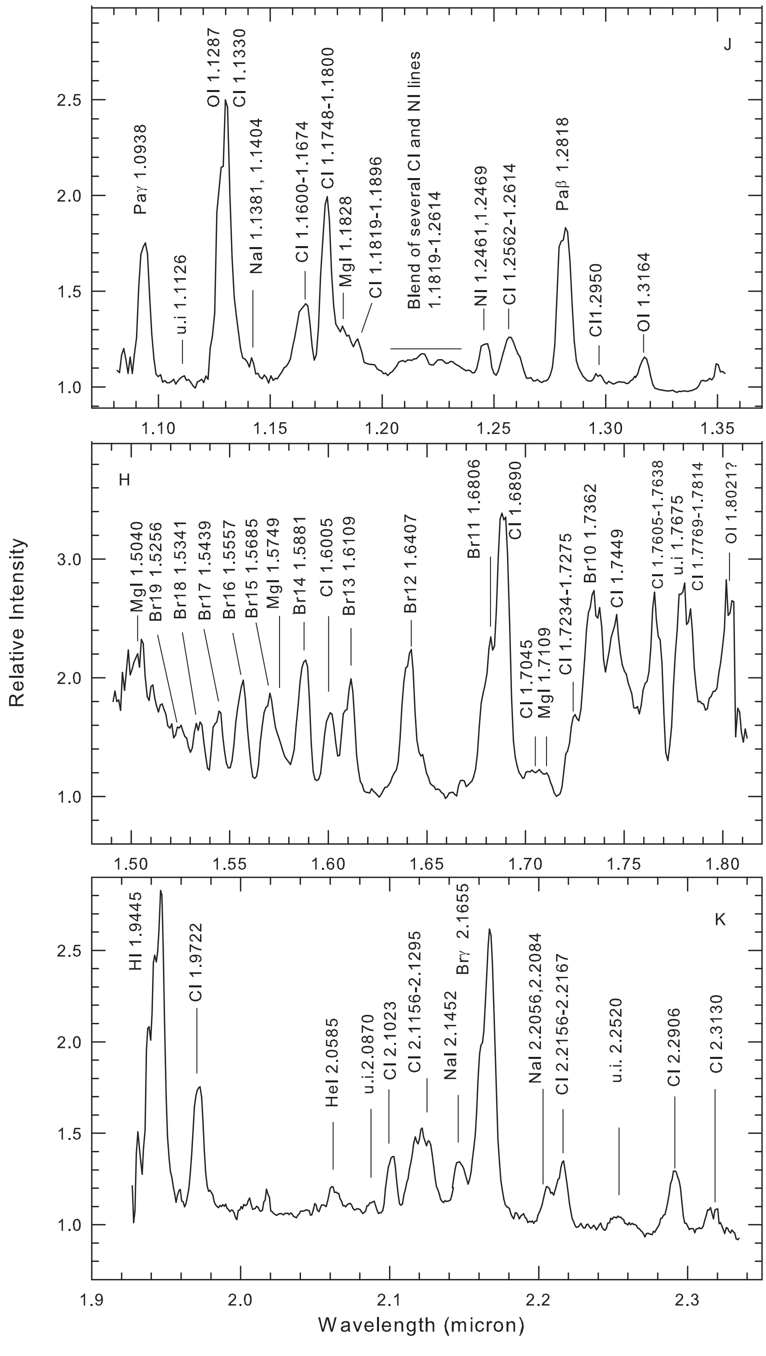

Figure 3.6: *The line identification is shown for the spectra of 2008 May 3 in the JHK bands as given in Table 3.4.*

studied the fireball phase by obtaining spectral energy distribution (SED) covering the optical and near-IR region. The following optical magnitudes B = 7.6, V = 6.87, R_C = 6.23 and I_C = 5.55 at maximum brightness from AAVSO along with the present JHK magnitudes of 2008 April 23.988 UT were used in deriving the SED. The observed magnitudes were corrected for extinction using Koornneef's (1983) relations (see Chapter 2) and A_V=2.23 mag. From a blackbody fit to the SED shown in top panel of Figure 3.6, we obtain a formal temperature of $T_{bb} = 8900 \pm 400$ K which is consistent with the A to F spectral type for the pseudo-photospheres displayed by novae at outburst (Gehrz 1988). However, this temperature T_{bb} estimate is likely to have additional errors as all the observed flux values used in the fit lie on the Rayleigh-Jeans part of the spectral energy distribution. Further, the B band flux value is also susceptible to significant errors since it has the largest interstellar extinction correction. The list of corrected broad band flux values for the optical and near-infrared bands is given in Table 3.5. The blackbody angular diameter θ_{bb} in arcseconds is calculated using the relation given by Ney & Hatfield (1978), namely,

$$\theta_{bb} = 2.0 \times 10^{11} (\lambda F_\lambda)^{1/2}_{max} \times T_{bb}^{-2} \tag{3.3}$$

where $(\lambda F_\lambda)_{max}$ is in W cm^{-2} and T_{bb} is in Kelvin. From the model blackbody fit of 8900 K shown in Figure 3.7 (upper panel), we find $(\lambda F_\lambda)_{max}$ = 3.64 $\times$ 10^{-14} W cm^{-2}. We accordingly obtain a value of $\sim$ 0.5 milliarcsec for the angular diameter. This value for the angular diameter can be used to estimate the distance to the nova by invoking constant expansion rate for the ejecta and the relation given by Gehrz (2008), namely,

$$d = 1.15 \times 10^{-3} (V_{ej}) t / \theta_{bb} \tag{3.4}$$

where d is in kpc, V_{ej} in km s^{-1}, t in days since outburst began and θ_{bb} in milliarcsec. Taking a value of 1500 km s^{-1}, the typical FWHM of H I lines for V_{ej} and t = 5d corresponding to the epoch of optical maximum we get d = 17.3 kpc which is four times larger than the estimate done in section 3.1 using the MMRD relation. The reason for this discrepancy is not clear. A likely reason is that the pseudo photosphere behaves as a grey body with reduced emissivity in the fireball phase. The estimate of θ_{bb} will always be a lower limit since it is applicable for a blackbody (Ney & Hatfield 1978; Gehrz et al. 1980). For a grey body, the observed angular size can be larger, since the right hand side of equation 3.3 should be divided by $\epsilon^{1/2}$, where ϵ the emissivity has a value less than unity.

A similar discrepancy was noticed by Das et al. (2008) in the case of V1280 Sco, where the blackbody angular diameters were smaller by a factor of three than the values derived from the interferometric measurements. It should be noted that the value of t is likely to have an error due to the uncertainty in the determination of the start of the outburst. For V5579 Sgr, Yamaoka, Haseda & Fujii (2008) and Liller & Camilleri (2008) report that no object brighter than 11.5 and 11.0 mag respectively was seen on their patrol images taken around 2008 April 15.743 UT and 2008 April 16.22 UT. Thus our estimate of t is likely to have an error of $\sim$ 2 days which worsens slightly the discrepancy between the distances determined using the MMRD and the blackbody angular diameter relations.

Table 3.4: A list of the lines identified from the JHK spectra shown in Figure 3.6. The additional lines contributing to the identified lines are listed and the unidentified lines are mentioned as u.i.

Wavelength (μm)	Species	Other contributing lines and remarks
1.0938	Pa γ	
1.1126	u.i	Fe II ?
1.1287	O I	
1.1330	C I	
1.1381	Na I	C I 1.1373

Continued on next page.

Table 3.4 – *Continued from previous page.*

Wavelength (μm)	Species	Other contributing lines and remarks
1.1404	Na I	C I 1.1415
1.1600-1.1674	C I	strongest lines at 1.1653, 1.1659,1.16696
1.1746-1.1800	C I	strongest lines at 1.1748, 1.1753,1.1755
1.1828	Mg I	
1.1819-1.2614	several C I and N I	strongest lines at 1.1880, 1.1896
1.2461,1.2469	N I	blended with O I 1.2464
1.2562,1.2569	C I	blended with O I 1. 2570
1.2818	Pa β	
1.2950	C I	
1.3164	O I	
1.5040	Mg I	blended with Mg I 1.5025, 1.5048
1.5256	Br 19	
1.5341	Br 18	
1.5439	Br 17	
1.5557	Br 16	
1.5701	Br 15	
1.5749	Mg I	blended with Mg I 1.5741, 1.5766,C I 1.5788
1.5881	Br 14	blended with C I 1.5853
1.6005	C I	
1.6109	Br 13	
1.6407	Br 12	
1.6806	Br 11	

Continued on next page.

Table 3.4 – *Continued from previous page.*

Wavelength (μm)	Species	Other contributing lines and remarks
1.6890	C I	
1.7045	C I	
1.7109	Mg I	
1.7234-1.7275	C I	several C I lines
1.7362	Br 10	affected by C I 1.7339 line
1.7449	C I	
1.7605-1.7638	C I	
1.7675	u.i	
1.7769-1.7814	C I	
1.8021	O I ?	
1.9445	H I	
1.9722	C I	
2.0585	He I	
2.0870	u.i	
2.1023	C I	
2.1156-2.1295	C I	
2.1452	Na I	
2.1655	Br γ	
2.2056,2.2084	Na I	
2.2156-2.2167	C I	
2.2520	u.i	
2.2906	C I	
2.3130	C I	

Table 3.5: List of broad band flux values close to the optical maximum corrected for $A_V = 2.23$ use to derived the spectral energy distribution during the fireball phase.

Band	Flux ($\mathrm{Wcm^{-2}\mu m^{-1}}$)
B	8.8×10^{-14}
V	5.1×10^{-14}
R	3.7×10^{-14}
I	2.3×10^{-14}
J	8.0×10^{-15}
H	2.6×10^{-15}
K	1.0×10^{-15}

3.3.5 Dust formation and ejecta mass estimate

The light curve showed a sharp fall about 15 days after the visual maximum indicating onset of dust formation. The thermal emission from the dust contributes to the near-IR bands and one expects a brightening at these wavelengths. The present near-IR photometric observations presented in Figure 3.2 clearly show the onset of dust formation associated with the fall in the visual light curve around 2008 May 8 accompanied simultaneously thereafter by a steady increase in the near-IR magnitudes, especially in the K band.

The SED of the dust component in the ejecta is constructed using the observed JHK magnitudes on 2008 May 14.919 UT and shown in the lower panel Figure 3.7. The contribution of the thermal emission from the dust given in Table 3.6 is seen increasing upto the K band indicating that it may peak at even longer wavelengths. We estimate a value of 1700 $\pm$ 200 K for the temperature of the dust shell. However, this estimate of temperature for

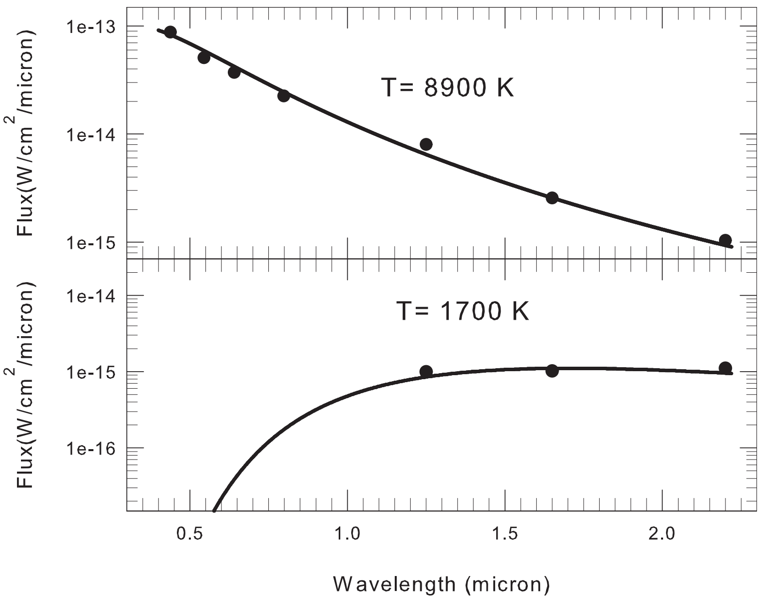

Figure 3.7: *The top panel shows spectral energy distribution for the fireball phase data of April 23.988 UT with blackbody temperature fit of 8900 K. The bottom panel shows a similar fit for the data of May 14.919 UT with blackbody temperature fit of 1700 K after dust formation.*

Table 3.6: List of near-infrared broad band flux values corrected for $A_V = 2.23$ for 2008 May 14.919 UT corresponding to dust formation phase.

Band	Flux ($Wcm^{-2}\mu m^{-1}$)
J	9.9×10^{-16}
H	1.0×10^{-15}
K	1.1×10^{-15}

the dust shell has large uncertainty as observations in only three wavelengths are used in fitting the SED of which the dust is contributing mostly in the K band. The list of corrected broad band flux is given in Table 3.6. Russell et al (2008) have estimated the dust shell temperature to be 1370 K based on the observations spanning the wavelength range upto 5.2 μm. The likely reason for the higher value for the dust temperature derived by us is the restricted spectral coverage extending upto K band only that may have emphasized the contribution at shorter wavelengths.

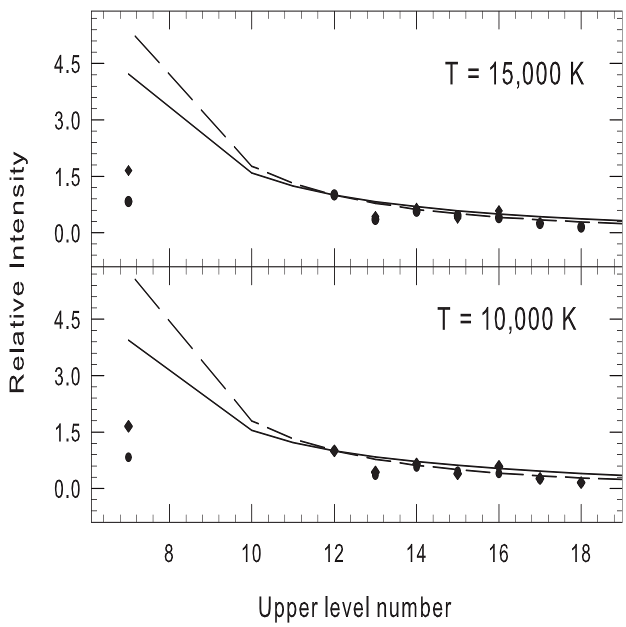

Figure 3.8: *Recombination analysis for the hydrogen Brackett lines in V5579 Sgr on 2008 May 3 and 8. The abscissa is the upper level number of the Brackett series line transition. The line intensities are relative to that of Br 12. The Case B model predictions for the line strengths are also shown for a temperature of* $T = 10^4$ *K and electron densities of* $n_e = 10^{12}$ cm^{-3} *(dashed line) and* 10^8 cm^{-3} *(solid line).*

The mass of the dust shell can be calculated from the thermal component of the SED of 2008 May 14 UT shown in Figure 3.7. Woodward et al. (1993) have given the expression for the mass of the dust shell as

$$M_{dust} = 1.1 \times 10^6 (\lambda F_\lambda)_{max} d^2 / T_{dust}^6 \tag{3.5}$$

In the expression above, mass of the dust shell M_{dust} is in units of $M_\odot$, $(\lambda F_\lambda)_{max}$ is in W cm^{-2} measured at peak of the SED, the black-body temperature of the dust shell T_{dust} is in units of 10^3 K, and the distance to the nova d is in kpc. It is assumed that the dust is composed of carbon particles of size less than 1 μm with a density of 2.25 gm cm^{-3}. The early dust formation, high dust temperature and SED in the near-infrared that resembles black-body in the case of V5579 Sgr are indicative of presence of carbon grains in the dust shell (Clayton & Wickramsinghe 1976). In addition the occurrence of strong carbon spectral features in the observed spectra indicate that our assumption that the dust is made up of carbon/graphite is reasonable. We obtain $M_{dust} = 2.12 \times 10^{-9}$ $M_\odot$ for 2008 May 14 taking the observed parameters of $(\lambda F_\lambda)_{max} = 2.42 \times 10^{-15}$ W cm^{-2}, $T_{dust}= 1.7 \times 10^3$ K and d = 4.4 kpc. The observed ratio for the M_{gas} to M_{dust} range from 1.8×10^2 for LW Ser that formed optically thick dust shell (Gehrz et al. 1980) to 2.5×10^4 for V1425 Aql that formed optically thin dust shell (Mason et al. 1996). Taking a canonical value of 200 for the gas to dust ratio, we get $\sim 4.2\times 10^{-7}$ $M_\odot$ for the gaseous component of the ejecta. This value is smaller than the typically observed value of 10^{-4} to 10^{-6} $M_\odot$ in novae. One definite reason for the dust mass being underestimated is that our SED is based on data extending upto only 2.2 μm and certainly neglects contribution from dust emission at longer wavelengths. In this process we are overestimating the derived dust temperature considerably as is evident from Russell et al. (2008) who get T_{dust} = 1370 K on 2008 May 9, five days before the date being considered in this analysis, which further cools down quickly to 1070 K by 2008 May 22 (Rudy et al. 2008). The formulation used for the dust mass estimate is very sensitive to T_{dust}. Further, since the Rudy et al. (2008) and Russell et al. (2008) reports show that the dust emission peaks at longer wavelengths, we are also underestimating $(\lambda F_\lambda)_{max}$. Correct use of both T_{dust} and $(\lambda F_\lambda)_{max}$ values should considerably enhance the dust mass estimate made here.

Table 3.7: List of near-infrared line flux values corrected for $A_V = 2.23$ for Case B analysis.

Brackett line	Flux ($\mathrm{Wcm^{-2}\mu m^{-1}}$)	
	3 May 2008	8 May 2008
7	1.0×10^{-13}	3.2×10^{-14}
12	1.3×10^{-13}	1.9×10^{-14}
13	4.3×10^{-14}	8.5×10^{-15}
14	7.0×10^{-14}	1.3×10^{-14}
15	5.6×10^{-14}	7.5×10^{-15}
16	5.0×10^{-14}	1.1×10^{-14}
17	3.0×10^{-14}	5.1×10^{-15}
18	1.8×10^{-14}	3.0×10^{-15}

Among all the fast novae that were mentioned above, only N Cyg 2006 (V2362 Cyg) and N Aql 1995 (V1425 Aql) formed optically thin dust. It should be noted that V2362 Cyg showed a pre-maximum rise lasting for $\sim$ 2.8 days and also a second maximum at $\triangle t$ = 239 d, after the optical maximum and dust formed around $\triangle t$ = 251 d. In case of V1425 Aql there was an indication of dust in the ejecta around $\triangle t$ = 22 d, while the present observations show that dust formation took place even earlier around $\triangle t$ = 15 d after the optical maximum in V5579 Sgr. Thus the IR data presented here for V5579 Sgr along with the results of Kamath et al. (1997) on V1425 Aql indicate that the earliest dust formation time scale for an Fe II nova lies in the range of 15 - 22 days.

We have alternatively explored the possibility of estimating the ejecta mass using recombination line analysis of H I lines for 2008 May 3 and 2008 May 8 (Figure 3.8). However, we find that the strengths of these lines, relative to each other, deviate considerably from Case B values on all epochs indicating that the lines are optically thick. Hence we are unable to estimate the ejecta mass from recombination analysis. The list of corrected line flux is given in Table 3.7 for H I lines.

3.3.6 A discussion of the P Cygni phase

We qualitatively discuss the P Cygni profiles seen around maximum light as they can help estimate the radius of the white dwarf's (WD) photosphere (r_{ph}) at this epoch. Kato & Hachisu (1994) have shown from theoretical considerations of the photospheric optical depth that $r_{ph} \geq 100$ $R_\odot$ at maximum. This is a substantial increase by a factor of almost 10^4 in the WD's radius between quiescence to maximum. Subsequent refinements in their modeling of novae light curves reaffirm that after the thermonuclear runaway sets in on a mass-accreting WD, its envelope expands greatly to $r_{ph} \geq 100$ $R_\odot$ (Hachisu & Kato, 2001; Hachisu & Kato, 2006) the evolution of r_{ph} with time is illustrated diagrammatically in the above works. It is desirable to have observational confirmation for such estimates of r_{ph} and P Cygni profiles may provide an assessment of this physical parameter.

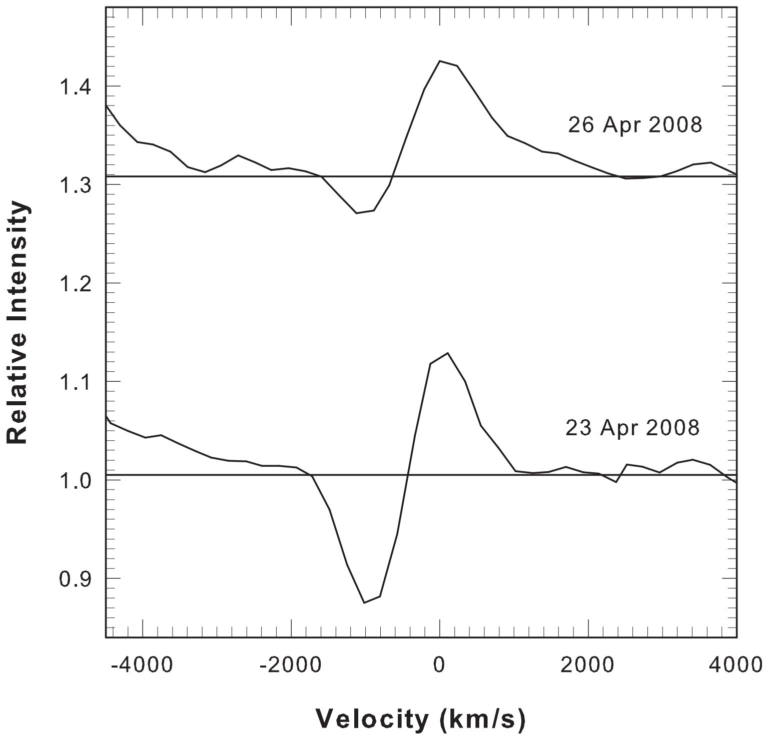

Figure 3.9: *The time evolution of Paβ 1.2818 μm line showing the evolution of the P Cygni feature. For more details see section 3.3.6.*

The generic formation of P Cygni profiles, following Lamers & Cassinelli (1999), can be understood by considering a spherical symmetric outflowing wind (in our case the mass loss from the nova outburst) in which the velocity necessarily increases outwards i.e., the wind is accelerated outwards till it reaches a terminal velocity. To the outside observer, it is the matter in the form of a tube in front of the stellar disc which scatters light from the continuum of the star that is responsible for the absorption component of the P Cygni profile (see Figure 2.4 in Lamers & Cassinelli 1999). The ratio of the strength of the emission and absorption components of the P Cygni profile depends on the size r_w of the wind region (i.e., size of the ejected material) relative to the size of the star. If the star is large compared to the size of the wind region the emission will be smaller than the absorption. When the wind region is large compared to the star's size we expect emission to dominate - this can be seen geometrically as the volume of the emitting gas becomes much larger than the volume causing the absorption component. Observationally consistent with this scenario, it is known that prominent P Cygni profiles in a nova outburst are inevitably seen and reported at maximum light and on one or two days following it. At such an epoch, it is therefore reasonable to use an approximation that the wind region size r_w is of the order of the stellar size r_{ph}. Since the wind region size r_w can be approximated kinematically ($r_w \sim v_{mean} \times t$, v_{mean} = mean velocity of ejecta, t = time after outburst), a qualitative estimate can be made of r_{ph}. This could be used as the rationale in estimating r_{ph}. As the ejected matter (the wind region) keeps expanding to larger sizes at later times following the maximum, the emission component strengthens and finally begins to dominate. This expected behaviour is reasonably in accordance with the early P Cygni profiles seen in V5579 Sgr as shown in Figure 3.9.

A simplistic order-of-magnitude estimate for r_{ph} may be obtained in the following way. Let a typical velocity of $v_{mean} \sim 1000$ km s^{-1} for the nova ejecta be assumed. Velocities in nova ejecta can range from few hundreds to few thousands of km s^{-1} and v_{mean} = 1000 km s^{-1} is a fairly representative value. For our choice of v_{mean}, and taking t = 1 d as the typical timescale when prominent P Cygni profiles are generally seen, the value of $r_w \sim 120$ $R_\odot$ encouragingly matches that expected for r_{ph}. However, we emphasize that this is purely a qualitative estimate. We hope to undertake a detailed modeling, which takes into account a realistic wind-velocity law in the ejecta, to try and reproduce observed P Cygni profiles in novae and their evolution with time.

It is theoretically expected that mass loss during a nova outburst is a sustained process. Spectroscopic evidence for such a sustained mass loss, obtained by tracing the evolution of a P Cygni feature in the Paβ line, is presented here allowing a lower limit of 8 - 12 days to be set for the mass-loss duration.

3.4 Summary

In this chapter, we have presented near-infrared spectroscopic and photometric results of Nova V5579 Sgr which erupted on 2008 April 18.784 UT. The spectra evolve from a P Cygni phase to an emission-line phase and at a later stage is dominated by emission from the dust that formed in this nova. It is theoretically expected that mass loss during a nova outburst is a sustained process. Spectroscopic evidence for such a sustained mass loss, obtained by tracing the evolution of a P Cygni feature in the Paβ line, is presented here allowing a lower limit of 8 - 10 days to be set for the mass-loss duration. From the optical lightcurve, the distance and the height from the galactic plane to the nova is estimated to be 4.4 $\pm$ 0.2 kpc and 232 $\pm$ 11 pc. The mass of the underlying white dwarf in V5579 Sgr is $M_{WD} \sim 1.12\ M_{\odot}$. The outburst luminosity of V5579 Sgr as calculated from M_V is $L_O = 2.7 \times 10^5\ L_{\odot}$. The light curve classification for V5579 Sgr is D(14). The infrared spectra indicate that the nova is of Fe II class. Evidence is seen from the JHK photometry and spectra for the formation of dust in the nova in mid-May 2008. The mass of the dust is estimated to be $M_{dust} = 2.12 \times 10^{-9}\ M_{\odot}$. In this context, the presence of emission lines from low ionization species like Na and Mg in the early spectra and subsequent formation of the dust supports the predictive property of these lines as indicators of dust formation as proposed by Das et al (2008). It may be noted that V5579 Sgr is one of the few fast Fe II class of novae (t_2 = 8 d) that formed dust. We have indicated the possible usefulness of the P Cygni profiles seen in the novae spectra around maximum brightness to study the physical parameters related to the central white dwarf. The summary of the nova is given in Table 3.8.

Table 3.8: Summary of the nova.

Parameter	Value
Name	Nova Sagitarii 2008, V5579 Sgr
Discovery Date	2008 April 18.784 UT
Date of optical maximum	2008 April 23.541 UT
Equatorial coordinates	18h 05m 58.88s -27d 13m 56s (J2000.0)
Galactic coordinates	3.7342, -3.0225 (J2000.0)
Speed class	Very fast
t_2	8 $\pm$ 0.5 days
t_3	$\sim$ 14 days
Reddening E(B-V)	0.72 $\pm$ 0.06
Extinction A_V	2.23 $\pm$ 0.08
M_V	-8.8 $\pm$ 0.1
Distance	4.4 $\pm$ 0.2 kpc
Galactic latitude	232 $\pm$ 11 pc
M_{WD}	$\sim$ 1.12 $M_\odot$
L_O	2.7 $\times$ 10^5 $L_\odot$
Emission lines	P Cygni profiles
Line widths (FWHM)	1500 km s^{-1}
Ejecta mass	$\sim$ 4.2$\times$ 10^{-7} $M_\odot$
Dust formation (mass of the dust)	Yes (2.12 $\times$ 10^{-9} $M_\odot$)

Chapter 4

Study of V496 Scuti

4.1 Introduction

Nova Scuti 2009 (V496 Sct) was discovered by Nishimura on 2009 November 8.370 UT at V = 8.8 (Nakano 2009) on two 10s unfiltered CCD images. Nishimura also reported that no object was visible on two CCD frames taken with the same instrument a day earlier on 2009 November 7.377 UT indicating that V496 Sct was discovered close to maximum brightness. This was confirmed spectroscopically soon after its discovery by the low resolution spectra obtained during the period 2009 November 9.73 UT to 10.08 UT which showed prominent Hα and Hβ emission lines with P Cygni components, along with the strong Fe II multiplets and O I lines indicating that V496 Scuti is an Fe II class nova near maximum light (Teyssier 2009, Munari et al. 2009a, Balam & Sarty 2009). The typical FWHM of the P Cygni components ranged from 700 to 950 km s^{-1} with the absorption component blue shifted by 700 km s^{-1}. Munari et al. (2009a) report that the overall resemblance is that of a typical nova of Fe II class observed close to the maximum brightness. The follow-up observations by Munari et al. (2009b) showed a post-discovery brightening for about 10 days before the onset of fading with maximum brightness V_{max} = 7.07 around 2009 November 18.716 UT. V496 Sct was observed in the infrared by Rudy et al. (2009) using Near Infrared Imaging Spectrograph on the 3m Shane reflector at Lick Observatory on 2009 November 27.08 UT and

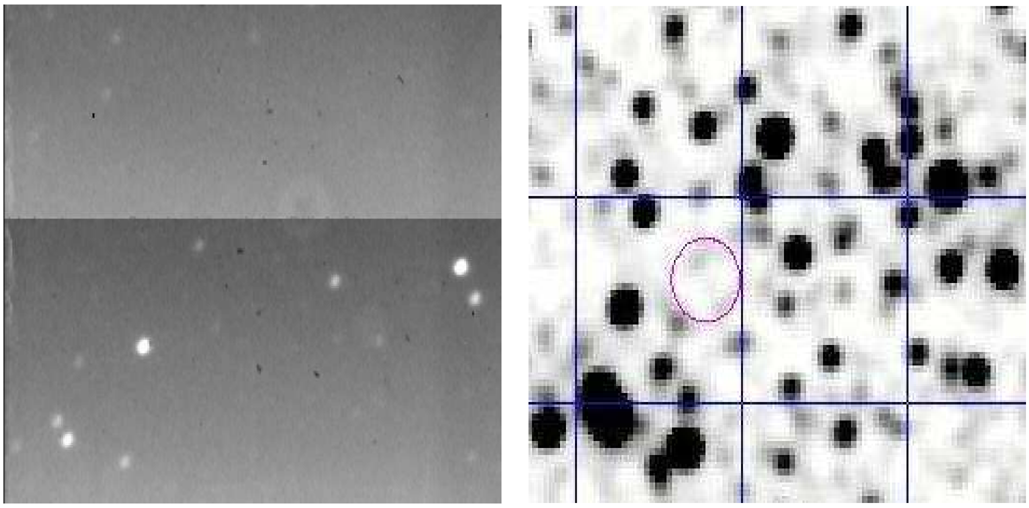

Figure 4.1: *The J band images (2 × 2 arcmin) of V496 Sct. The left panel shows the image obtained during the outburst from Mt. Abu and the right panel is 2MASS image with suggested progenitor marked with a circle. North is on the top and East is to the right.*

revealed strong first overtone CO emission bands - an extremely short lived feature that is seen in only a few novae. They also found several prominent C I emission lines with the strongest line accompanied by P Cygni type absorption component. As the novae that display first overtone CO in emission and strong C I emission in early phases form dust, Rudy et al. (2009) predicted that dust formation in V496 Sct is almost certain. Following this interesting prediction an observational campaign of V496 Sct was initiated at Mt. Abu IR Observatory and the first result by Raj, Ashok & Banerjee (2009) showed the continuation of CO emission during the period 2009 December 3.55 UT to 8.55 UT. V496 Sct could not be observed after 2009 December 9 as it become inaccessible due to its conjuntion with the sun. Subsequent observations by Russell et al. (2010) after V496 Sct came out of the solar conjunction showed dust formation on 2010 February 10. The CO emission seen in 2009 November was absent.

An inspection by Guido & Sostero (2009) of the Digitized Sky Survey (DSS) plate (limiting red magnitude about 20) obtained on 1996 August 13 to look for the progenitor did not reveal any clear and unambiguous object at the position of V496 Sct. The limiting red magnitude of 20 for the DSS plate makes V496 Sct one of the large amplitude ($\triangle R \geq 13.5$) novae.

The nova V496 Sct was studied at Mt. Abu IR Observatory of Physical Research Laboratory in India, at Asiago Observatory operated by the University of Padova and INAF Astronomical Observatory of Padova and Schiaparelli Observatory in Italy.

This chapter discuss the infrared and optical observations in Section 4.2. The results of the optical light curve, characteristics of the infrared and optical spectra, detection and evolution of the CO emission and physical parameters of the nova ejecta are presented in Section 4.3. In section 4.4 the summary of the results are given.

4.2 Observations

4.2.1 Infrared observations

Near-IR photometric and spectroscopic observations were obtained using the 1.2m telescope of Mt. Abu Infrared Observatory from 2009 November 19 to 2011 April 23. After the first observation on 2009 November 19, the observations were done from 2009 December 3 after the detection of CO first overtone bands in emission on 2009 November 27.08 UT by Rudy et al. (2009). In the intervening period no observations could be done due to the non-availability of telescope time. The availability of V496 Sct for short duration during 2009 December resulted in restricted photometric coverage. The log of the spectroscopic and photometric observations are given in Table 4.1 for 520 days from optical maximum. The details of the spectroscopic reduction of the data is given in Chapter 2. The procedure is briefly summarized below. The spectra were obtained at a resolution of $\sim$ 1000 using a Near-Infrared Imager/Spectrometer with a 256 $\times$ 256 HgCdTe NICMOS3 array. In each of the JHK bands a set of spectra was taken with the nova off-set to two different positions along the slit. The wavelength calibration was done using the OH

Table 4.1: Parameters of the standard stars used for spectral and photometric reduction.

Name	Equatorial and Galactic co-ordinates (2000)	V	J	H	K	Spectral type
SAO 144150	20h 11m 18.27s -00d 49m 17.31s (41.58, -18.08)	3.242	3.293	3.278	3.295	B9.5 III
SAO 142612	18h 46m 54.7s -07d 34m 44.84s (25.67, -2.48)	7.24	6.551	6.509	6.44	B9

sky lines that register with the stellar spectra. The spectra of the comparison star SAO 144150 and SAO 142612 were taken at similar airmass as that of V496 Sct to ensure that the ratioing process (nova spectrum divided by the standard star spectrum) removes the telluric features reliably. To avoid artificially generated emission lines in the ratioed spectrum, the H I absorption lines in the spectra of standard star were removed by interpolation before ratioing. The ratioed spectra were then multiplied by a blackbody curve corresponding to the standard star's effective temperature to yield the final spectra.

Photometry in the JHK bands was done in clear sky conditions using the NICMOS3 array in the imaging mode. Several frames, in 4 dithered positions, offset by $\sim$ 30 arcsec were obtained in all the bands. The sky frames, which are subtracted from the nova frames, were generated by median combining the dithered frames. The star SAO 142612 located close to the nova was used for photometric calibration. The data is reduced and analyzed using the $IRAF$ package.

4.2.2 Optical photometry

Optical photometry of V496 Sct was obtained with ANS Collaboration telescope number R030 located in Cembra (Trento, Italy). A detailed description of ANS Collaboration instruments, operation modes and results on the mon-

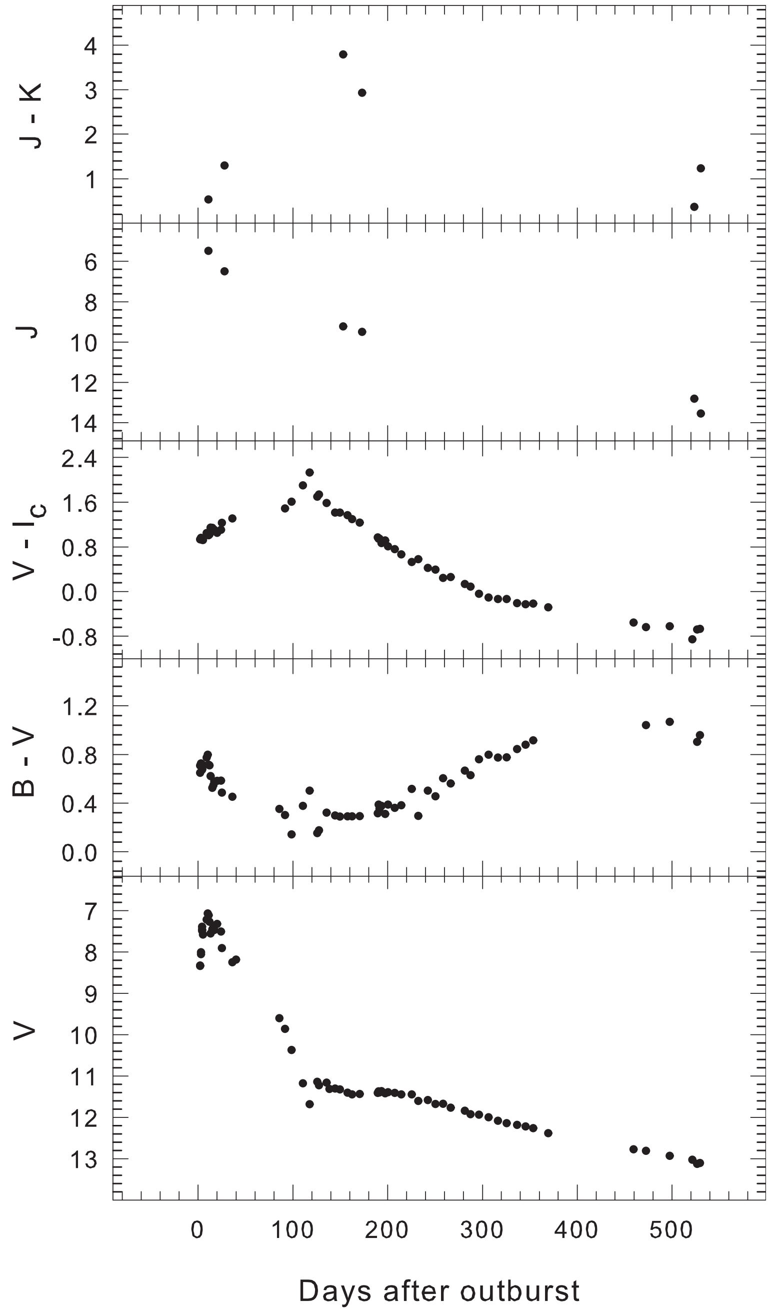

Figure 4.2: *The light curve and the optical and the infrared colors of V496 Sct from Asiago and Mt. Abu data.*

Table 4.2: Log of the Mt. Abu near-infrared observations of V496 Sct. The date of optical maximum is taken as 2009 November 18.716 UT.

Date of	Days since	Integration time (s)			Integration time (s)			Nova Magnitude		
Observation	optical max	J-band	H-band	K-band	J-band	H-band	K-band	J-band	H-band	K-band
		Spectroscopic Observations			Photometric Observations					
2009 Nov. 19.57	0.854	60	–	–	10	25	50	5.49±0.02	5.20±0.02	4.96±0.10
2009 Dec. 03.58	14.864	–	–	60	–	–	–	–	–	–
2009 Dec. 05.56	16.844	60	60	120	–	–	–	–	–	–
2009 Dec. 06.56	17.844	90	60	120	5	10	10	6.50±0.16	5.82±0.21	5.21±0.14
2009 Dec. 07.54	18.824	–	–	120	–	–	25	–	–	5.67±0.20
2009 Dec. 08.54	19.824	90	70	120	–	–	25	–	–	5.45±0.20
2009 Dec. 09.22	20.504	–	90	120	–	–	25	–	–	5.27±0.07
2010 Apr. 10.97	143.254	–	–	–	250	275	50	9.24±0.15	7.74±0.15	5.45±0.20
2010 Apr. 11.97	144.254	120	120	80	–	–	–	–	–	–
2010 Apr. 21.94	154.224	300	200	200	–	–	–	–	–	–
2010 Apr. 22.94	155.224	120	80	60	–	–	–	–	–	–
2010 Apr. 23.93	156.214	120	80	60	–	–	–	–	–	–
2010 Apr. 29.92	162.204	150	100	100	–	–	–	–	–	–
2010 Apr. 30.92	163.204	300	–	–	625	550	50	9.50±0.09	7.99±0.09	6.57±0.10
2011 Apr. 15.95	513.234	–	–	–	1000	500	105	12.82±0.15	13.03±0.15	12.46±0.20
2011 Apr. 22.96	520.244	–	–	–	1000	750	105	13.55±0.12	13.28±0.10	12.32±0.12

itoring of novae is provided by Munari et al. (2012) and Munari & Moretti (2012). Telescope R030 is a 0.30-m Meade RCX-400 f/8 Schmidt-Cassegrain telescope, equipped with a SBIG ST-9 CCD camera, 512×512 array, 20 μm pixels $\equiv 1.72''$/pix, providing a field of view of $13' \times 13'$. The B filter is from Omega and the UVR_CI_C filters from Custom Scientific. The BVR_CI_C photometry of Nova Sct 2009 is presented in Table 4.3. The median values for the total error budget are σ(V)=0.008, σ(B - V)=0.014, σ(V - R)=0.012, σ(V - I)=0.027, which include both the Poissonian components and the uncertainty in the transformation from the local to the standard Landolt (1992) system. The observations and data reduction were co-ordinated by Munari.

4.2.3 Optical spectroscopy

Spectroscopic observations of V496 Sct were obtained with the 0.6m telescope of the Schiaparelli observatory in Varese, equipped with a multi mode spectrograph (Echelle + single dispersion modes) and various reflection gratings, as part of the ANS Collaboration monitoring of nova outbursts (Munari et al. 2012). A journal of the spectroscopic observations is provided in Table 4.4, where the time is counted from the V band maximum. The resolving power of the Echelle spectra is $\sim$ 20,000. The spectra were exposed with a 2 arcsec wide slit, oriented along the instantaneous parallactic angle. All spectra (including Echelle ones) were calibrated in absolute fluxes by observations of several spectrophotometric standards each night, at similar airmasses and both immediately before and after the exposure on the nova. Their zero-points were then checked against simultaneous $BVRI$ photometry by integrating the band transmission profiles on the fluxed spectra, with the differences almost never exceeding 0.1 mag. The observations and data reduction were co-ordinated by Munari.

Table 4.3: Log of the optical photometric observations of V496 Sct. The date of optical maximum is taken to be 2009 November 18.716 UT.

Date (UT)	Days since optical maximum	*V*	*B-V*	*V-Rc*	*V-Ic*
2009					
Nov. 10.692	-8.024	8.341	0.647	0.471	0.933
Nov. 10.710	-8.006	8.329	0.707		
Nov. 11.693	-7.023	8.057	0.725	0.506	0.961
Nov. 11.705	-7.011	8.009	0.709		
Nov. 12.698	-6.018	7.393	0.712		
Nov. 12.700	-6.016	7.463	0.680	0.479	0.935
Nov. 12.736	-5.980	7.487	0.672	0.469	0.913
Nov. 13.732	-4.984	7.585	0.711	0.457	0.914
Nov. 17.706	-1.010	7.219	0.772	0.508	1.051
Nov. 18.716	0.000	7.070	0.797	0.526	1.037
Nov. 19.710	0.994	7.115	0.713	0.472	1.000
Nov. 20.699	1.983	7.271	0.708	0.495	1.021
Nov. 21.706	2.990	7.554	0.620	0.572	1.144
Nov. 23.687	4.971	7.455	0.524	0.567	1.144
Nov. 24.687	5.971	7.401	0.545	0.542	1.107
Nov. 25.690	6.974	7.473	0.578	0.550	1.101
Nov. 28.686	9.970	7.327	0.581	0.549	1.053
Dec. 2.681	13.965	7.508	0.583	0.550	1.109
Dec. 3.682	14.966	7.907	0.484	0.668	1.212
Dec. 14.688	25.972	8.250	0.450	0.759	1.251
Dec. 18.692	29.976	8.190			1.097

Continued on next page.

Table 4.3 – *Continued from previous page.*

Date (UT)	Days since optical maximum	*V*	*B-V*	*V-Rc*	*V-Ic*
2010					
Feb. 2.221	75.505	9.607	0.351		1.402
Feb. 8.212	81.496	9.861	0.301	1.053	1.436
Feb. 15.204	88.488	10.373	0.141	1.154	1.561
Feb. 27.196	100.480	11.178	0.375	1.477	1.764
Mar. 6.163	107.447	11.684	0.501	1.796	2.003
Mar. 14.172	115.456	11.143	0.152	1.412	1.588
Mar. 16.165	117.449	11.229	0.175	1.500	1.591
Mar. 24.168	125.452	11.162	0.320	1.461	1.465
Mar. 27.172	128.456	11.314			1.375
Apr. 2.141	134.425	11.306	0.297	1.412	1.259
Apr. 7.119	139.403	11.327	0.288	1.409	1.244
Apr. 15.110	147.394	11.405	0.290	1.417	1.182
Apr. 20.128	152.412	11.466	0.290	1.375	1.127
Apr. 28.094	160.378	11.439	0.292	1.313	1.037
May. 17.020	179.305	11.411	0.315	1.117	0.823
May. 18.089	180.374	11.377	0.387	1.074	0.794
May. 19.067	181.352	11.401	0.352	1.087	0.770
May. 21.040	183.324	11.371	0.376	1.005	0.742
May. 25.004	187.289	11.424	0.310	1.090	0.740
May. 28.008	190.293	11.395	0.386	0.994	0.678
Jun. 4.004	197.289	11.413	0.359	0.920	0.653
Jun. 10.978	204.262	11.447	0.381	0.877	0.557
Jun. 21.950	215.235	11.448	0.516	0.711	0.416
Jun. 28.918	222.202	11.607	0.293	0.816	0.464
Jul. 8.947	232.232	11.584	0.501	0.641	0.315

Continued on next page.

Table 4.3 – *Continued from previous page.*

Date (UT)	Days since optical maximum	*V*	*B-V*	*V-Rc*	*V-Ic*
Jul. 16.906	240.191	11.680	0.455	0.657	0.268
Jul. 24.914	248.199	11.677	0.602	0.514	0.170
Aug. 1.962	256.246	11.770	0.559	0.513	0.171
Aug. 16.905	271.189	11.841	0.666	0.396	0.052
Aug. 22.883	277.167	11.925	0.627	0.404	0.012
Aug. 31.866	286.150	11.937	0.759	0.302	-0.044
Sep. 10.859	296.080	11.999	0.796	0.238	-0.111
Sep. 20.774	305.995	12.085	0.772	0.212	-0.136
Sep. 29.844	315.065	12.141	0.774	0.193	-0.139
Oct. 10.752	325.973	12.188	0.843	0.139	-0.211
Oct. 19.777	334.998	12.225	0.878	0.098	-0.230
Oct. 27.762	342.984	12.267	0.915	0.097	-0.220
Nov. 12.744	358.965	12.387			
2011					
Feb. 10.212	448.433	12.773			-0.557
Feb. 23.190	461.411	12.813	1.040	-0.234	-0.642
Mar. 20.151	486.372	12.933	1.066	-0.287	-0.624
Apr. 13.141	511.362	13.029			-0.858
Apr. 18.087	516.308	13.128	0.901	-0.187	-0.683
Apr. 21.088	519.309	13.109	0.957	-0.256	-0.672

Table 4.4: Log of the Varese optical spectroscopy of V496 Sct. The date of optical maximum is taken as 2009 November 18.716 UT.

date	UT	expt (sec)	disp (Å/pix)	λ range (Å)	Days since optical maximum
2009 11 09	18:26	1500	2.12	3960-8600	-8.955
10	18:15	3600	echelle	3950-8640	-7.960
12	17:06	900	2.12	3955-8595	-6.005
12	17:50	1800	echelle	3880-8640	-5.987
19	16:52	360	2.12	3955-8590	0.972
19	17:57	3600	echelle	3950-8650	1.016
21	16:53	420	2.12	3965-8610	2.973
21	17:54	3600	echelle	4180-8650	3.015
24	17:46	2700	echelle	3955-8645	6.012
28	17:07	2700	echelle	4020-8655	9.995
12 01	17:23	900	echelle	3955-8645	13.002
01	17:58	900	2.12	3945-8590	13.017
05	17:09	3600	echelle	3950-8645	16.996
10	17:04	1800	echelle	3950-8640	21.994
10	17:34	300	2.12	3945-8597	22.007
2010 03 13	04:43	1020	4.24	3800-8385	114.469
04 28	02:39	2400	2.12	3965-8600	160.384
06 06	01:13	3600	2.12	3975-8615	199.331
06 22	23:07	3600	2.12	3975-8600	216.245
07 15	23:24	3600	echelle	3950-8640	239.252
10 05	19:16	3600	2.12	3925-8565	321.082
2011 04 19	02:47	5400	2.12	4000-8640	516.387

4.3 Results

4.3.1 The optical light curve:

the pre-maximum rise, outburst luminosity, reddening and distance

The optical light curve based on Table 4.2 is presented in Figure 4.2. There is a good photometric coverage of the nova's rise to maximum which lasts for almost 10 days culminating in a peak brightness of V_{max} = 7.07 on 2009 November 18.716 UT. The early decline after the maximum was observed till mid - December and subsequently the solar conjunction of V496 Sct resulted in lack of its observational coverage till early 2010 February. We determine the rate of decline by doing a least square regression fit to the post maximum light curve and estimate t_2 to be 59 ± 5 d. The estimated value of t_2 makes V496 Sct as one of the moderately fast Fe II class of novae in recent years. V496 Sct is one of the large amplitude novae observed in recent years with $\triangle R \geq 13.5$ magnitudes (Guido & Sostero 2009). These observed values of the amplitude and t_2 for V496 Sct put it above the upper limit in the observed spread of the amplitude versus decline rate plot for classical novae presented by Warner (2008, Figure 2.3) which shows $\triangle V$ = 8 - 11 for t_2 = 59 days. Using the maximum magnitude versus rate of decline (MMRD) relation of della Valle & Livio (1995), we determine the absolute magnitude of the nova to be M_V = -7.0 ± 0.2. The reddening is derived using the intrinsic colors of novae at peak brightness, namely (B-V) = 0.23 ± 0.06, as derived by van den Bergh & Younger (1987). We have used our optical photometry data to calculate E(B-V). The observed (B-V) = 0.797 ± 0.014 at optical maximum on 2009 November 18.716 UT results in E(B-V) = 0.57 ± 0.06. We have also estimated E(B-V) using the interstellar lines and diffuse interstellar band (DIB) registered in our high resolution optical spectra. The Na I line is composed of at least five independent components, of which three are well isolated and the remaining two are blended. Following Munari & Zwitter (1997) we estimate a total value of E(B-V) = 0.65 from these five components. The interstellar line of K I, though underexposed in the observed spectra, gives a value of E(B-V) $\sim$ 0.60 and the DIB λ6614 gives E(B-V) = 0.65. These estimates of interstellar reddening are in good agreement with each other, and in the rest of the discussion in this Chapter we adopt E(B-V) = 0.57 $\pm$ 0.06 and A_V = 1.77 $\pm$ 0.06 for a standard reddening law R = 3.1. In their study of the spatial distribution of the interstellar extinction, Neckel & Klare (1980) have shown that close to the direction of V496 Sct, A_V shows a value of $\sim$ 1.8 mag around 3 kpc and moderate value of A_V estimated by us appears reasonable. By using (MMRD) relation of della Valle & Livio (1995) and taking the value of E(B-V) = 0.57 $\pm$ 0.06 we obtain the distance d = 2.9 $\pm$ 0.3 kpc to the nova. The height from the galactic plane is estimated to be z = 89 $\pm$ 3 pc to the nova. By using the relations for the blackbody angular diameter and temperature, expansion rate for the ejecta and distance to the nova given by Ney & Hatfield (1978) and Gehrz (2008) respectively, we estimate a value $\sim$ 9 kpc for the distance to the nova. This value is more than 3 times the value estimated by (MMRD) relation of della Valle & Livio (1995). A likely reason for this discrepancy is the behaviour of the pseudo-photosphere as a grey-body with reduced emissivity in the fireball phase as seen earlier in the case of V1280 Sco (Das et al. 2008) and V5579 Sgr described earlier in Chapter 3 and reported in our paper (Raj, Ashok & Banerjee 2011).

We have estimated the white dwarf mass by using the derived value of the absolute magnitude M_V and relation given by Livio (1992); Warner (1995b):

$$M_V = -8.3 - 10\ log\ M_{WD}/M_{\odot} \tag{4.1}$$

The mass of the underlying white dwarf (M_{WD}) in V496 Sct is estimated to be $M_{WD} \sim 0.7\ M_{\odot}$. The outburst luminosity of V496 Sct as calculated from M_V is $L_O = 5.1 \times 10^4\ L_{\odot}$.

4.3.2 The nature of the light curve

A classification system for the optical light curves for novae, based on a large sample of the data from American Association of Variable Star Observers

(AAVSO), has been presented by Strope et al. (2010). As discussed earlier in Chapter 3, their classification system defines seven classes based on the time to decline by 3 mag from the peak, t_3, and the shape of the light curve. The shape of the optical light curves of V496 Sct presented in Figure 4.2 has all the characteristics of D class of nova. The early decline following the rise to the maximum is interrupted by fast decline around 90 days after the outburst reaching minimum brightness close to 120 days near the center of the dust dip. The brightness recovered to a value below the original decline. Thus the classification of the optical light curve for V496 Sct is D(90), as the estimated value of t_3 is $\sim$ 90 days for V496 Sct. The t_3 value obtained by us is consistent with relation $t_3 = 2.75\ (t_2)^{0.88}$ which gives $t_3 = 99$ days (Warner 1995a).

4.3.3 Line identification, evolution and general characteristics of the JHK spectra

The JHK spectra are presented in Figures 4.3 to 4.5 respectively; the observed line list is given in Table 4.5. The infrared observations presented here cover all the phases with the first J band spectrum taken on 2009 November 19 very close to the visual maximum. This J band spectrum is dominated by the lines of H I, N I, C I and O I all displaying deep P Cygni profiles. The full width at half maximum (FWHM) of the emission and the absorption components of Pβ line are 700 km s^{-1} and 270 km s^{-1} respectively. The absorption component is blue shifted by 960 km s^{-1} from the emission component. The next set of spectra taken beginning from 2009 December 3 show the disappearance of P Cygni profiles and predominant emission components for all the lines. The typical FWHM of the H I lines are 1230 $\pm$ 50 km s^{-1}. The ratio of the observed strength of the O I lines, W (1.1287)/W (1.3164) $\sim$ 3 indicates that Lyβ fluorescence is the dominating pumping mechanism and this is corroborated by the strong O I 8446 line seen in the optical spectra discussed later. A noticeable feature of these early spectra is the presence of lines due to Na I and Mg I. In the spectra taken on 2009 December 5 the Na I lines at 1.1404μm,

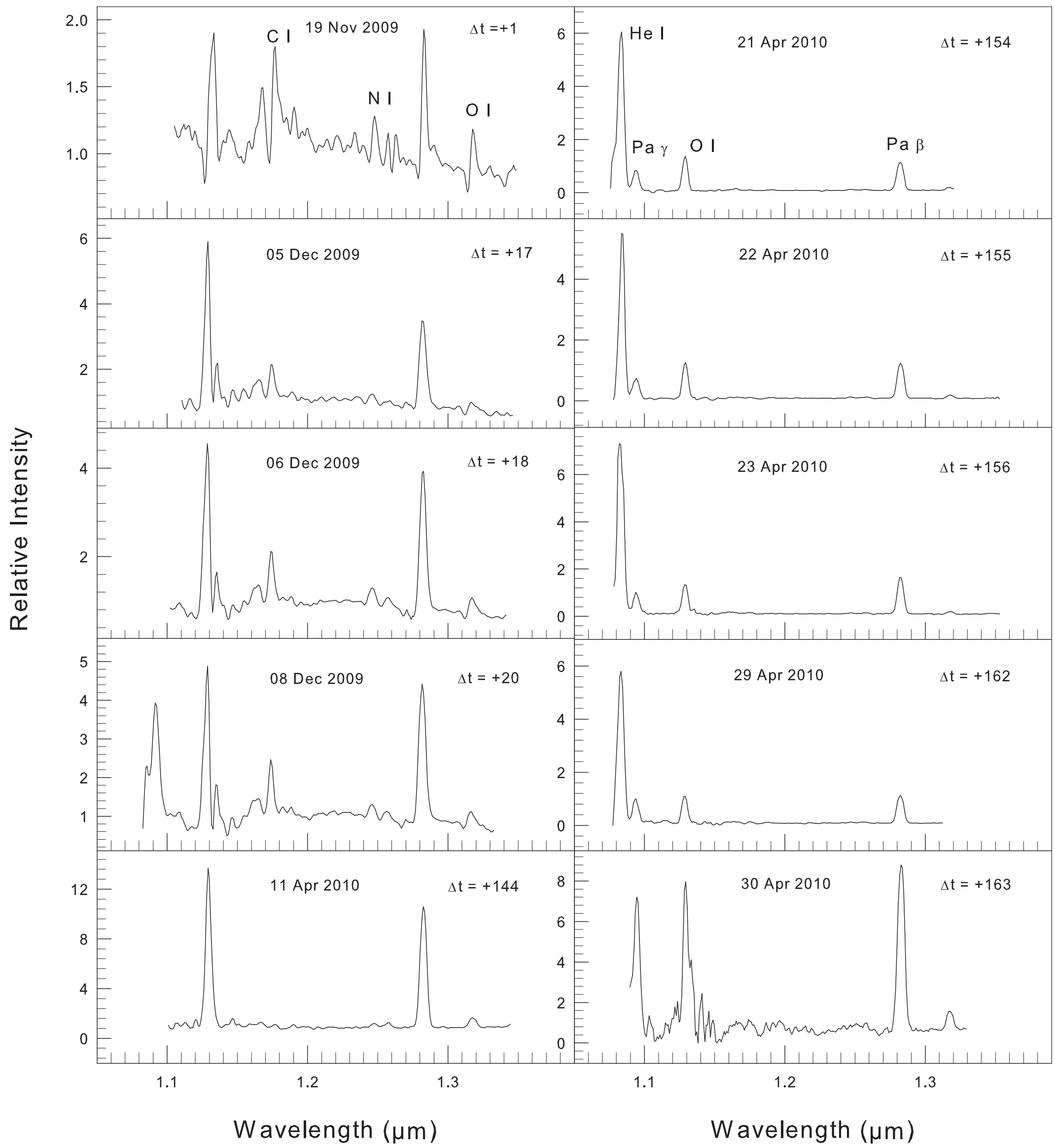

Figure 4.3: *The J band spectra of V496 Sct are shown at different epochs. The relative intensity is normalized to unity at 1.25 μm. The time from optical maximum are given for each spectrum.*

2.1452μm, 2.2056μm and 2.2084μm and Mg I lines at 1.1828μm, 1.5040μm, 1.5749μm and 1.7109 μm are clearly seen. In an earlier study of V1280 Sco, Das et al. (2008) had suggested that the presence of spectral lines of low ionization species like Na I and Mg I in the early spectra are indicators of low temperature zones conducive to dust formation in the nova ejecta and this is very well borne out in the case of V496 Sct. We would like to point out the presence of a large number of strong lines of neutral carbon seen in the JHK bands. These are typical of Fe II type nova as seen in the case of V1280 Sco (Das et al. 2008), V2615 Oph (Das, Banerjee & Ashok 2009) and V5579 Sgr as discussed earlier in Chapter 3.

The most interesting spectral features seen in the spectra of V496 Sct taken in 2009 December are the prominent first overtone CO bands in the K band and they are discussed in the following subsection 4.3.4. The last spectra, before V496 Sct became inaccessible due to its conjunction with the sun, was taken on 2009 December 9.

The set of spectra taken in 2010 April, after V496 Sct emerged from its solar conjunction, show strong He I lines at 1.0830μm in the J band and 2.0581μm in the K band. The He I 1.0830μm line exceeds in strength compared to H I lines indicating higher excitation conditions in the nova ejecta. The other weaker He I lines at 1.7002μm and 2.1120 - 2.1132μm are also seen. The rising continuum seen in the spectra taken on 2010 April 11 indicates that the dust detected by Russell et al. (2010) on 2010 February 10 is still present.

Table 4.5: A list of the lines identified from the JHK spectra. The additional lines contributing to the identified lines are listed.

Wavelength (μm)	Species	Other contributing lines and remarks
1.0830	He I	

Continued on next page.

Table 4.5 – *Continued from previous page.*

Wavelength (μm)	Species	Other contributing lines and remarks
1.0938	Pa γ	
1.1287	O I	
1.1404	Na I	C I 1.1415
1.1600-1.1674	C I	strongest lines at 1.1653, 1.1659,1.16696
1.6872	Fe II	
1.1746-1.1800	C I	strongest lines at 1.1748, 1.1753,1.1755
1.1828	Mg I	
1.1880	C I	
1.2074	N I	
1.2187,1.2204	N I	
1.2249,1.2264	C I	
1.2329	N I	
1.2382	N I	
1.2461,1.2469	N I	blended with O I 1.2464
1.2562,1.2569	C I	blended with O I 1. 2570
1.2818	Pa β	
1.2950	C I	
1.3164	O I	
1.5040	Mg I	blended with Mg I 1.5025, 1.5048
1.5256	Br 19	
1.5341	Br 18	
1.5439	Br 17	
1.5557	Br 16	
1.5701	Br 15	

Continued on next page.

Table 4.5 – *Continued from previous page.*

Wavelength (μm)	Species	Other contributing lines and remarks
1.5749	Mg I	blended with Mg I 1.5741, 1.5766,C I 1.5788
1.5881	Br 14	blended with C I 1.5853
1.6005	C I	
1.6109	Br 13	
1.6407	Br 12	
1.6806	Br 11	
1.6890	C I	
1.7002	He I	
1.7045	C I	
1.7109	Mg I	
1.7234-1.7275	C I	several C I lines
1.7362	Br 10	affected by C I 1.7339 line
1.7449	C I	
1.7605-1.7638	C I	
2.0581	He I	
2.1120,2.1132	He I	
2.1156-2.1295	C I	
2.1452	Na I	
2.1655	Br γ	
2.2056,2.2084	Na I	
2.2156-2.2167	C I	
2.29-2.40	CO	Δv=2 bands
2.2906	C I	
2.3130	C I	

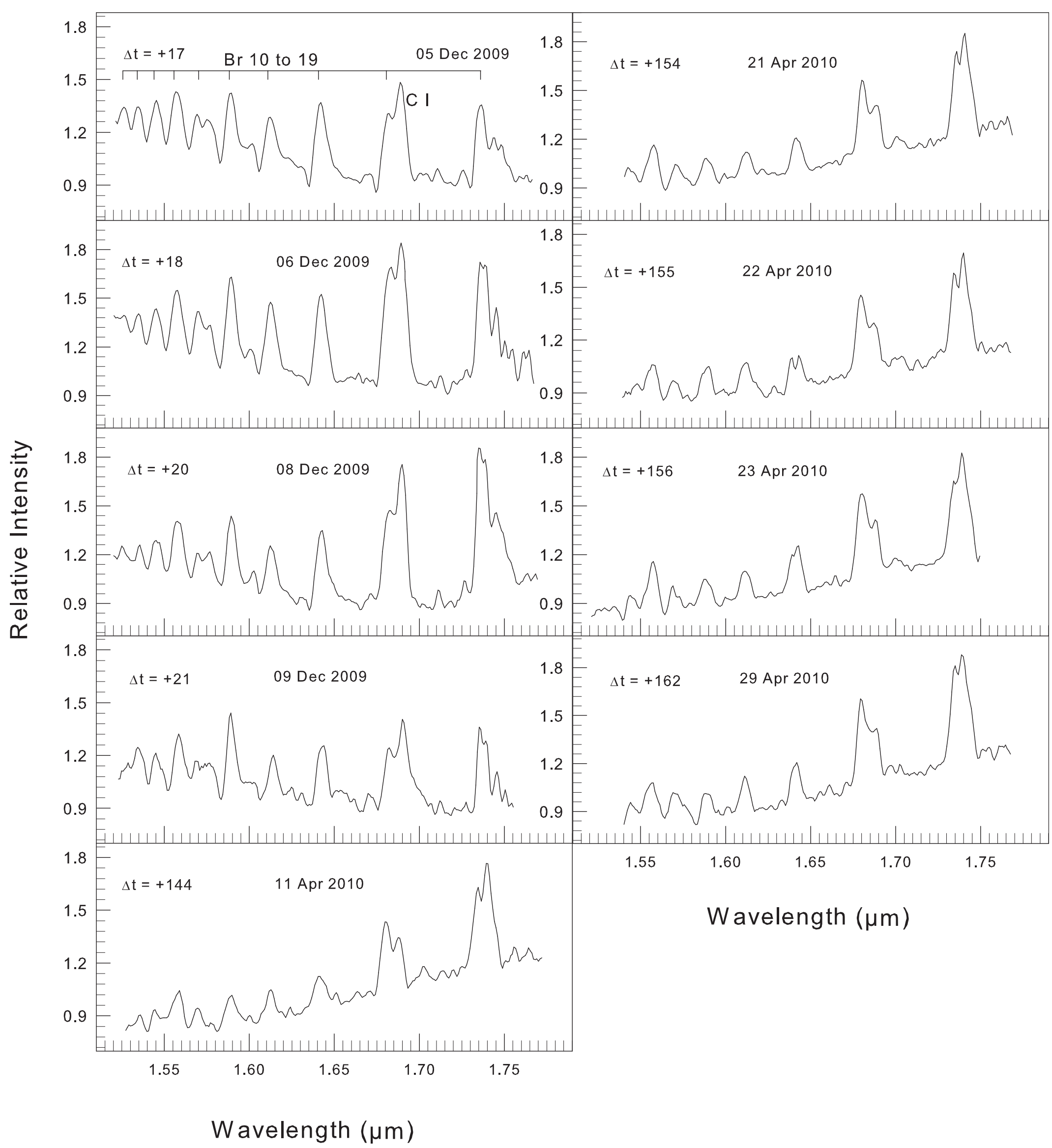

Figure 4.4: *The H band spectra of V496 Sct are shown at different epochs. The relative intensity is normalized to unity at 1.65 μm. The time from optical maximum are given for each spectrum.*

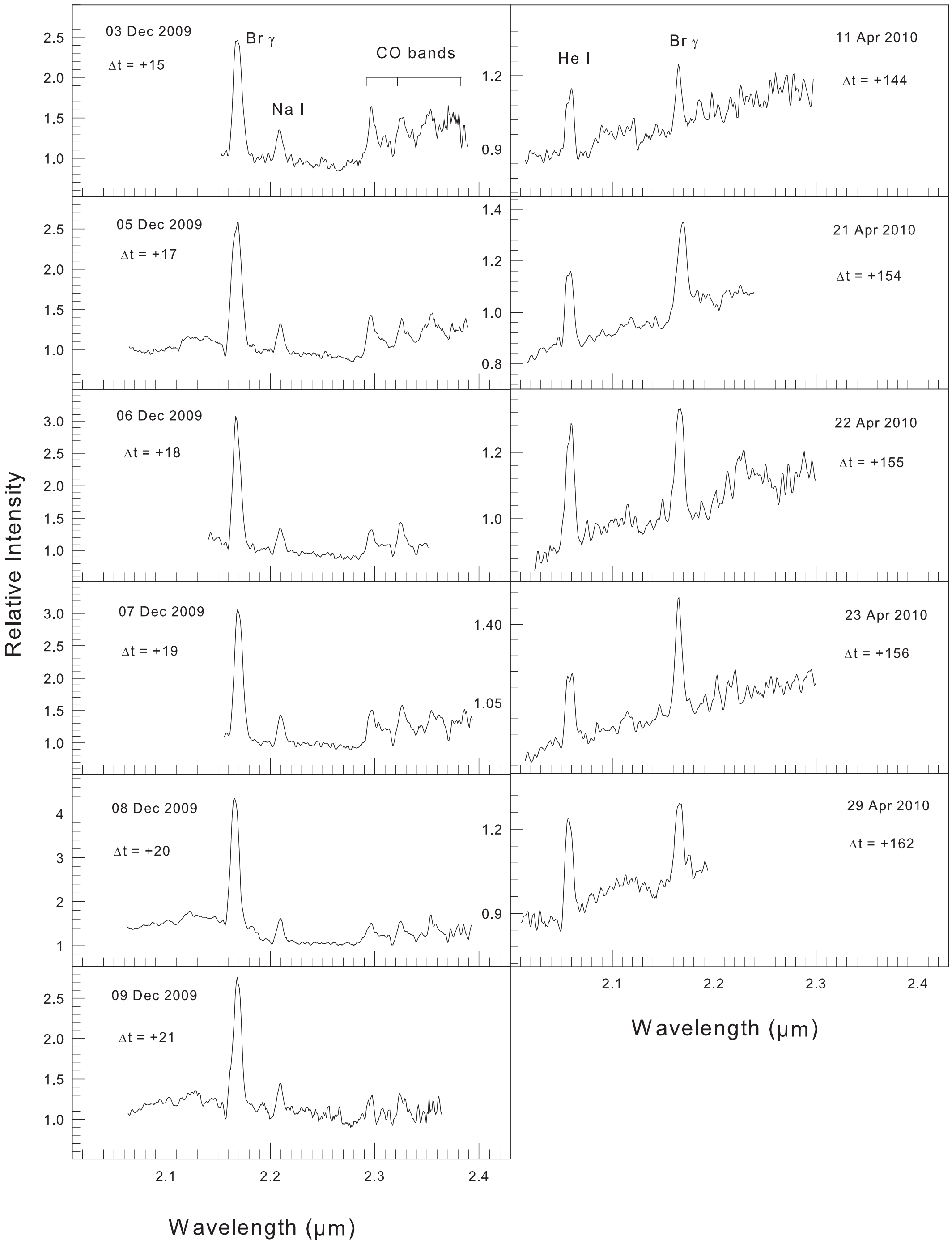

Figure 4.5: *The K band spectra of V496 Sct are shown at different epochs. The relative intensity is normalized to unity at 2.2 μm. The time from optical maximum are given for each spectrum.*

4.3.4 Modeling and evolution of the CO emission

We adopt the model developed in the earlier work on V2615 Oph by Das, Banerjee & Ashok (2009) to characterize the CO emission. Briefly, in this model the CO gas is considered to be in thermal equilibrium with the same temperature for calculating the level populations of rotation and vibration bands. It is assumed that the rotational levels are gaussian in shape. The populations of different levels can be determined from the Boltzmann distribution with the energy $E_{J,v}$ of any individual rovibrational level, with rotational and vibrational quantum numbers (J, v), being given by

$$E_{J,v} = BJ(J+1) - DJ^2(J+1)^2 + w_e(v+1/2) - w_e(v+1/2)^2(x_e - y_e) \quad (4.2)$$

The first two terms in the above equation correspond to the rotational energy (higher order terms are neglected) and the remaining terms to the vibrational energy. The values used for the rotational constants are B = 57635.96828(12) MHz and D = 183.5058(22) KHz respectively for $^{12}C^{16}O$ and 55101.0138(23) MHz and 167.668(5) KHz for $^{13}C^{16}O$ respectively. In addition to $^{12}C^{16}O$ the other isotopic species included in the calculations is $^{13}C^{16}O$. The isotopic species like $^{12}C^{17}O$ and $^{12}C^{18}O$ are not considered in our calculations as they are expected to have low abundances. For the vibrational equilibrium constants the values used are w_e = 2169.75589(23) cm^{-1}, $w_e x_e$ = 13.28803(5) cm^{-1}, $w_e y_e$ = 0.0104109(43) cm^{-1} for ^{12}CO; w_e = 2141.162 cm^{-1} , $w_e x_e$ = 12.711 cm^{-1}, $w_e y_e$ = 0.0107 cm^{-1} for ^{13}CO. All the molecular constants are taken from the NIST database except for the vibrational constants for ^{13}CO which are adopted from Benedict et al. (1962).

The model luminosity E which is in units of erg s^{-1} is converted to erg cm^{-2} s^{-1} μm^{-1} by dividing with $4\pi d^2$ where d is the distance to the source and scaling to a unit wavelength. The peak intensities of the vibration bands are analytically determined such that the integrated area under the curve matches the expected observed quantity E/$4\pi d^2$. An appropriate continuum determined from the K band photometry for a particular date is added to the model CO emission so that it can be compared with the observed CO emission

Table 4.6: List of temperatures of CO gas at different days. The typical errors are ± 500 K.

Date (2009)	Temperature (K)
3 December	4000
5 December	4000
6 December	3800
7 December	3600
8 December	3300
9 December	2800

bands. The input parameters to the model are the total mass of the CO gas (M_{CO}), the $^{12}C/^{13}C$ ratio denoted as a constant α and the gas temperature T_{CO}. For a given set of values for M_{CO}, α, T_{CO} and d the CO flux estimated from the model is an absolute quantity. The representative model spectra matching the observed data for 2009 December 5 and 7 are shown in Figure 4.6.

The best fit model spectra to the observed data are obtained by varying the input parameters M_{CO}, α, T_{CO}. The expected changes to the model spectra by varying these input parameters may qualitatively be summarized as follows. The increase in M_{CO} enhances the absolute level of the CO emission while the increase in T_{CO} changes the relative intensities of different vibrational bands in addition to changing the absolute level of the emission. The CO emission is assumed to be optically thin. The C I lines at 2.2906 and 2.3130 μm and Na I lines at 2.3348 and 2.3379 μm are also likely to be present in the spectral region covered by the CO emission giving rise to some deviations between the best model fit and the observed spectra. In addition, since a comparison of the relative strengths of the vibrational bands within the first overtone allows the gas temperature to be determined, we are handicapped by being able to detect only three of the bands (ν = 2 - 0, 3 - 1, 4 - 2). Within these constraints we have done formal model fits for the observations during the period 2009 december 3 to 9. The typical errors to the formal model fits are $\pm$ 500 K. The model spectra with a reasonably similar range in mass of $M_{CO} = 1.5 - 2 \times 10^{-8}$ $M_\odot$ fit the observed spectra. There is an indication of decreasing trend in the temperature as seen from the values listed in Table 4.6 during the period of our observations starting with a value 4000 $\pm$ 500 K on 2009 December 3 and 2800 $\pm$ 500 K on 2009 December 9. The representative fits for 2009 December 5 and 7 are shown in Figure 4.6. The model calculations also show that the $v = 2 - 0$ bandhead of ^{13}CO at 2.3130 μm becomes discernibly prominent if the ^{12}C/^{13}C ratio is $\leq$ 1.5. As this spectral feature is not clearly detected in our observed spectra, we place a lower limit of $\sim$ 1.5 for the ^{12}C/^{13}C ratio. However we add a cautionary note that the signal to noise ratio in the region of ^{12}CO and ^{13}CO bands is about 15 - 20 and better quality spectra may permit a more accurate determination of the CO gas parameters. The lower limit of $\sim$ 1.5 for the ^{12}C/^{13}C ratio reported here is the lowest value till date among the novae that have displayed the first overtone bands of CO.

It may be helpful to compare the observed ^{12}C/^{13}C ratio in V496 Sct with the values for other novae that have displayed the first overtone bands of CO and also the model predicted values. The observed values for the ^{12}C/^{13}C ratio available in the literature are ^{12}C/^{13}C $\geq$ 5 in V705 Cas (Evans et al. 1996), ^{12}C/^{13}C $\geq$ 3 in NQ Vul (Ferland et al. 1979), ^{12}C/^{13}C $\geq$ 2 in V2615 Oph (Das, Banerjee & Ashok, 2009), ^{12}C/^{13}C $\simeq$ 2.9 in V842 Cen (Wichmann et al. 1991) and ^{12}C/^{13}C $\simeq$ 1.2 in V2274 Cyg (Rudy et al. 2003). The thermonuclear runaway (TNR) responsible for the nova outburst is one of the important source for the production of ^{13}C isotopes (Starrfield et al. 1972; Starrfield, Sparks & Truran 1974 and Romano & Matteucci 2003). Hajduk et al. (2005) have pointed out that the outburst of born-again giants like V4334 Sgr are another source for ^{13}C isotopes in the galaxy; a low value for the ratio

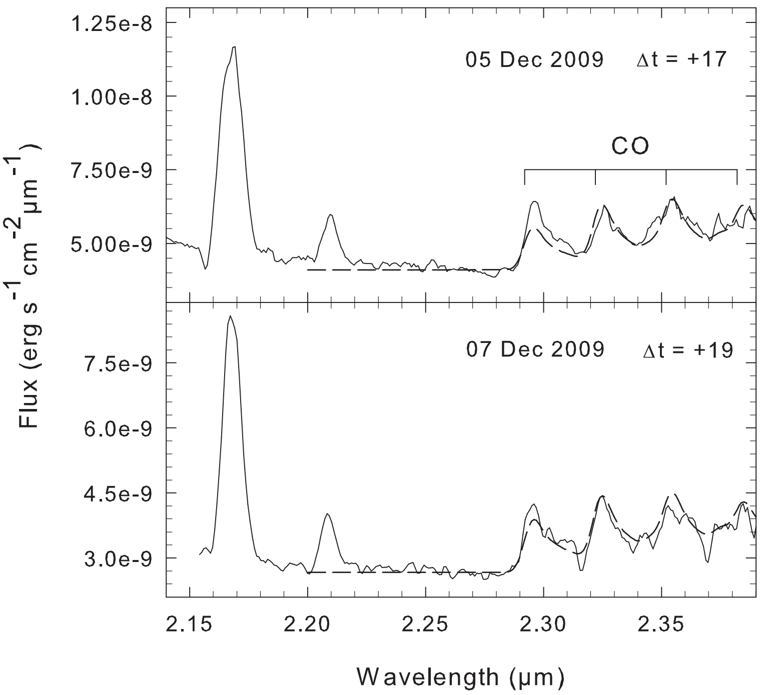

Figure 4.6: *The model fits are shown as dashed lines to the observed first overtone CO bands in V496 Sct for 2009 December 5 and 7. The fits are made for a constant CO mass of 2 × 10^{-8} $M_\odot$ on both the days while the temperature of the gas T_{CO} is 4000 K and 3600 K respectively. The time from optical maximum are given for each spectrum.*

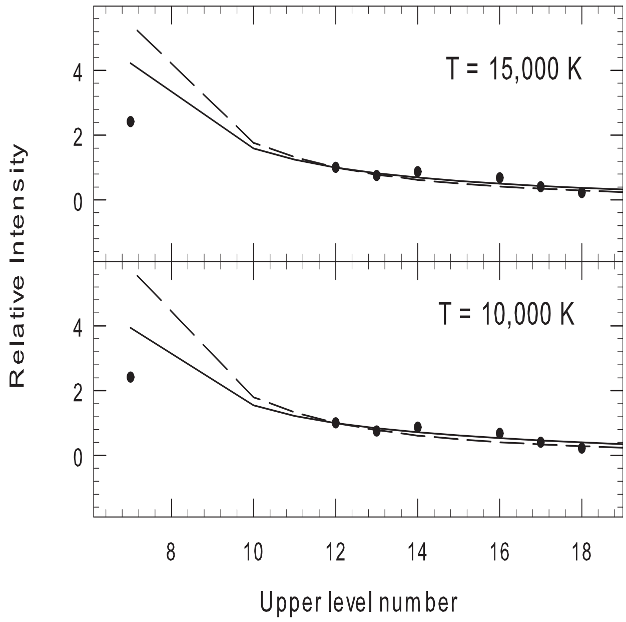

Figure 4.7: *The two panels show the case B analysis for 2009 December 6 for two different temperatures. The abscissa is the upper level number of the Brackett series line transition. The line intensities are relative to that of Br 12. The Case B model predictions for the line strengths are also shown for a temperature of $T = 10^4$ K and electron densities of $n_e = 10^{12}$ cm^{-3} (dashed line) and 10^8 cm^{-3} (solid line).*

${}^{12}C/{}^{13}C = 5$ was observed by Pavlenko et al. (2004) in V4334 Sgr.

In the hydrodynamical models of nova outbursts the ${}^{12}C/{}^{13}C$ ratio will depend on parameters like the mass of the underlying white dwarf, the accretion history and mixing of the accreted material from the companion star with the surface material of the white dwarf (Jose & Hernanz 1998; Starrfield et al. 1997; Yaron et al. 2005). The estimated lower limits as well as the observed values for ${}^{12}C/{}^{13}C$ ratio in case of novae discussed above indicate that ${}^{13}C$ is possibly not synthesized at the high values predicted by these theoretical models.

In the novae mentioned above that displayed CO bands, the estimated M_{CO} ranges from 2.8×10^{-10} $M_\odot$ (V705 Cas) to 3×10^{-8} $M_\odot$ (V2615 Oph). The present value of M_{CO} = 1.5 - 2 $\times$ 10^{-8} $M_\odot$ for V496 Sct lies within this range and is similar to the CO mass determined in V2615 Oph.

We have also tried to estimate the ejecta mass by using recombination line analysis of H I lines for 2009 December 6 (Figure 4.8). However, we find that the strengths of these lines, relative to each other, deviate considerably (specially for Brγ, Figure 4.8) from Case B values for 2009 December 6 indicating that the lines are optically thick. Hence we are unable to estimate the ejecta mass from recombination analysis. The list of corrected line flux is given in Table 4.7 for H I lines.

Table 4.7: A list of the prominent emission lines identified from the optical spectra.

Wavelength (A)	Species
3970	Ca II and Hϵ
4101	Hδ
4129	Fe II(27)
4173	Fe II(27)
4233	Fe II(27)
4303	Fe II(27)
4340	Hγ
4351	Fe II(27)
4363	[O III]
4555	Fe II(37)
4586	Fe II(38)
4634	N III
4649	O II
4686	He II
4861	Hβ

Continued on next page.

Table 4.7 – *Continued from previous page.*

Wavelength (A)	Species
4924	Fe II(42)
4959	[O III]
5007	[O III]
5018	Fe II(42)
5046	Si II
5159	[Fe VI] + [Fe VII]
5169	Fe II + Mg I
5235	Fe II(49)
5270	[Fe III]
5276	Fe II(49+48)
5309	[Ca V]
5316	Fe II(49)
5361	Fe II(48)
5415	He II
5535	Fe II(55) + N II
5676	N II
5755	[N II](3)
5876	He I
5890	Na I
5909	Fe II
5942	N II(28)
5991	Fe II(46)
6086	[Ca V] + [Fe VII]
6084	Fe II(46)
6157	O I
6243	Fe II + N II
6300	[O I]

Continued on next page.

Table 4.7 – *Continued from previous page.*

Wavelength (A)	Species
6347	Si II(2)
6363	[O I]
6419	Fe II(74)
6431	Fe II(40)
6456	Fe II
6563	Hα
6678	He I
6726	O I(2)
7065	He I
7139	[Ar III]
7234	C II(3, blend of 7231 and 7236)
7330	[O II]
7774	O I
8446	O I
8498	Ca II triplet
8542	Ca II triplet

4.3.5 Line identification, evolution and general characteristics of the optical spectra

The optical spectra presented here cover the pre-maximum rise, the optical maximum brightness, the early decline and the nebular phase. There are very few novae for which the spectral evolution before the maximum brightness has been documented: V1280 Sco (Naito et al. 2012, Kuncarayakti et al. 2008) and V2615 Oph (Munari et al. 2008). The spectral evolution of V496 Sct during the pre-maximum, maximum and optically thick branch of the decline phase is presented in Figure 4.7, while the subsequent evolution during the optically thin and nebular phase is covered by Figure 4.8. Figure 4.9 documents the complex evolution of profiles of Fe II λ5018 line, and Figure 4.10 the temporal evolution of the velocity of the absorption components of Fe II λ5018 line. A summary of emission lines identified in the optical spectra is provided in Table 5, and de-reddened fluxes (according to E(B-V) = 0.57 and a R = 3.1 reddening law) of the prominent emission lines relative to Hβ are given in Table 6 for some representative dates.

4.3.6 Pre-maximum rise and optical maximum

There is considerable interest in studying the spectral evolution during the pre-maximum rising phase of classical novae, an evolutionary phase rarely observed. The pre-maximum spectra of V496 Sct in Figure 4.7 are characterized by emission lines confined to just Fe II (multiplets 27, 28, 37, 38, 42, 48, 49, 55 and 74) and hydrogen Balmer series, with feeble O I 7772, 8446.

During the rise toward maximum the baricentric and terminal velocity of P Cygni absorptions, and the FWHM of both absorption and emission components declined with time (see Figure 4.7). The terminal and core velocity of P Cygni absorption component of Hα line in Figure 4.7 declined from -2000 and -700 km s^{-1} on day -9 to -1200 and -600 km s^{-1} on day -6, while at the same time the FWHM of the absorption and emission components declined from 1000 to 700 km s^{-1}. The P Cygni components essentially vanished at the time of maximum brightness. When they reappeared later into early decline they were much sharper (FWHM=250 km s^{-1}) and blue-shifted (core velocity = -1350 km s^{-1}) than at pre-maximum. The high resolution Echelle spectra listed in Table 3 show that the broad and single P Cygni absorption components observed on 2009 November 10 and 12 of H I and Fe II multiplets are replaced by two narrow components on 2009 November 19. The two absorption components in case of Fe II 5018, shown in Figure 4.9, are located at heliocentric velocities of -785 and -360 km s^{-1}.

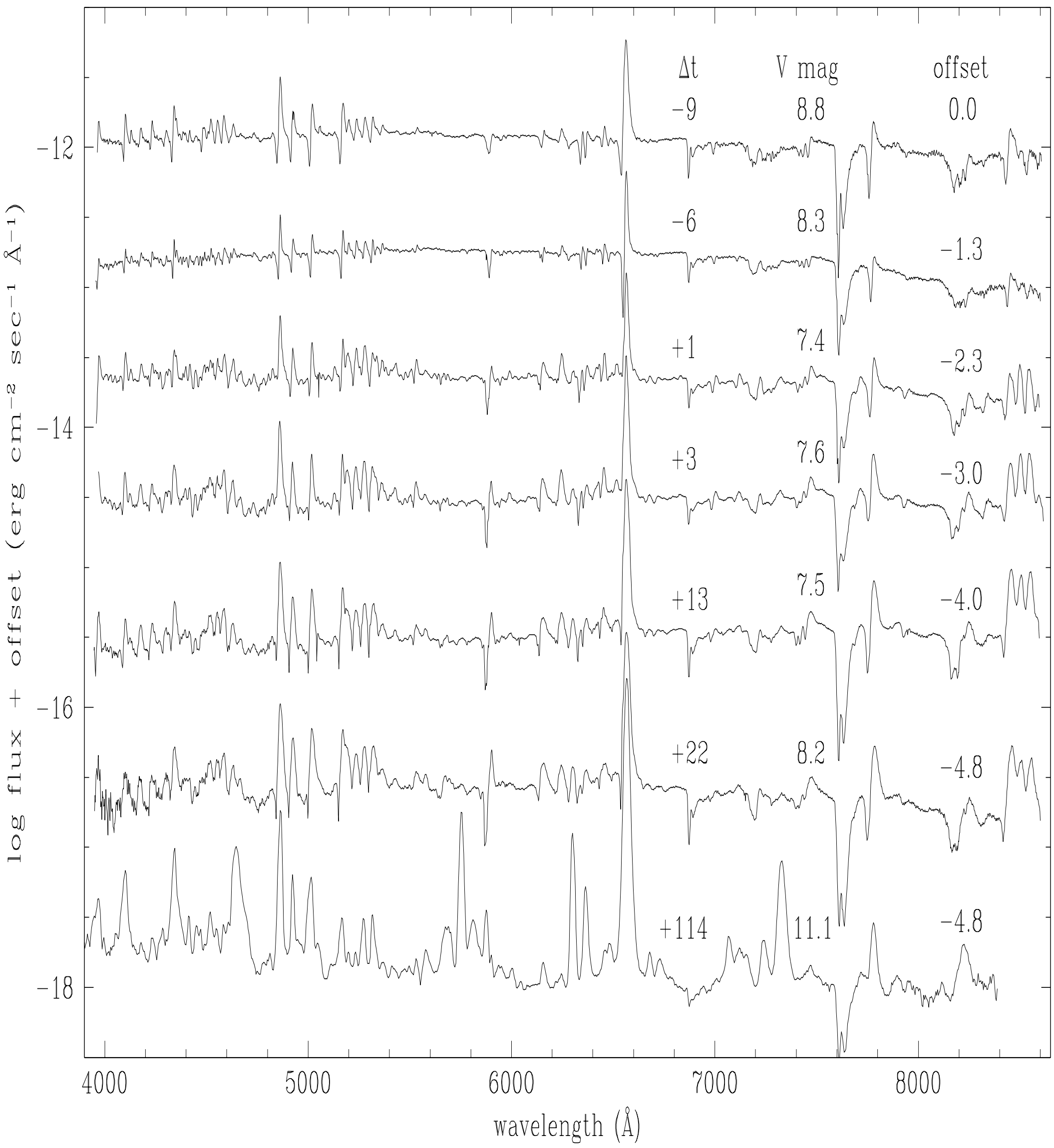

Figure 4.8: *Low-res spectroscopic evolution of V496 Sct from pre-maximum to the end of the optically thick branch (pre-nebular stage) of the light-curve. For the first month of the evolution the emission lines are mostly due to Fe II and H I, with also O I 7772, 8446, Na I 5893, and Ca II 8498, 8542. The last spectrum in plotted for commonality also in Figure 4.8. The time from optical maximum, the V band magnitude and the offset in log flux are given for each spectrum.*

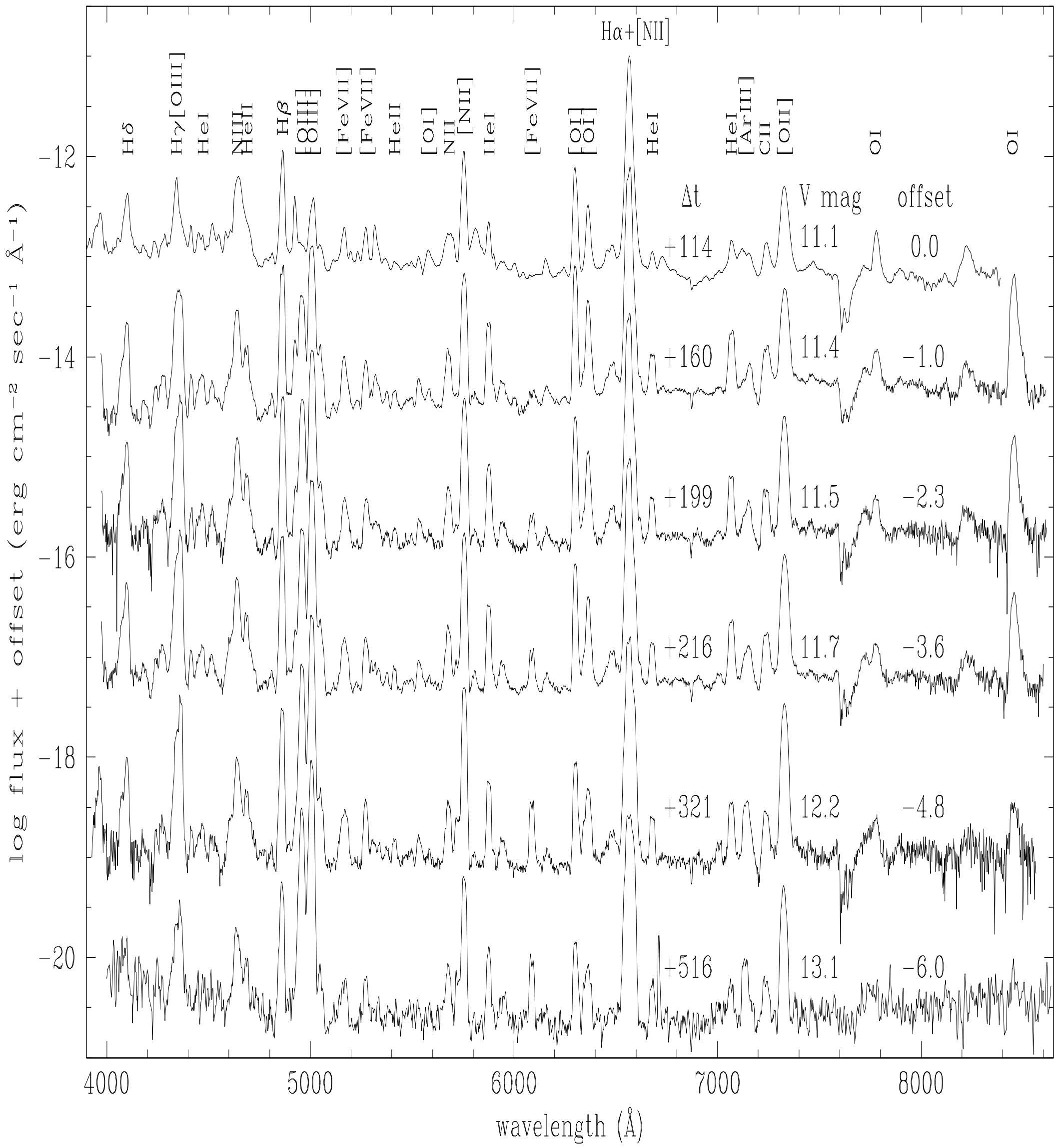

Figure 4.9: *Low-res spectroscopic evolution of V496 Sct during the optically thin branch (nebular condition) of the lightcurve, with time from optical maximum, the V band magnitude and the offset in log flux are given for each spectrum. The major emission lines are identified.*

4.3.7 Absorption systems during early decline

The Echelle spectra offer the possibility to observe at high resolution the evolution of the absorption components. As illustrated in Figure 4.9, when the nova reached its maximum brightness, the broad single absorption component of P Cygni line profile was replaced by two components, whose intensity gradually faded in parallel with the decline in brightness of the nova. A similar behaviour was exhibited by V2615 Oph where two absorption components are seen in addition to the emission component following the optical maximum (Munari et al. 2008). Figure 4.9 presents line profiles for Fe II 5018 from the high resolution echelle spectra to illustrate the evolution of the two absorption components. Both absorption components increased their negative radial velocity with time, with a linear trend as illustrated in Figure 4.10 and the best fit lines are given by the following expressions:

$$V_A = -343 - (9.2 \times t) \tag{4.3}$$

$$V_B = -763 - (18.5 \times t) \tag{4.4}$$

where t is the time after optical maximum. The approaching conjunction with the Sun prevented further observations of V496 Sct after our 2009 December 10, 22 days past optical maximum, and the next set of observations were resumed from 2010 March 13. Novae usually display different absorption systems, which behave similarly from object to object, and that have been studied in detail by McLaughlin (1960, hereafter McL60), who introduced a handy nomenclature for them. An impressive graphical representation of them has been offered by Hack and Struve (1970, Figure 4i) from very high resolution observation of Nova Del 1967 by Ch. Fehrenbach. The A and B components of Eq. (1) and (2) shown in Figure 4.10 nicely correspond to the principal and diffuse enhanced absorption systems described by McL60, who noted a clear correlation between the t_2, t_3 decline times and the mean velocity of these absorption systems. McL60 also noted how the radial velocity of these absorption systems generally increase with time, as seen here in V496 Sct.

Table 4.8: List of near-infrared line flux values corrected for $A_V = 1.77$ for Case B analysis.

Brackett line	Flux ($\mathrm{Wcm^{-2}\mu m^{-1}}$) 2009 Dec. 6
7	8.9×10^{-14}
12	3.7×10^{-14}
13	2.7×10^{-14}
14	3.2×10^{-14}
16	2.5×10^{-14}
17	1.5×10^{-14}
18	8.0×10^{-15}

The McL60 velocity relation for the principal system is $\log v_{\rm prin}$ = 3.57 - 0.5 $\log t_2$, and predicts a mean -485 km s^{-1} for the t_2=59 day of V496 Sct. The agreement with Figure 4.10 is evident, considering in particular that the approaching conjunction with the Sun prevented to extend the observations to later epoch characterized by larger radial velocities for both systems. The McL60 velocity relation for the diffuse enhanced system is $\log v_{\rm diff-enh}$ = 3.71 - 0.4 $\log t_2$, and it predicts -1005 km s^{-1} for the t_2=59 day of V496 Sct, again in good agreement with Figure 4.10. Munari et al. (2008) have pointed out similar agreement of the observed velocities for the absorption systems of Hα in case of V2615 Oph with the predicted values using the statistical relations by McL60.

For a few days around optical maximum, the high resolution spectra displayed a rich ensemble of very sharp absorption lines of modest radial velocity displacement, due to low ionization metals like Ti II, which will be investigated elsewhere. They are similar to the transient heavy element absorption systems resulting from the episodic mass ejection from the secondary star seen in novae by Williams et al. (2008).

The permitted lines of Fe II are the strongest non-Balmer lines both during the pre-maximum rise, near optical maximum and early decline indicating P$_{fe}$ spectral class for V496 Sct during these phases (Williams et al. 1991; Williams, Phillips & Hamuy 1994).

4.3.8 Nebular phase

The spectral evolution during the optically thin branch (nebular phase) is shown in Figure 4.8. The evolution has been pretty standard, with [O III] 4363, 4959, 5007, [N II] 5755, 6548, 6584, [O II] 7325 and [O I] 6300, 6364 being the dominant lines. The [O I] 6300/6364 flux ratio, that during the early phases was close to 1 and indicative of a large optical depth in the lines, with the thinning of the ejecta, the opacity increased toward the 3.1 normal ratio. The Lyβ fluorescent OI 8446 line, has remained strong throughout the outburst and begun declining around day +200 when the optical thinning of ejecta reduced the trapping of Lyβ photons and therefore the fluorescent pumping of O I atoms. The ionization conditions have been steadily increasing with advancing decline, with He I, He II and [Fe VII] lines monotonically increasing in intensity with respect to the other lines. The presence of a feable [Fe X] 6375 component could compatible with the profile for the [O I] 6360 + [S II] 6347, 6371 blend of the day +516 spectrum in Figure 4.8, a firmer conclusion requiring a spectrum of higher S/N and resolution. The spectra shown in Figure 4.8 show how the transition of V496 Sct from *permitted* to *nebular* phase occurred at an intermediate time after the last permitted spectrum of 2010 March 13 and the first nebular spectrum of 2010 April 28 where [O III] doublet lines λ4959 and λ5007 are seen prominently. We assign A_o spectral class for V496 Sct (Williams et al. 1991; Williams, Phillips & Hamuy 1994).

The presence of an emission feature at λ4924 coinciding with Fe II(42) line in the spectra taken during 2010 March till June is little puzzling. As the other prominent Fe II lines at λ4584 and λ5018 are absent as expected in the nebular phase, this feature is unlikely to be associated with Fe II multiplet. We would like to point out the presence of the emission feature at λ4924 as an unidentified feature similar to several such features seen in the spectra of many novae.

4.3.9 Physical parameters

The emission line fluxes of hydrogen and other elements can be used to estimate the physical parameters of the nova ejecta. In the early decline phase when the electron number densities are large, it is necessary to take in to account the optical depth τ while deriving the physical parameters. We determine the optical depth for [O I] λ6300 line using the formulation of Williams (1994), viz.,

$$\frac{j_{6300}}{j_{6364}} = \frac{1 - e^{-\tau}}{1 - e^{-\tau/3}} \tag{4.5}$$

where j is the line emissivity. For the period 2010 April 28 to 2010 October 5 we get τ in the range 0.54 - 3.21. Now from the optical depth and the electron

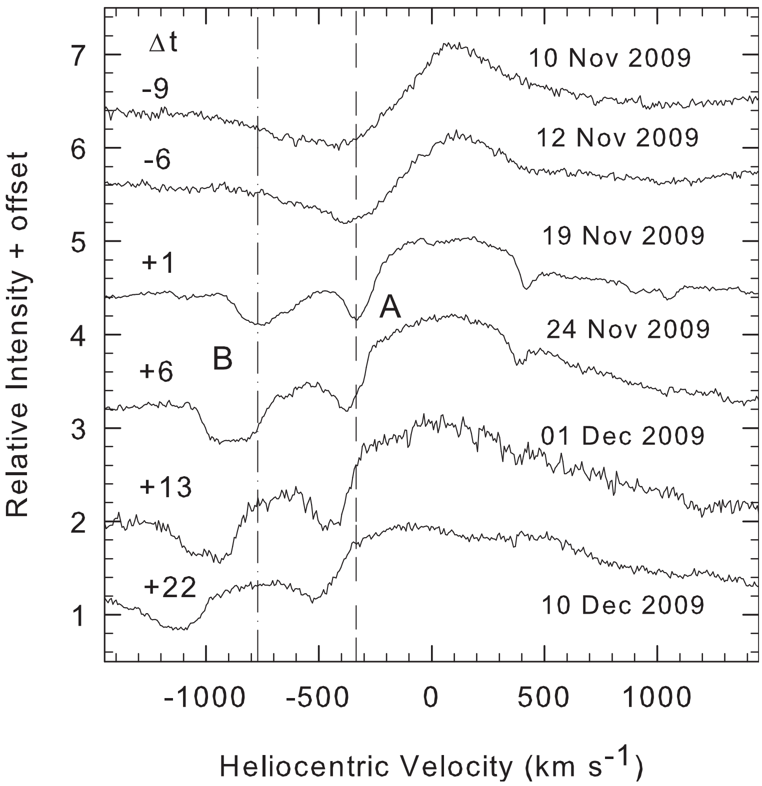

Figure 4.10: *Profiles of Fe II $\lambda 5018$ line in the pre-maximum rise, near optical maximum and the early decline phases. The initial positions of the two narrow absorption components are shown by the broken lines. The time from optical maximum are given for each spectrum.*

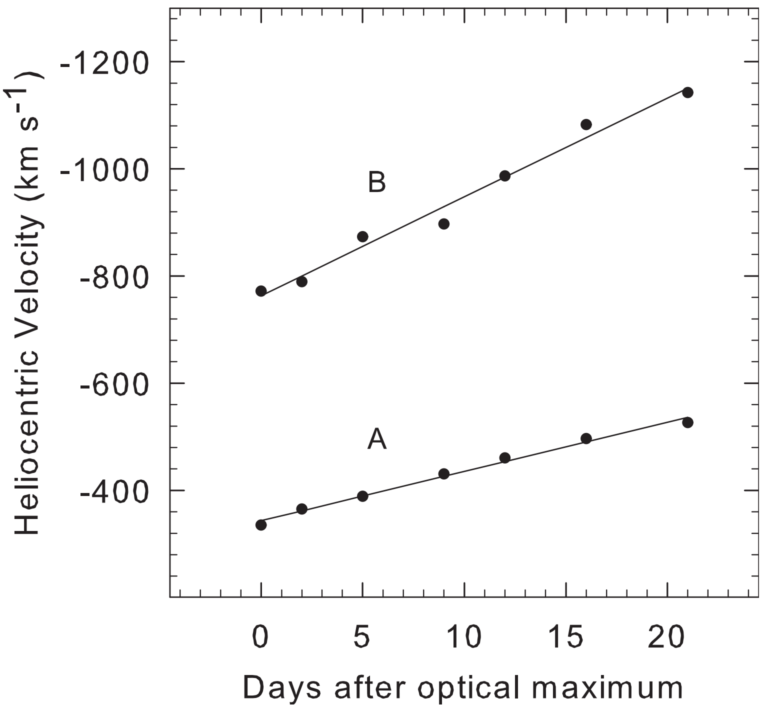

Figure 4.11: *The time evolution of radial velocities of the two absorption components of Fe II λ5018 line.*

temperature we can estimate the mass of oxygen in the ejecta using the λ6300 line.

$$M_{OI} = 152 d^2 e^{22850/T_e} \times 10^{1.05E(B-V)} \frac{\tau}{1-e^{-\tau}} F M_\odot \tag{4.6}$$

where, F is the flux of λ6300 line. Taking typical value of $T_e = 5000$ K for the electron temperature (Ederoclite et al. 2006) we find M_{OI} in the range 1.18×10^{-5}-2.28×10^{-6} $M_\odot$. The electron number density N_e can be determined by [O III] line as given in Osterbrock (1989)

$$\frac{j_{4959} + j_{5007}}{j_{4363}} = 7.73 \frac{e^{3.29\times10^4/T_e}}{1 + 4.5\times10^{-4}\frac{N_e}{T_e^{1/2}}} \tag{4.7}$$

The values we obtained are in the range 10^4 to 10^6 cm^{-3} close to the lower limit of the critical densities to give rise to nebular and auroral lines. This indicates that these lines are arising in relatively low density regions. Following Osterbrock (1989) we have a relation between the intensity of the Hβ emission line and the mass of hydrogen in the emitting nebula of pure hydrogen as

$$m(H)/M_\odot = \frac{d^2 \times 2.455 \times 10^{-2}}{\alpha^{eff} N_e} I(H\beta) \tag{4.8}$$

where α^{eff} is the effective recombination coefficient and I(Hβ) is the flux for Hβ line. The mass of hydrogen m(H) in the ejecta is $(6.3 \pm 0.2)\times10^{-5}M_\odot$. As noted earlier in section 3.2 V496 Sct formed dust. The infrared observations by Russell et al. (2010) showed the presence of dust on 2010 February 10 which is still present on 2010 April 11 as indicated by the large (J - K) colour and the rising continuum. A sharp decline around 2010 February 8 seen in the V band light curve presented in Figure 4.2 also indicates the onset of dust formation. It would be interesting to make an estimate of the dust mass M$_{dust}$ in V496 Sct and compare it with other novae that formed dust in their ejecta using the thermal component of the spectral energy distribution (SED). We adopt the method described by Woodward et al. (1993) that uses $(\lambda F_\lambda)_{max}$ and T$_{dust}$ values obtained from the thermal component of the spectral energy distribution (SED). It is pertinent to point out that the present JHK photometric observations cover mostly the increasing part of the SED and thus the estimate of the temperature for the dust T$_{dust}$ likely to have large uncertainty. We obtain M$_{dust}$ = 1-5$\times10^{-10}$M$_\odot$ for 2010 April 30 from the best fit value T$_{dust}$ = 1500 $\pm$ 200 K (with χ^2 minimization) for the temperature of the dust shell, $(\lambda F_\lambda)_{max}$ = 2.62 $\times10^{-16}$ W cm^{-2} and d = 2.9 kpc. The estimated masses for different constituents of the ejecta like hydrogen, oxygen and dust derived from the optical and the infrared observations may be usefully utilized to derive the gas to dust mass ratio in novae. Gehrz et al. (1998) have presented a compilation of M$_{gas}$ and M$_{dust}$ along with ratio M$_{gas}$/M$_{dust}$ ranging from 5 in case of V705 Cas and 3×10^4 in case of QU Vul. In case of V2362 Cyg, a very fast Fe II nova, Munari et al. (2008) have derived a value of 3×10^5 for M$_{gas}$/M$_{dust}$. Taking the average fractional yield (by mass) of hydrogen to be 0.32 $\pm$ 0.10 for white dwarf masses ranging from 0.6 to 1.25 M$_\odot$ as per calculations of Jose & Hernanz (1998) and Starrfield et al. (1997), the total gas mass based on the mass of hydrogen gas (determined here as 6.3×10^{-5}M$_\odot$) is estimated to be 2.0 $\pm$ 0.6 $\times10^{-4}$M$_\odot$. Hence the gas to dust ratio is found to be M$_{gas}$/M$_{dust}$ $\sim$ 1.3 - 6.3 $\times10^5$ indicating that a small amount of dust was formed in V496 Sct comparable to 3 $\times10^5$ observed in the case of V2362 Cyg by Munari et al. (2008).

4.4 Summary

In this chapter we have presented near-infrared and optical spectroscopy and photometry of nova V496 Sct which erupted on 2009 November 8. From the optical lightcurve, the absolute magnitude and the distance to the nova are estimated to be M_V = -7.0 ± 0.2 and d = 2.9 ± 0.3 kpc respectively. The height from the galactic plane to the nova is estimated to be 89 ± 3 pc. The mass of the underlying white dwarf in V496 Sct is $M_{WD} \sim 0.7$ $M_\odot$. The outburst luminosity of V5579 Sgr as calculated from M_V is $L_O = 5.1 \times 10^4$ $L_\odot$. The light curve classification for V496 Sct is D(90). The infrared and optical spectra indicate that the nova is of the Fe II class. The evolution of the spectra are shown from the initial P Cygni phase to an emission-line phase and finally to a dust formation stage. The characteristics of the JHK spectra are very similar to those observed in a nova outburst occurring on a carbon-oxygen white dwarf. Evidence is seen from the JHK photometry for the formation of dust in the nova in 2010 April. In this context, the presence of emission lines from low ionization species like Na and Mg in the early spectra and subsequent formation of the dust supports the predictive property of these lines as indicators of dust formation as proposed by Das et al (2008). The highlight of the observations is the detection of the first overtone bands of carbon monoxide (CO) in the 2.29 - 2.40 μm region. The CO bands are modeled to estimate the temperature and mass of the emitting CO gas and also to place limits on the $^{12}C/^{13}C$ ratio. V496 Sct is one of the moderately fast Fe II class of novae (t_2 = 59 d) that showed CO emission before the dust formation.

The various phases of the spectral evolution of V496 Sct have been identified using the Tololo classification system for novae (Williams et al. 1991; Williams, Phillips & Hamuy 1994). The permitted lines of Fe II were the strongest non-Balmer lines in the pre-maximum as well as the early decline

Table 4.9: Fluxes of prominent emission lines relative to Hβ = 100. The fluxes of the emission lines including Hβ are corrected for E(B-V) = 0.57.

Wavelength (A)	Species	2009 Nov. 09	2009 Nov. 19	2009 Dec. 10	2010 Apr. 28
3970	Ca II and Hϵ	28.3	39.4	30.0	
4101	Hδ	45.2	36.6	7.2	54.2
4173	Fe II(27)	27.7	24.7	18.0	
4340	Hγ	21.1	11.8	36.2	141.5
4584	Fe II(38)	48.2	37.3	19.8	
4635	N III	13.3	42.9	14.2	41.5
4686	He II				9.3
4861	Hβ	100	100	100	100
4924	Fe II(42)	31.3	44.7	39.8	5.9
4959	[O III]				48.3
5007	[O III]				182.2
5018	Fe II	36.8	35.0	58.5	
5169+5176	Fe II + Mg I + N II	36.8	21.7	64.2	11.0
5535	Fe II(55) + N II	3.6	8.1	6.1	
5577	O I			3.7	
5675	N II				10.2
5755	[N II](3)				66.1
5876	He I				22.0
5890	Na I		10.5	11.4	
6157	O I	2.4	10.7	10.6	
6243	Fe II + N II	12.7	29.0	14.0	
6300	[O I]			12.3	58.5
6363	[O I]			6.8	28.0
6456	Fe II	6.0	19.9	11.8	
6563	Hα	234.9	195.7	240.3	690.7 [a]
6678	He I				8.5
7065	He I				15.3
7330	[O II]				44.9
7774	O I	18.1	12.5	19.1	5.1
8446	O I	6.0	14.2	16.9	47.5
8498	Ca II triplet		20.3	5.4	
8542	Ca II triplet		16.6	9.1	
Hα/Hβ		2.4	2.0	2.4	6.9
Hβ	10^{-11}erg cm^{-2} s^{-1}	16.6	71.8	97.0	11.8

[a] [NII] 6548, 6584 expected to contribute significantly to the overall flux of Hα blend.

phase indicating P_{fe} class for the nova. The nova had evolved to the auroral phase A_o in 2010 March as the [N II] 5755 auroral line was the strongest non-Balmer line. We note the absence of [Fe X] 6375 coronal emission line in the spectra taken as late as 2011 April 19. Thus the optical spectra show that the nova evolved in the $P_{fe}A_o$ spectral sequence. The summary of the nova is given in Table 4.9.

Table 4.10: Summary of the nova.

Parameter	Value
Name	Nova Scuti 2009, V496 Sct
Discovery Date	2009 November 8.370 UT
Date of optical maximum	2009 November 18.716 UT
Equatorial coordinates	18h 43m 45.57s -7d 36m 42s (J2000.0)
Galactic coordinates	25.2838, -1.7678 (J2000.0)
Speed class	Moderately fast
t_2	59 ± 5 days
t_3	$\sim$ 90 days
Reddening E(B-V)	0.57 ± 0.06
Extinction A_V	1.77 ± 0.06
M_V	-7.0 ± 0.2
Distance	2.9 ± 0.3 kpc
Height from the Galactic plane	89 ± 3 pc
M_{WD}	$\sim 0.7\ M_\odot$
L_O	$5.1 \times 10^4\ L_\odot$
Emission lines	complex, saddle-like profiles
Line widths (FWHM)	1230 ± 50 km s^{-1}
Ejecta mass	$6.3 \pm 0.2 \times 10^{-5}\ M_\odot$
Dust formation (mass of the dust)	Yes ($1\text{-}5 \times 10^{-10}\ M_\odot$)

Chapter 5

Study of KT Eridani

5.1 Introduction

Nova KT Eri was discovered on 2009 November 25.536 UT by K. Itagaki at V = 8.1 (Yamaoka et al. 2009) with 0.21m patrol system. An image taken soon after the discovery by Itagaki using 0.60m reflector on 2009 November 25.545 UT confirmed the presence of KT Eri. Itagaki also noted the presence of a faint object near the position of KT Eri in his archival patrol images. Yamaoka pointed out that All Sky Automated Survey (ASAS-3) system (Pojmanski 1997) had detected KT Eri on 3 occasions prior to the discovery announcement of Yamaoka. These pre-discovery magnitudes along with additional detections are listed in Table 5.1. In addition Yamaoka suggested that the discovery of KT Eri might be the result of brightening of a 15th magnitude blue star contained in many catalogues with one of the identifications being USNO-B1.0 0798-0048707. Guido & Sostero (2009) confirmed the discovery of KT Eri using their CCD observations using 0.25m reflector and pointed out the presence of a star of $\sim$ 15 mag close to the position of KT Eri on the DSS red plate of 1990 November 23 UT. The nature of KT Eri as a nova was confirmed by several low resolution optical spectra obtained during 2009 November 26.5 - 26.6 UT by Fujji, Arai & Isogai and Imamura (Maehara 2009). These spectra showed broad Balmer emission (FWHM of Hα 3200 - 3400 km s^{-1}) together with prominent emission features of He I, N I, N II, Na I D, O I and Mg II leading Maehara to suggest that KT Eri is a nova of the He/N class. Rudy et al. (2009) also suggested KT Eri to be a nova of He/N class on the basis of their near-infrared spectra obtained on 2009 November 26.4 UT spanning the spectral range of 0.9 to 2.5 μm. The He I line at 1.083 μm was already the strongest line in the spectrum with a P Cygni absorption extending to 3600 km s^{-1}. The emission lines of H I, N I and O I were very strong and broad with FWHM $\sim$ 4000 km s^{-1}. The reports of clear detection of KT Eri prior to its discovery has resulted in additional studies by different groups to obtain its pre-discovery light curves. Drake et al. (2009) carried out a search of Catalina Sky Survey data covering the location of KT Eri during period 2005 January 17 to 2009 November 18. KT Eri was clearly seen in outburst in the images taken on 2009 November 18 and they pointed out that the outburst occurred after 2009 November 10.41 UT. The study of pre-discovery light curve has shown clear variations of approximately 1.8 magnitudes. The association of an unresolved fainter companion to the 15th magnitude star to be the progenitor of KT Eri would mean a very high level of variability. As this possibility is unlikely Drake et al. (2009) conclude that the 15th magnitude star is most likely associated with KT Eri. Ragan et al. (2009) have estimated that the optical maximum of KT Eri occurred around 2009 November 15 UT with $V \sim$ 5.6 mag on the basis of the photometry from the "Pi of the sky" consortium data and the AAVSO data. Using this epoch for the optical maximum they derived the decline times of t_2 = 8 & t_3 = 15 days. An average value of M$_V$ $\sim$ -8.7 mag was estimated from different MMRD relations. The equivalent width of the interstellar Na I D line from the echelle spectra was used by Ragan et al. (2009) to calculate a value of E(B-V) $\sim$ 0.08 from the relation of Munari & Zwitter (1997). They derived a distance of $\sim$ 6.5 kpc to KT Eri and pointed out that the 15th magnitude star located close to the KT Eri position in pre-discovery images is too bright to be its progenitor. The high galactic latitude (-32 deg) location of the star can explain the small value estimated for E(B - V). Hounsell et al. (2010) have obtained an impressive high cadence optical light curve of KT Eri through its initial rise, peak and early decline using USAF/NASA Solar Mass Ejection Imager (SMEI) on board the Coriolis Satellite (Eyles, 2003). These observations are spread over the period 2009 November 1.13 to 30.62 UT. The light curve, obtained by SMEI indicates that the initial rise of the nova is steep (rising 4.1 magnitudes over 2.7 days) with evidence of a pre-maximum halt occurring on 2009 November 13.90 $\pm$ 0.04 UT at $m_{SMEI} \sim 6$. The duration of this halt would seem to be only a few hours, which is appropriate for the speed of the nova (e.g. Payne-Gaposchkin 1964). The nova reached maximum light on 2009 November 14.67 $\pm$ 0.04 UT with an unfiltered SMEI apparent magnitude of $m_{SMEI} \sim 5.42 \pm 0.02$. It subsequently declined rapidly with a t_2 value of 6.6 days confirming KT Eri as a very fast nova. The SMEI observations are consistent with the observed high expansion velocities (FWHM $\sim$ 3400 km s^{-1}) and assignment of He/N spectral class to KT Eri described earlier. Nesci et al. (2009) have used the pre-outburst spectrum of the suspected 15th magnitude progenitor available in the Digitized First Byurakan Survey of the field containing KT Eri to study its nature. The spectra taken on 1971 January 25 shows a strong UV continuum with several emission lines that include [Ne V]3426, [Ne III]3868 and a large blend around Hγ. As these features are typical of cataclysmic variables Nesci et al. (2009) favour the identification of the 15th magnitude star with the actual progenitor of KT Eri and point out that the forbidden lines of [Ne III] & [Ne V] were also seen in the transient source CSS 081007: 030559+054715 (HV Cet) suggested to be a possible He/N nova located at high galactic latitude -43.7 deg (Prieto et al. 2008, Pejcha et al. 2008). A search for previous outburst of KT Eri was done by Jurdana-Sepic et al. (2011) using the Harvard College Observatory archive plates spanning the period 1883 to 1952. As no earlier outbursts were found they have suggested that if KT Eri is a recurrent nova, recurrence time is likely to be on a time scale of centuries. Jurdana-Sepic et al. (2011) find a periodicity at quiescence of 737 days for the 15th magnitude progenitor that may arise from reflection effects and/or eclipses in the underlying binary system in KT Eri.

Later KT Eri has been detected as a luminous soft X-ray source (Bode et

Table 5.1: Pre-discovery CCD magnitudes of KT Eri from IAUC 9098.

Date in UT 2009 November	Magnitude	Observers
10.236	< 14.0	ASAS
14.572	5.7	Ootsuki
14.632	5.4	Watanabe & Miyasaita
14.813	5.6	Ootsuki & Ohshima
17.226	6.9	Hankey
17.758	6.7	Tanaka
17.807	6.6	Kawamura
18.760	7.0	Yamamoto
18.809	7.0	Yamamoto
19.241	7.34	ASAS
22.179	7.98	ASAS
24.269	8.12	ASAS

al. 2010, Ness et al. 2010, Beardmore et al. 2010) and also in radio (O'Brien et al. 2010). The details of these observations are described below.

5.1.1 X-ray detection

KT Eri has been extensively studied at X-ray wavelengths using SWIFT (Bode et al. 2010; Beardmore et al. 2010) and CHANDRA (Ness et al. 2010) observatory. The SWIFT observations started from 2009 November 27 UT, 2 days after the announcement of the outburst and corresponding to day 13.1 after optical maximum. There was no evidence of X-ray observations until day 39.9 when a relatively hard X-ray source was seen. The highlight of subsequent regular observations was the emergence of a bright and highly variable Supersoft X-ray Source (SSS) starting from day 55.5. Bode et al. (2010) note that the time scale for emergence of SSS in KT Eri is very similar to that in

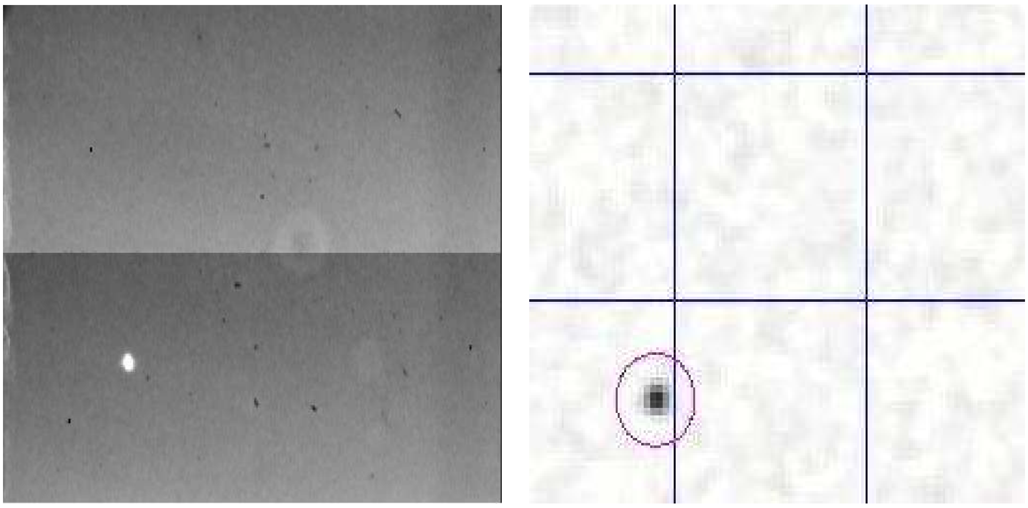

Figure 5.1: *The J band images (2 × 2 arcmin) of KT Eridani. The left panel shows the image obtained during the outburst and the right panel is 2MASS image with suggested progenitor marked with a circle. North is on the top and East is to the right.*

the recurrent nova LMC 2009a & fast and rapid variability with count rates changing by a factor of 20 in $\sim$ 3 hours during day 65.61 to 65.76 after the optical maximum is similar to that seen in the 2006 outburst of recurrent nova RS Oph. Beardmore et al. (2010) have searched for variability on shorter time scales using the data from day 66.60 to 79.25 and find the presence of quasi-periodic oscillation (QPO) with a period of 35 second. They have also done a time series analysis of CHANDRA data set of KT Eri during day 70.283 to 70.457 and find a marginal detection of 35 second periodicity. These observations show that KT Eri is the second example after the recurrent nova RS Oph where $\sim$ 35 sec oscillation is seen in the SSS X-ray emission. Beardmore et al. (2010) favour a possible residual nuclear-burning white dwarf pulsation for the identical $\sim$ 35 sec QPOs seen in KT Eri and RS Oph instead of rotation based origin for this modulation. The high resolution X-ray spectrum of KT Eri taken between day 70.31 to 70.49 after the optical maximum by Ness et al. (2010) shows bright Supersoft Source along with deep absorption feature from nitrogen and carbon.

5.1.2 Radio detection

KT Eri has been observed at Australia Telescope Compact Array (ATCA), Giant Metrewave Radio Telescope (GMRT), Multi-Element Radio Linked Interferometer Network (MERLIN) and Very Large Array (VLA) radio observatories as Target of Opportunity during the period 2009 December 4 to 2010 February 3 (O'Brien et al. 2010). The observations during 2009 December 4 to 8 at MERLIN, 2009 December 28 at VLA and 2010 January 10 at GMRT resulted in 3σ upper limits at 5 GHz, 1.4 GHz and 610 MHz respectively. The first clear detection of KT Eri at radio wavelengths was done at VLA on 2009 December 28 at 5 GHz with a peak flux of 0.21 mJy. Subsequent observations on 2010 January 14 and February 3 at ATCA have shown the brightening of KT Eri at 5.5 GHz and 9 GHz. These observations show that KT Eri was on the rising part of the radio light curve during this period.

This chapter discusses the near-infrared photometric and spectroscopic observations in Section 5.2. The results of the analysis of V band light curve, characteristics of the near-infrared spectra, recombination analysis of the H I lines, evidence for bipolar flow and evolution of the continuum are presented in Section 5.3. In Section 5.4 the nature of the progenitor, mass of the underlying white dwarf and the possibility of KT Eri being a recurrent nova are discussed. The summary of the results obtained from the near-infrared observations are given in Section 5.5.

5.2 Observations

Near-IR observations were obtained using the 1.2m telescope of Mt. Abu Infrared Observatory from 2009 November 28 to 2010 March 3. The log of the spectroscopic and photometric observations is given in Table 5.2. The spectra were obtained at a resolution of $\sim$ 1000 using a Near-Infrared Imager/Spectrometer with a 256 $\times$ 256 HgCdTe NICMOS3 array. In each of the JHK bands a set of spectra was taken with the nova off-set to two different positions along the slit. Spectral calibration was done using the OH sky lines that register with the stellar spectra. The spectra of the comparison star SAO 131794 were taken at similar airmass as that of KT Eri to ensure that the ratioing process (nova spectrum divided by the standard star spectrum) removes the telluric features reliably. To avoid artificially generated emission lines in the ratioed spectrum, the H I absorption lines in the spectra of standard star were removed by interpolation before ratioing. The ratioed spectra were then multiplied by a blackbody curve corresponding to the standard star's effective temperature to yield the final spectra.

Photometry in the JHK bands was done in clear sky conditions using the NICMOS3 array in the imaging mode. Several frames, in 4 dithered positions, offset by $\sim$ 30 arcsec were obtained in all the bands. The sky frames, which are subtracted from the nova frames, were generated by median combining the dithered frames. The star SAO 131500 located close to the nova was used for photometric calibration. The details of the standard stars are given in Table 5.3. The data is reduced and analyzed using the $IRAF$ package (details are given in Chapter 2).

5.3 Results

Before presenting the results proper, we estimate some of the useful parameters like reddening, distance and latitude for KT Eri.

5.3.1 General characteristics of V and JHK light curves

The light curves based on the V band data of AAVSO and JHK magnitudes from Mt. Abu are presented in Figure 5.2. The AAVSO data span the period 2009 November 27 to 2010 March 20. We have used the pre-discovery observations presented in Table 5.1 from IAUC 9098 to adopt the epoch of optical maximum for KT Eri as 2009 November 14.632 UT when it reached a value of V_{max} = 5.4. This matches with the value of 2009 November 14.67 $\pm$ 0.04 UT obtained by Hounsell et al. (2010) using the SMEI data. This is slightly smaller than the value of t_2 = 6.6 days estimated by Hounsell et al. (2010).

Table 5.2: Log of the Mt. Abu near-infrared observations of KT Eri. The date of optical maximum is taken as 2009 November 14.632 UT.

Date of Observation	Days since optical maximum	Integration time (s)			Integration time (s)			Nova Magnitude		
		J-band	H-band	K-band	J-band	H-band	K-band	J-band	H-band	K-band
		Spectroscopic Observations			Photometric Observations					
2009 Nov. 28.854	14.222	90	90	90	25	55	105	7.39±0.03	7.45±0.03	7.04±0.04
2009 Dec. 01.813	17.181	120	90	120	25	55	105	7.89±0.03	7.91±0.04	7.37±0.06
2009 Dec. 03.844	19.212	–	–	–	75	165	105	7.88±0.06	7.79±0.04	7.35±0.04
2009 Dec. 04.834	20.202	120	120	120	–	–	–	–	–	–
2009 Dec. 05.844	21.212	120	90	120	75	110	105	8.21±0.08	8.08±0.04	7.69±0.05
2009 Dec. 06.813	22.181	90	90	120	–	–	–	–	–	–
2009 Dec. 07.865	23.233	90	90	120	75	110	105	8.36±0.01	8.39±0.02	7.95±0.06
2009 Dec. 08.834	24.202	120	90	120	–	–	–	–	–	–
2009 Dec. 09.823	25.191	120	90	120	75	110	105	8.39±0.05	8.42±0.07	8.02±0.06
2009 Dec. 15.776	31.144	120	90	120	75	110	105	8.80±0.03	8.82±0.10	8.35±0.02
2009 Dec. 16.782	32.150	120	90	120	–	–	–	–	–	–
2009 Dec. 17.786	33.154	–	–	–	100	110	105	9.06±0.06	8.94±0.04	8.55±0.07
2009 Dec. 27.779	43.147	–	–	–	100	220	105	9.44±0.05	9.34±0.05	9.02±0.13
2009 Dec. 29.767	45.135	–	–	–	125	220	105	9.53±0.14	9.36±0.03	8.93±0.12
2009 Dec. 31.757	47.125	–	–	–	100	165	105	9.30±0.06	9.19±0.04	8.85±0.09
2010 Jan. 03.750	50.118	–	–	–	250	550	105	9.30±0.05	9.91±0.04	8.67±0.07
2010 Jan. 25.755	72.123	–	–	–	500	825	105	10.58±0.06	10.41±0.05	9.50±0.04
2010 Jan. 27.744	74.112	–	–	–	750	1100	105	10.65±0.02	10.51±0.03	9.51±0.10
2010 Feb. 28.735	106.103	–	–	–	600	660	63	11.23±0.08	11.01±0.08	9.99±0.10
2010 Mar. 01.725	106.828	–	–	–	600	660	63	11.26±0.04	11.05±0.10	9.89±0.10
2010 Mar. 03.734	108.837	–	–	–	–	825	63	–	11.05±0.10	9.89±0.10

Table 5.3: Parameters of the standard stars used for spectral and photometric reduction.

Name	Equatorial and Galactic co-ordinates (2000)	V	J	H	K	Spectral type
SAO 131794	05h 07m 50.99s -05d 05m 11.21s 205.34, -25.32	2.79	2.47	2.44	2.4	A3 III
SAO 131500	04h 48m 13.84s -09d 30m 24.13s 207.31, -31.65	7.15	7.35	7.413	7.399	A0

From a least square regression fit to the post maximum light curve we estimate t_2 to be 5.7 $\pm$ 0.2 d, making KT Eri one of the fast He/N class of novae in recent years. Using the maximum magnitude versus rate of decline (MMRD) relation of della Valle & Livio (1995), we determine the absolute magnitude of the nova to be M_V = -8.9 $\pm$ 0.1. The reddening E(B - V) = 0.09, is derived from Shlegel et al. (1998) towards nova direction and we get A_V = 0.29 for R = 3.1. Based on the above we obtain a value of the distance d = 6.3 $\pm$ 0.1 kpc to the nova. Using the value of d we estimated the latitude z = 3.3 $\pm$ 0.1 kpc from the Galactic plane. It shows that the value of E(B - V) taken by us is appropriate for the nova. The outburst luminosity of KT Eri as calculated from M_V is $L_O = 2.9 \times 10^5$ $L_\odot$.

The near-infrared observations presented in Table 5.2 cover the period 2009 November 28 to 2010 March 3. The optical and JHK lightcurves show additional small amplitude outburst near day 40 from the optical maximum. A plateau was also seen in the V band light curve after 80 days from optical maximum. The duration of the plateau was more than 60 days as the nova went in to conjunction with Sun afterwards.

The observed value of the amplitude $\triangle V$ = 9 and t_2 = 5.7 days for KT Eri is well below the lower limit in the amplitude versus decline rate plot for classical novae presented by Warner (2008) which shows $\triangle V$ = 12 - 15 for t_2 =

Table 5.4: A list of the lines identified from the JHK spectra.

Wavelength (μm)	Species
1.0830	He I
1.0938	Pa γ
1.1287	O I
1.2818	Pa β
1.5256	Br 19
1.5341	Br 18
1.5439	Br 17
1.5557	Br 16
1.5701	Br 15
1.5881	Br 14
1.6109	Br 13
1.6407	Br 12
1.6806	Br 11
1.7002	He I
1.7362	Br 10
1.9451	Br 8
2.0581	He I
2.1120,2.1132	He I
2.1655	Br γ

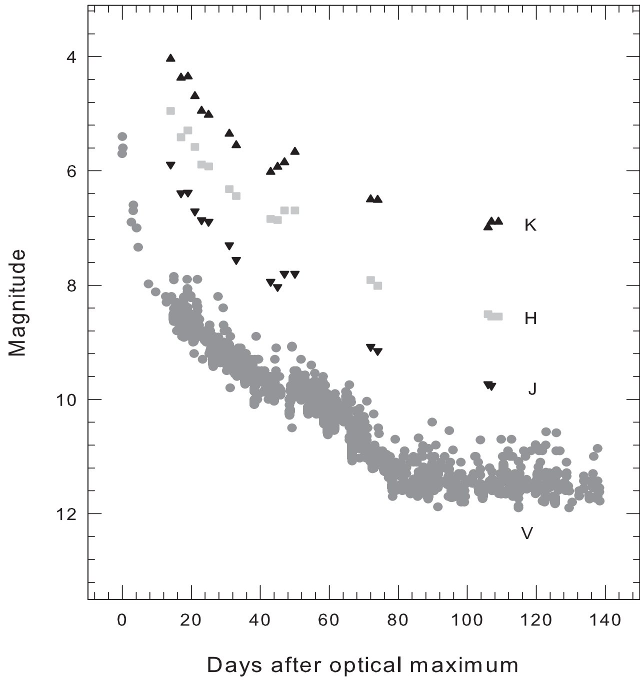

Figure 5.2: *The V and JHK band lightcurve of KT Eri from AAVSO and Mt. Abu data respectively.*

5.7 days. The most likely reason for the small value of the outburst amplitude is the possibility of KT Eri being a recurrent nova.

5.3.2 The nature of the light curve

As discussed earlier, (Chapter 1, 3 & 4) a classification system for the optical light curves for novae have been presented by Strope et al. (2010). The classification is based on the time to decline by 3 mag from the optical maximum (t_3) and the shape of the light curve. The shape of the optical light curve of KT Eri presented in Figure 5.2 has all the characteristics of P class of nova. The P class light curve show smooth decline but as the light curve approaches 3 - 6 mag below peak, the smooth decline is interrupted by a long lasting, nearly flat interval that abruptly ends and is followed by a steeper decline. Such a flattened interval is a plateau as seen in the case of KT Eri after 80 days from optical maximum. These plateaus range in duration from 15 to 500 days and vary slightly in slopes. Strope et al. (2010) have clsssified 8 RNe on the basis of their light curve in which 6 have shown P class characteristics as in KT Eri but they also pointed out that the plateau phase only is not the signature for a nova to be recurrent one. So on the basis of light curve we can not say that KT Eri is a recurrent nova. Thus the classification of the optical light curve for KT Eri is P(9), as the estimated value of t_3 is $\sim$ 9 days for KT Eri. The t_3 value obtained by us is less than the value obtained by the relation $t_3 = 2.75\ (t_2)^{0.88}$ (Warner 1995a).

5.3.3 Line identification, evolution and general characteristics of the JHK spectra

The JHK spectra are presented in Figures 5.3 to 5.5 respectively; line identification is given in Table 5.4. The infrared observations presented here cover the phases after optical maximum with the first infrared spectra taken on 2009 November 28. In case of He/N class of novae a small number of spectral lines are normally seen as relatively weaker individual lines blend with each other due to large expansion velocities and become indistinguishable against the underlying continuum. The prominent lines seen in case of KT Eri are H I, O I and He I. The typical FWHM of the H I lines range from 1900 to 2300 km s^{-1} with full width at zero intensity (FWZI) reaching a value of $\sim$ 4000 km s^{-1}. A noticeable feature of these early spectra is the presence of lines due to He I. In the spectra taken on 2009 November 28 the He I lines at 1.0830 μm, 1.7002 μm, 2.0581 μm, 2.1120 μm and 2.1132 μm are clearly seen. These He I lines are seen to strengthen and become even stronger as the nova evolves. There is and indication of He I line at 2.0581 μm decreasing in strength after 2009 December 7. The absence of the emission lines from low ionization species like Na and Mg is consistent with no dust formation seen in the nova ejecta. In addition, the absence of C I lines also supports the lack of dust formation in KT Eri. We would like to point out the decrease in intensity of O I line at 1.1287μm with respect to Paβ and He I line at 2.0581μm with respect to Brγ from 2009 December 8. The reason for this change is not clear.

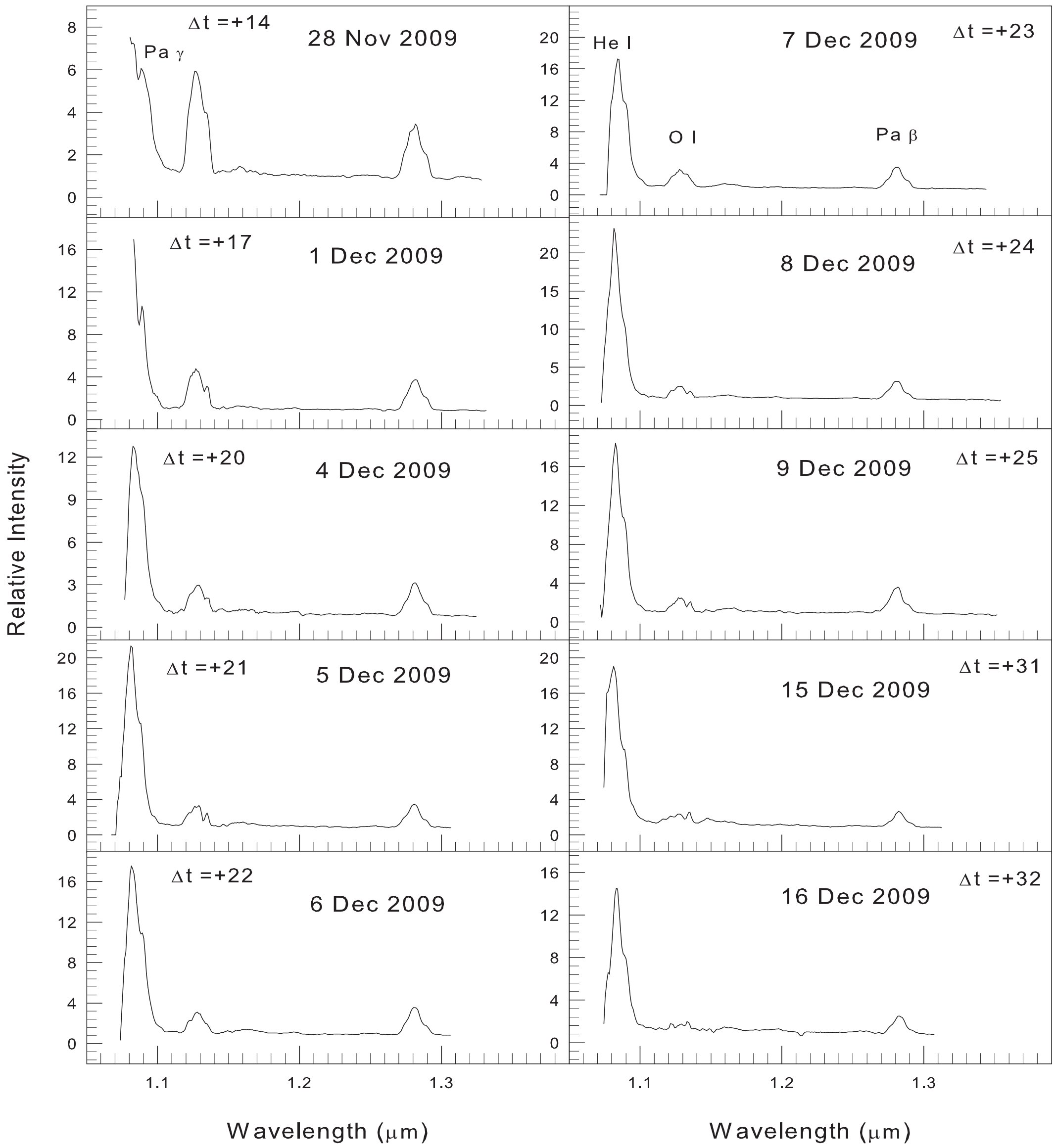

Figure 5.3: *The J band spectra of KT Eri are shown at different epochs. The relative intensity is normalized to unity at 1.25 μm. The time from optical maximum are given for each spectrum.*

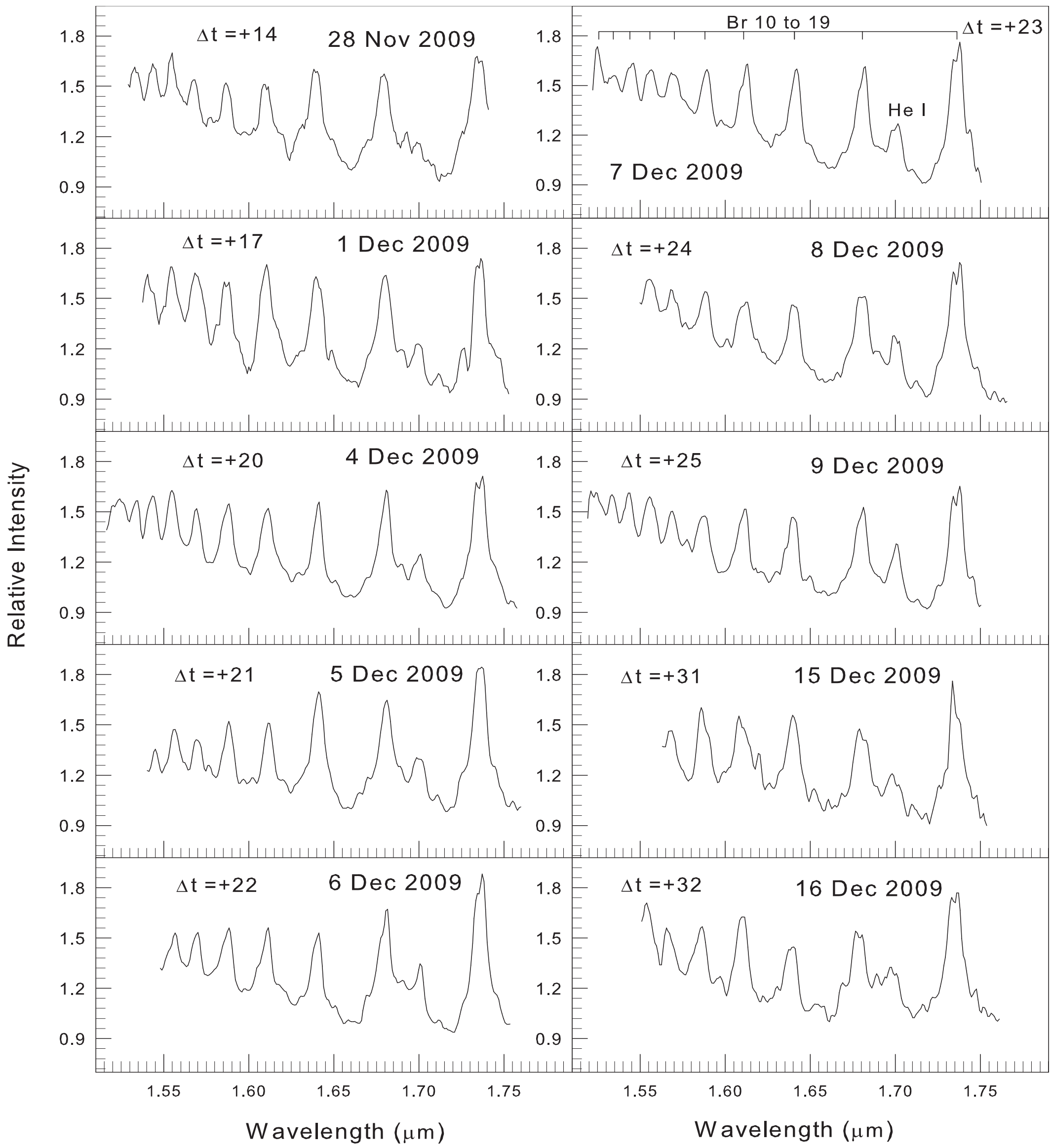

Figure 5.4: *The H band spectra of KT Eri are shown at different epochs. The relative intensity is normalized to unity at 1.65 μm. The time from optical maximum are given for each spectrum.*

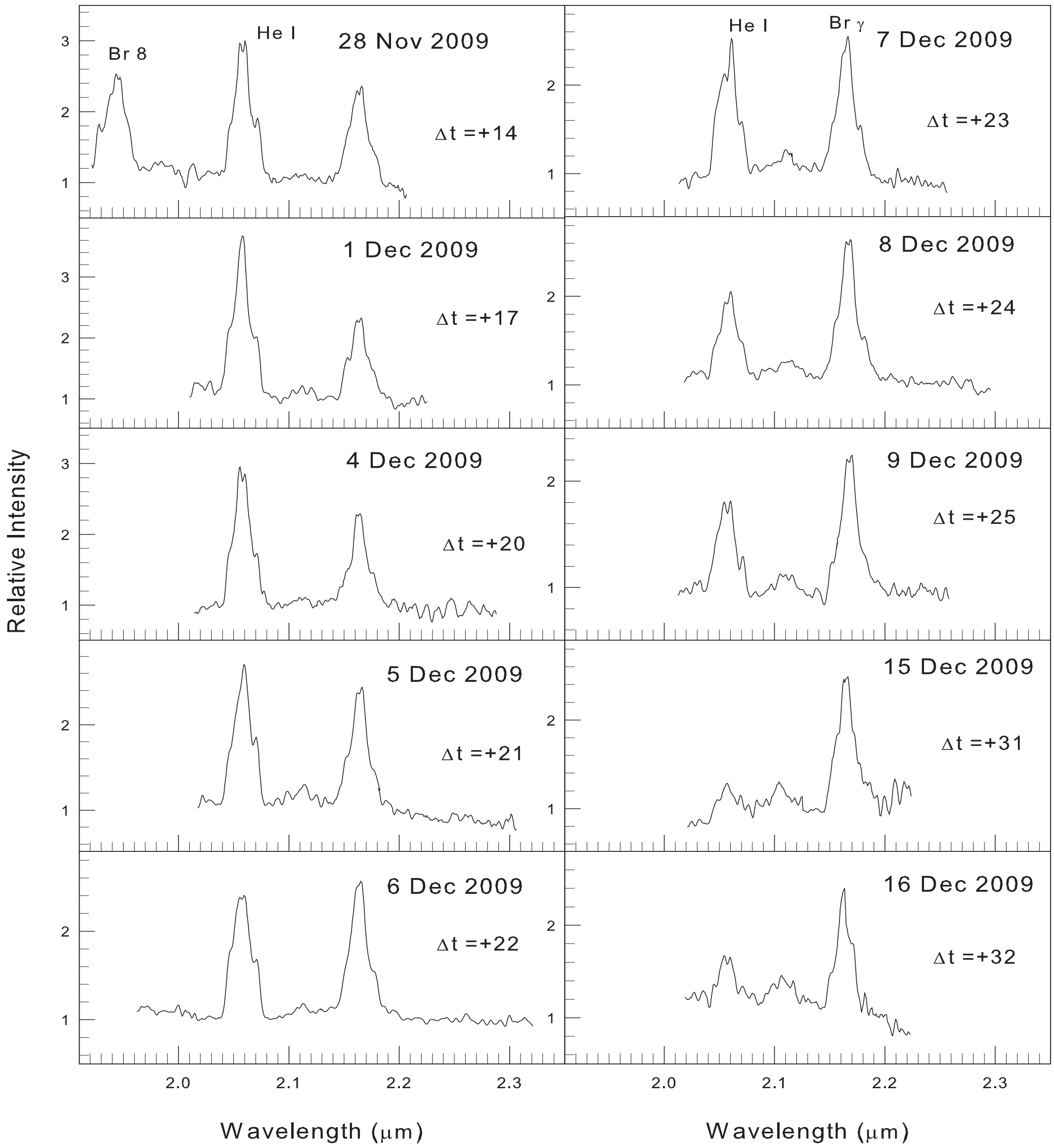

Figure 5.5: *The K band spectra of KT Eri are shown at different epochs. The relative intensity is normalized to unity at 2.2 μm. The time from optical maximum are given for each spectrum.*

5.3.4 Recombination analysis of the H I lines and mass estimation of ejecta

The recombination case B analysis for the H I lines was carried out for all the observed spectra, and the representative results for four epochs of our observations are shown in Figure 5.6. We have plotted in Figure 5.6 the observed relative strength of Brackett series lines with the line strength of Br12 as unity along with the predicted values for three different recombination case B emissivity values from Storey & Hummer (1995). These predicted values cover a representative temperature of T = 10^4 K and the electron densities of $n_e = 10^8$, 10^9 and 10^{11} cm^{-3}. High electron densities are considered because the ejecta material is expected to be dense in the early stages after the outburst. Figure 5.6 shows that the observed line intensities clearly deviate from case B values in the initial phase of our observations. Specifically, Brγ, which is expected to be relatively stronger than the other Br lines, is observed to be considerably weaker in the early observations. This is most likely due to optical depth effects in the Brackett lines (Lynch et al. 2000).

Such deviations from the recombination case B conditions during the early stages after outburst can be expected and have been observed in other novae too, for example V2491 Cyg and V597 Pup (Naik, Banerjee & Ashok 2009), RS Oph (Banerjee et al. 2009) etc. However, after 25 days from optical maximum, on 2009 December 9 (fourth panel of Figure 5) there is an indication that case B conditions have begun to prevail. For 2009 December 9, it is found that the observed data match well with the predicted values for the recombination case B values of T = 10^4 K and an electron density $n_e = 10^9$ cm^{-3}. The mass of the emitting gas is given by

$$M = (4\pi d^2 (m_H)^2 (fV/\epsilon))^{0.5} \tag{5.1}$$

where d is the distance, m_H the proton mass, f the observed flux in a particular line, ϵ the corresponding case B emissivity; V is the volume of the emitting gas, which is $[4/3\pi\ (vt)^3\ \phi]$, where ϕ, v, and t are the filling factor, velocity and time after outburst, respectively. Using the value of temperature and electron

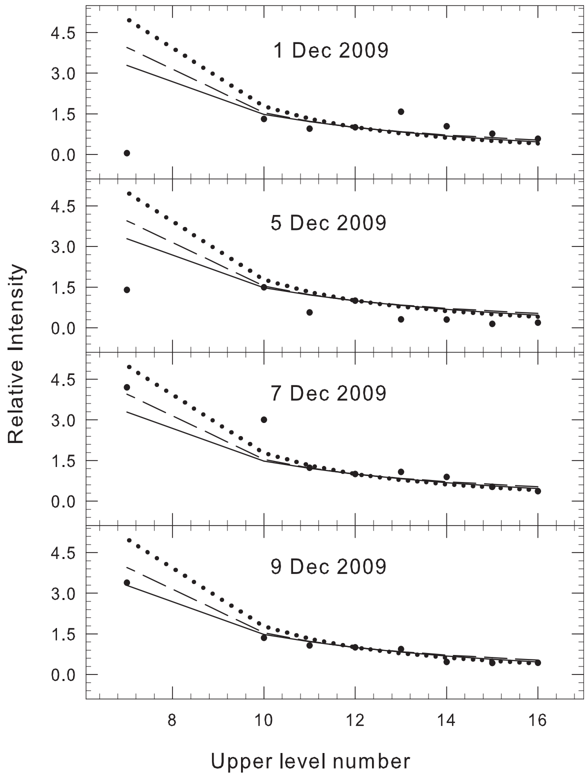

Figure 5.6: *Recombination analysis for the hydrogen Brackett lines in KT Eri on selected dates. The abscissa is the upper level number of the Brackett series line transition. The line intensities are relative to that of Br 12. The Case B model predictions for the line strengths are also shown for a temperature of* $T = 10^4$ *K and electron densities of* $n_e = 10^{11}$ *cm*$^{-3}$ *(dotted line),* 10^9 *cm*$^{-3}$ *(solid line) and* 10^8 *cm*$^{-3}$ *(dashed line).*

density we calculated the mass of the gas in the ejecta in the range 2.4 - 7.4 $\times 10^{-5} M_{\odot}$. As the filling factor $\phi < 1$, this range is an upper limit for the mass of the ejecta.

Ederoclite et al. (2006) have derived the filling factor to lie in the range $\sim 7.1 \times 10^{-2}$ - 7.9×10^{-4} for V5114 Sgr. Additional values reported in the literature for the filling factor are 10^{-2} - 10^{-5} for T Pyx (Shara et al. 1997), 0.1 for N Vel 1999 (della Valle et al. 2002), 0.1 - 10^{-3} for N SMC 2001 (Mason et al. 2005) and 10^{-2} - 10^{-4} for N LMC 2002 (Mason et al 2002). These values clearly demonstrate that the filling factor in nova ejecta are smaller that 1.

Table 5.5: List of line flux corrected for $A_V = 0.29$ for Case B analysis.

Brackett line	Flux ($Wcm^{-2}\mu m^{-1}$) 2009 Dec. 1	Flux ($Wcm^{-2}\mu m^{-1}$) 2009 Dec. 5	Flux ($Wcm^{-2}\mu m^{-1}$) 2009 Dec. 7	Flux ($Wcm^{-2}\mu m^{-1}$) 2009 Dec. 9
7	1.5×10^{-16}	7.6×10^{-15}	7.3×10^{-15}	6.4×10^{-15}
10	4.6×10^{-15}	8.2×10^{-15}	5.3×10^{-15}	2.6×10^{-15}
11	3.3×10^{-15}	3.1×10^{-15}	2.2×10^{-15}	2.0×10^{-15}
12	3.5×10^{-15}	5.5×10^{-15}	1.8×10^{-15}	1.9×10^{-15}
13	5.5×10^{-15}	1.7×10^{-15}	1.9×10^{-15}	1.8×10^{-15}
14	3.6×10^{-15}	1.6×10^{-15}	1.6×10^{-15}	8.7×10^{-16}
15	2.7×10^{-15}	7.7×10^{-16}	9.2×10^{-16}	8.0×10^{-16}
16	2.0×10^{-15}	1.0×10^{-15}	6.3×10^{-16}	8.1×10^{-16}

5.3.5 Evidence for bipolar flow

A significant finding that has emerged from the studies of KT Eri is the presence of extended structure in the ejected material. Such bipolar structure is commonly encountered in planetary nebulae and explained on the basis of the ejecta interacting with a non-uniform circumstellar environment. Alternatively, the ejection of the material could be intrinsically isotropic or anisotropic which we can see here. In the anisotropic scenario, the pre-existing circumstellar material has a density enhancement in the equatorial plane then the outflowing ejecta is impeded from expanding in the equatorial region while expanding relatively more freely in the polar direction. This leads to a constriction of the nebula in the equatorial region thereby giving rise to an hourglass shape. Kinematically, this would imply that the matter in the poles would flow out with a high velocity relative to the matter in the waist of the hourglass. But in the isotropic scenario the velocity of the ejecta will be almost same. The evidence for a bipolar flow is also seen from our near-IR data. To illustrate this, we present in Figure 5.7, representative profiles of the Paβ and Brγ lines on December 7.865 UT. As can be seen, the profiles have a strong central component flanked by two weaker components. In both panels of Figure 5.7, we have fitted the profile with three Gaussians a central Gaussian for the core emission component and two Gaussians for the satellite components in the wings (the Gaussians are shown by continuous black lines, their sum by the dashed line and the observed data by the grey line).

It is seen that a three-component Gaussian fits the data reasonably well. The fits indicate the presence of two high velocity components at radial velocities of -1530 and 2090 km s^{-1} for Paβ and at -1940 and 1930 km s^{-1} for the Brγ lines, respectively (these high velocity components appear to be associated with the faster structure reported by Bode et al. (2010)). The central components have full width at half-maximum (FWHM) of 2340 and 1930 km s^{-1} for the Paβ and Brγ lines, respectively. We can interpret the results of Figure 5.7 as follows viz. the core emission can be associated with the slower expanding material from the waist of the bipolar ejecta while the higher velocity satellite

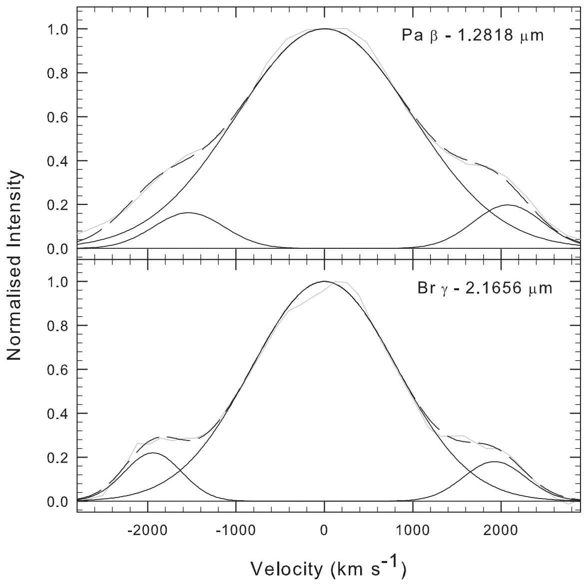

Figure 5.7: *Line profiles of the Paβ and Brγ lines on December 7.865 showing broad wings indicative of a bipolar flow. A multi-Gaussian fit of the profiles is shown - a Gaussian for the central component and two Gaussians for the satellite components in the wings. The Gaussians are shown by continuous black lines, their co-added sum by the dashed line and the observed data by the grey line. Further details are provided in Section 5.3.5.*

components are associated with the flow from the polar regions.

Ribeiro et al. 2011 have modeled the Hα line showing the bipolar flow with a dumbbell shape with a 1/r density profile, and got the expansion velocity and inclination angle as V$_{exp}$ = 2800 $\pm$ 200 km s^{-1} and 58^{+6}_{-7} degrees respectively.

The spectra presented by Imamura & Tanabe (2012) shows the decline rate of FWHM of Hα $\sim$ 30 km s^{-1} per day. After 12.2 days from optical maximum the FWHM of Hα is approximately 3400 km s^{-1} but about 70 days after the optical maximum is around 1500 km s^{-1}. An asymmetric profiles at the earlier stages for Hα suggests the existence of the non-spherical expanding gas shell.

We would like to point out the detection of similar high velocity bipolar flow in the case of the 2006 outburst of the recurrent nova RS Oph by Banerjee et al. (2009) on the basis of the broad wings in the line profiles of Paβ and Brγ.

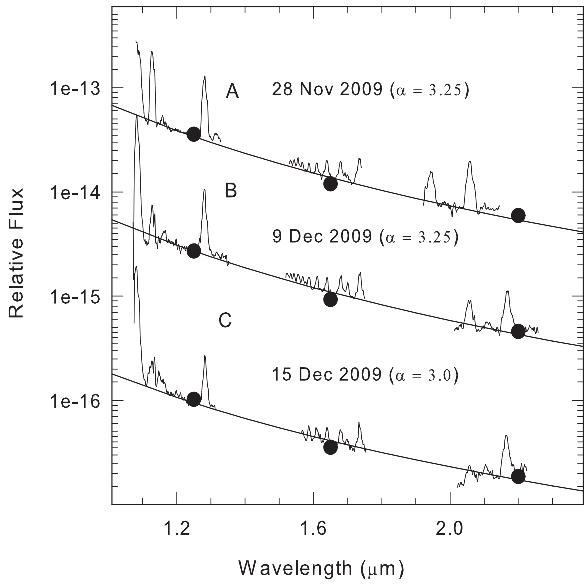

Figure 5.8: *The composite JHK spectra of KT Eri for three representative dates 2009 November 28, 2009 December 9 and 2009 December 15 are shown. Model fits to the data with a power law, $F_\lambda \alpha \lambda^{-\alpha}$, are shown by the continuous lines with the broad band fluxes represented as filled circles. A decreasing trend in the power law index α is seen indicating the decrease in the optical depth of the ejecta.*

5.3.6 Evolution of the continuum

We analyze and discuss the evolution of the continuum spectra of KT Eri. At the time of outburst, a nova's continuum is generally well described by a blackbody distribution from an optically thick pseudo-photosphere corresponding to a stellar spectral type A to F (Gehrz 1988). The spectral energy distribution (SED) then gradually evolves into a free-free continuum as the optical depth of the nova ejecta decreases (Ennis et al. 1977; Gehrz 1988). The evolution of the continuum of KT Eri is shown in Figure 5.8 wherein we have shown representative spectra sampling the duration of our observations. The spectra in Figure 5.8 were flux calibrated using the broad-band JHK photometric observations presented in Table 5.2.

At the epoch of optical maximum a blackbody fit with an index of $\alpha = 4.0$

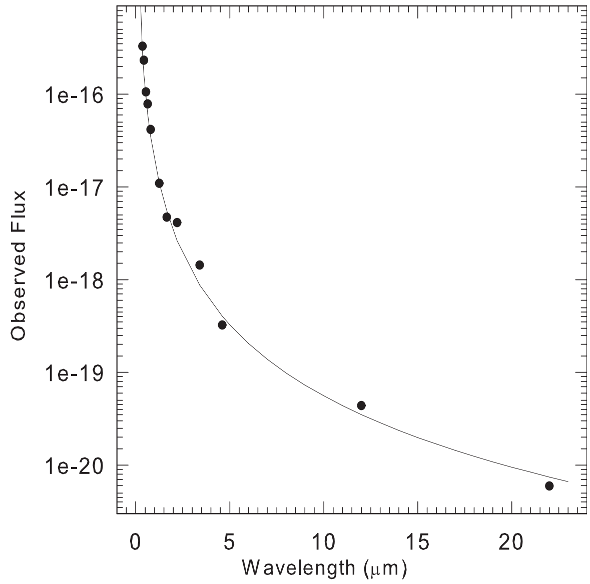

Figure 5.9: *The spectral energy distribution (SED) during the plateau phase is shown using UBVRI fluxes in the optical from AAVSO, JHK fluxes in the near-infrared from Mt. Abu and mid-infrared fluxes from WISE data spread over 2010 February 21 to 28. A power law fit with index α = 2.55 is found to fit the data.*

is expected to fit the continuum flux distribution. As our observations begin from day 14 after optical maximum, we have done power law fits, $F_\lambda \ \alpha \ \lambda^{-\alpha}$, to see the evolution of continuum spectra shown in Figure 5.8. In the beginning of our observation, i.e. on 2009 November 28 (14 d after optical maximum) and 2009 December 9, the continuum spectrum closely matches for a spectral index $\alpha = 3.25$.

The subsequent spectrum on 2009 December 15 has become flatter with a slope of $\alpha = 3.0$. This slow change in the slope of the continuum spectrum is also evident in case of other novae, for example, V4643 Sagittarii where it changed from a slope of about 3 to 2 within about three months (Ashok et al. 2006). However, in the case of another nova viz. V4633 Sagittarii (Lynch et al. 2001) the change in the slope of the continuum was found to be in the opposite direction, i.e. the slope changed from 2 to 2.7 in observations taken 525 and 850 days after outburst. Therefore, it is, necessary to follow the nova

Table 5.6: List of broad band flux corrected for A_V = 0.29 for optical IR & mid IR data.

Band	Flux ($Wcm^{-2}\mu m^{-1}$)
U	3.3×10^{-16}
B	2.3×10^{-16}
V	1.1×10^{-16}
R	7.8×10^{-17}
I	4.2×10^{-17}
J	1.1×10^{-17}
H	4.7×10^{-18}
K	4.1×10^{-18}
$W1$	1.4×10^{-18}
$W2$	3.2×10^{-19}
$W3$	4.4×10^{-20}
$W4$	5.9×10^{-21}

outburst more regularly to have a better spectral coverage to understand the behaviour of the nova continua.

Further we tried to fit the SED for 2010 February 21 to 28 in Figure 5.9 and found that the spectral index α is flattened up to 2.55. In Figure 5.9 we have used the $UBVRI$ data from AAVSO, JHK from Mt. Abu and $W1W2W3W4$ from WISE (Wide Field Infrared Survey). The central wavelengths for $W1W2W3W4$ are 3.4, 4.6, 12 and 22 micron, respectively.

5.4 Discussion

5.4.1 Nature of the suggested progenitor candidate

The possibility of the 15th magnitude star close to the position of KT Eri pointed out by different groups was discussed earlier in section 5.1. We have explored the likelihood of this possibility by examining the spectral energy distribution (SED) using the optical photometric data from USNO-B1 catalouge and the near-infrared photometric data from 2MASS catalouge. The estimated value of A_V = 0.29 mag derived in subsection 5.3.1 was used to correct for interstellar extinction. The corrected flux values are given in Table 5.7. The observed SED shown in Figure 5.10 is difficult to fit with a blackbody spectrum. Several blackbody fits at different temperatures were tried to fit the observed SED. We did not find a good blackbody fit to the SED and the closest fit to the data with T = 10,000 K is not satisfactory. The observed flux values decrease slower than the blackbody distribution. We have considered the possibility that the observed continuum distribution from the progenitor candidate of KT Eri is dominated by radiation from an accretion disk surrounding the white dwarf. In the case of a steady-state accretion disk around a white-dwarf, the continuum radiation from the disk can be described by a F_ν α $\nu^{1/3}$ relation (Mayo et al. 1980 and references therein). A F_ν α $\nu^{1/3}$ dependence falls less steeply than the relation expected for a blackbody in the Rayleigh-Jeans regime. This relation translates to F_λ α $\lambda^{-\alpha}$ where α = 2.33. We find that a power law spectrum with α = 2.88 fits the data of Figure 5.10 better than a black-body fit. This value of α = 2.88 is closer to the model value of α = 2.33 for the accretion disk compared to the value of α = 4.0 for the blackbody distribution. It may be reasonable to consider the power law distribution with α = 2.88 for the observed flux as some evidence for the presence of accretion disk in the progenitor candidate.

Jurdana-Sepic et al. (2012) have utilized the 2MASS infrared magnitudes to study the properties of the secondary star in KT Eri as this spectral region is more sensitive to the secondary star. They have calculated the absolute magnitudes of the secondary star to be $M_J = 0.48 \pm 0.03$, $M_H = 0.05 \pm 0.05$ and $M_{K_S} = 0.00 \pm 0.07$ using the distance and reddening of $d = 6.5$ kpc and E(B-V) = 0.08 given by Ragan et al. (2009). These magnitudes are brighter than those derived for the RN U Sco at quiescence from 2MASS ($M_J = 1.3 \pm 0.4$, $M_H = 0.9 \pm 0.4$ and $M_{K_S} = 0.9 \pm 0.4$. Theses are significantly brighter than typical quiescent CNe (Darnley et al. 2011). Furthermore, the colours are more in line with those of cool giant stars.

It is relevant to point out the nature of progenitors in two recent novae V2491 Cyg and V2672 Oph that have been suggested as possible recurrent novae. Darnley et al. (2011) have made a comparison of V2491 Cyg with U Sco while discussing its nature. They point out that their optical and near-infrared luminosities at quiescence and the outburst amplitude are very similar. They favour the suggestion of V2491 Cyg being a recurrent nova and point out that it contains a subgiant secondary and an accretion disk. Naik et al. (2009) have ruled out the possibility of V2491 Cyg being a RNe of RS Oph category with red giant secondary on the basis of the temporal evolution of the Paβ line profiles. In case of V2672 Oph, another candidate for RNe, Munari et al. (2011) have suggested that the mass losing companion star is not a red giant like that in RS Oph or T CrB.

5.4.2 Mass of the WD in KT Eri

We have estimated the white dwarf mass by using the derived value of the absolute magnitude M_V and relation given by Livio (1992); Warner (1995b):

$$M_V = -8.3 - 10 \; log \; M_{WD}/M_{\odot} \tag{5.2}$$

The mass of the underlying white dwarf (M_{WD}) in KT Eri is $M_{WD} \sim 1.15$ $M_{\odot}$. The determination of mass of the white dwarf in KT Eri by other investigators is briefly described. As the time for the emergence of the supersoft X-ray source (SSS) in KT Eri is much later than the case of recurrent novae RS Oph and U Sco (Hachisu et al. 2007; Kahabka et al. 1999, respectively), which have white dwarfs with masses very close to the Chandrasekhar limit, Jurdana-Sepic et

Table 5.7: List of broad band flux corrected for $A_V = 0.29$ of the progenitor system.

Band	Flux ($\mathrm{Wcm^{-2}\mu m^{-1}}$)
B	7.6×10^{-18}
R	2.0×10^{-18}
I	1.7×10^{-18}
J	4.8×10^{-19}
H	2.6×10^{-19}
K	9.4×10^{-20}

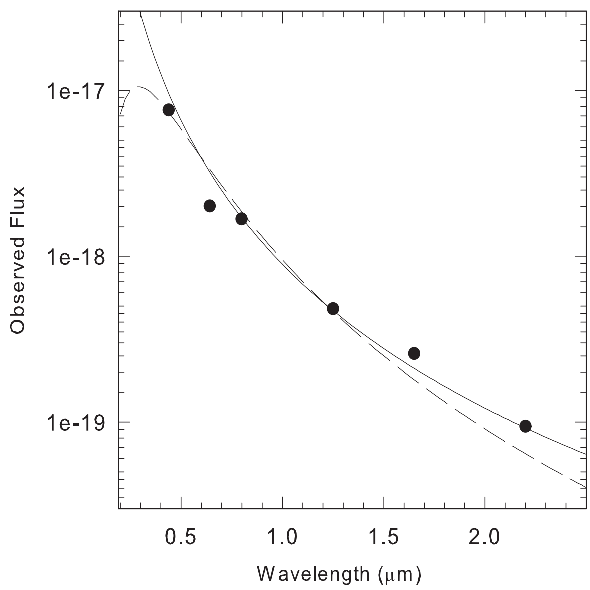

Figure 5.10: *The SED is shown for the progenitor of KT Eri.*

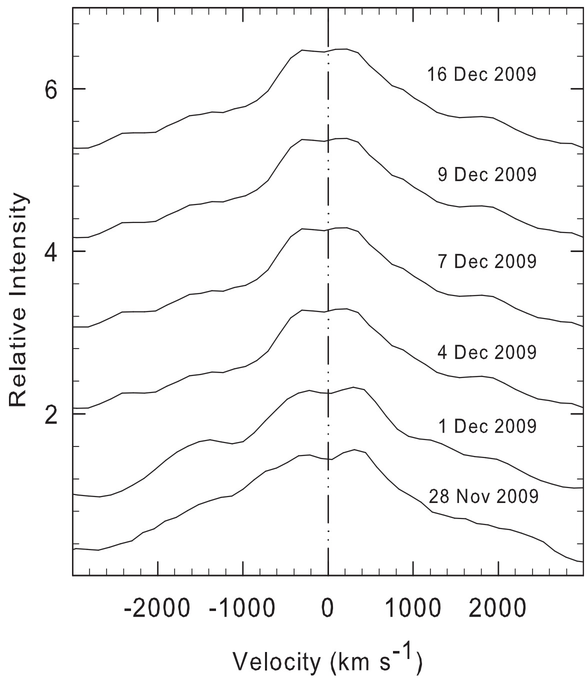

Figure 5.11: *The evolution of Brγ line throughout the near-IR observations of KT Eri.*

al. (2012) have constrained the mass for the WD in KT Eri system as $M_{WD} < 1.3\ M_\odot$. They also constrain the mass of the white dwarf $M_{WD} \geq 1.1\ M_\odot$ on the basis of Ne enrichment seen in the low-resolution spectra of the progenitor of KT Eri reported by Nesci et al. (2009).

5.4.3 KT Eri - a possible recurrent nova ?

The similarity of some of the properties of KT Eri with those of the recurrent novae has prompted the discussion in as to whether KT Eri could be a recurrent nova. We have made an attempt to test, to some extent, the hypothesis that KT Eri is a RNe from the IR observations presented in this chapter. A significant decrease in the width of the emission line profiles should be seen if KT Eri is a RNe of the RS Oph type. As the secondary star in RS Oph type RNe lose mass at a high rate, the nova ejecta expelled with high velocity will get decelerated as it moves through the wind of the companion. This deceleration results in fast temporal changes in the expansion velocity of the ejecta. Such effects have been reported by Das et al. (2006) in the case of 2006 outburst of RS Oph. We have investigated the evolution of one prominent emission lines viz. Brγ in KT Eri. The full width at half maximum (FWHM) is a good representation of the expansion velocity. The line profiles of Brγ for 6 days are shown in Figure 5.11. These line profiles do not show significant changes during the period 2009 November 28 to 2009 December 16.

The present observations thus rule out the possibility of a red giant nature of the binary companion to KT Eri, as in the case of RS Oph subgroup of RNe. The close monitoring of recent outbursts of recurrent novae has revealed mid-plateau phase in U Sco, CI Aql and RS Oph. These mid-plateau phase have been interpreted as arriving from the contribution of bright accretion disks that are irradiated by the central white dwarf. The mid-plateau phase is followed by a sharp decline in the nova light curves leading to the final decline to quiscence phase. The optical light curves of novae have been modeled. Hachisu & Kato (2006) have modeled the ultraviolet, optical and near-infrared light curve of well sampled novae and proposed a universal decline law based on the optically thick wind ejected following the nova outburst. The initiation of thermonuclear runaway in the accreted material on the surface of the WD results in a rapid expansion of its envelop to values $R_{ph} \geq 100\ R_{\odot}$ leading to the ejection of a large part of the envelop as a wind. The early decline of the novae light curves shows a power law dependence of the form $F_{\lambda}\ \alpha\ \lambda^{-\alpha}$. The initial early decline becomes steeper at later stages with α increasing from the range 1.5 - 2 to a value approaching ~ 3. The ejection of the outer envelop is accompanied by the shrinking of the WD pseudo photosphere. Hachisu & Kato (2006) have labeled their modeling of nova light curves as optically thick wind model as the acceleration takes place deep inside the photosphere.

The other recent examples of novae that could be recurrent novae are V2491 Cyg (Nova Cyg 2008) and V2672 Oph (Nova Oph 2009). In case of V2491 Cyg, similarities of the optical spectra with those of RNe V394 CrA and U Sco were pointed out by Tomov et al. (2008). Page et al. (2010) have presented extensive X-ray and UV observations and discussed the possibility of V2491

Cyg being a recurrent nova. They estimate recurrence time scale greater than 100 years if the mass of the WD is $\sim$ 1.3 $M_\odot$ and the source is located at a distance of 10.5 kpc. Schwarz et al. (2009) and Munari et al. (2011) have pointed out the similarities in the observed properties of V2672 Oph with U Sco, like rapid decline, extremely broad emission lines and early hard X-ray emission, thus suggesting that it could be a recurrent nova. They speculate that earlier outburst of V2672 Oph might have been missed due to several unfavourable characteristics like very fast decline rate (t_2 = 2.3d) and faint outburst brightness (V_{max} = 11.35).

5.5 Summary

In this chapter, we have presented near-infrared spectroscopy and photometry of nova KT Eri which erupted after 2009 November 10. From the optical lightcurve, the distance and latitude to the nova is estimated to be 6.3 $\pm$ 0.1 kpc and 3.3 $\pm$ 0.1 kpc. We have estimated the white dwarf mass $M_{WD} \sim 1.15$ $M_\odot$. The outburst luminosity of KT Eri as calculated from M_V is L = 2.9 $\times$ 10^5 $L_\odot$. The light curve classification for KT Eri is P(9). The infrared spectra indicate that the nova is of the He/N type. It may be noted that KT Eri is one of the very fats He/N type of novae (t_2 = 5.7 d) and also one of the very high latitude $z = 3.3 \pm 0.1$ kpc nova in last few years. We calculated the mass of the gas in the ejecta in the range 2.4-7.4 $\times$ 10^{-5} $M_\odot$. We also found the evidence for bipolar flow, which shows the presence of two high velocity components at radial velocities of -1530 and 2090 km s^{-1} for Paβ and at -1940 and 1930 km s^{-1} for the Brγ lines, respectively. The central components have full width at half-maximum (FWHM) of 2340 and 1930 km s^{-1} for the Paβ and Brγ lines, respectively. We have also discssed the possibility of 15th magnitude star to be the proginator. We also discussed the evolution of the continuum of the spectra. The summary of the nova is given in Table 5.8.

Table 5.8: Summary of the nova.

Parameter	Value
Name	Nova Eridani 2009, KT Eri
Discovery Date	2009 November 25.536 UT
Date of optical maximum	2009 November 14.632 UT
Equatorial coordinates	4h 47m 54.21s -10d 10m 43.1s (J2000.0)
Galactic coordinates	207.9863, -32.0202 (G2000.0)
Speed class	Very fast
t_2	5.7 $\pm$ 0.3 days
t_3	$\sim$ 9 days
Reddening E(B-V)	0.09
Extinction A_V	0.29
M_V	-8.9 $\pm$ 0.1
Distance	6.3 $\pm$ 0.1 kpc
Galactic latitude	3.3 $\pm$ 0.1 kpc
M_{WD}	$\sim$ 1.15 $M_\odot$
L_O	2.9 $\times$ 10^5 $L_\odot$
Emission lines	bipolar wings
Line widths (FWHM)	$\sim$ 2100 km s^{-1}
Ejecta mass	2.4-7.4 $\times$ 10^{-5} $M_\odot$
Dust formation (mass of the dust)	No

Chapter 6

Summary and Future Work

The work presented in this thesis is an attempt to explore many fundamental questions about classical nova outbursts. We summarize the work carried out in this thesis with emphasis on the important and new results that have been obtained. The scope for future work is also discussed. This work is based mainly upon our obsevations from 1.2m telescope of Mt. Abu Infrared Observatory (Mt. Abu IR Telescope) and also includes optical data from Asiago Observatory (Italy) for one nova. I have presented the analysis of 3 classical novae (of different types) that have exibited different aspects throughout a broad range of evolutionary stages of development from a few days to years after the outburst.

6.1 Summary

The thesis presents the near-infrared spectroscopic and photometric studies of the following three novae:

1. V5579 Sagittarii (V5579 Sgr), a classical nova. It was discovered on 2008 April 18.784 UT. Our observations of this nova commenced after 5 days of outburst and extended upto 26 days after outburst.

2. V496 Scuti (V496 Sct), a classical nova. It was discovered in outburst on 2009 November 8.370 UT. This object was observed for 530 days after outburst.

3. KT Eridani (KT Eri), a classical nova which showed some of the features of recurrent novae. This was discovered on 2009 November 25.812 UT and was followed for next 100 days.

The important results obtained from the extensive studies of these novae are described below.

6.1.1 Results from the study of V5579 Sgr

1. From the optical light curve, we determine the absolute magnitude of the nova to be M_V = -8.8 $\pm$ 0.1. The distance and the height from the galactic plane for the nova is estimated to be 4.4 $\pm$ 0.2 kpc and 232 $\pm$ 11 pc respectively. The mass of the underlying white dwarf in V5579 Sgr is estimated to be $M_{WD} \sim 1.12\ M_\odot$.

2. The outburst luminosity of V5579 Sgr as calculated from M_V is L = 2.7 $\times\ 10^5\ L_\odot$. We have also pointed out that V5579 Sgr is one of the few fast Fe II classes of novae (t_2 = 8 d) that formed dust. The light curve classification for V5579 Sgr is D(14).

3. The IR spectra indicate that the nova is of the Fe II class. The presence of emission lines from low-ionization species like Na and Mg in the early spectra and subsequent formation of the dust support the predictive property of these lines as indicators of dust formation as proposed by Das et al. (2008). Evidence is seen from the JHK photometry and spectra for the formation of dust in the nova in mid-May 2008. The mass of the dust and gas is estimated $M_{dust} = 2.12 \times 10^{-9}\ M_\odot$ and $\sim 4.2\times\ 10^{-7}\ M_\odot$, respectively.

4. We have indicated the usefulness of the P Cygni profiles seen in the nova spectra around maximum brightness to study the physical parameters related to the central WD. The presence of a persisting absorption structure in the Paβ line is interpreted as evidence for sustained mass-loss during the outburst and used to set a lower limit of 8 - 12 days for the mass loss duration.

6.1.2 Results from the study of V496 Sct

1. From the optical light curve, the absolute magnitude, distance and the height from the galactic plane for the nova are estimated to be M_V =-7.0 $\pm$ 0.2, d = 2.9 $\pm$ 0.3 kpc and z = 89 $\pm$ 3 pc. respectively.

2. The key observational result is the detection of first overtone bands of carbon monoxide (CO) in the 2.29 - 2.40 μm region. The CO bands are recorded over several epochs thereby allowing a rare opportunity to study its evolution from a phase of constant strength through a stage when the CO is destroyed fairly rapidly.

3. The modeling of the CO bands shows that in the initial phase the gas temperature and mass are found to be fairly constant in the range of 3600 - 4000K and 1.5 - 2 $\times$ 10^{-8} $M_\odot$ respectively.

4. From the modeling we estimate the ratio of $^{12}C/^{13}C$ to be $\sim$1.5. This implies that ^{13}C is possibly not synthesized to the high levels as predicted by the theoretical models.

5. The IR spectra indicate that the nova is of the Fe II class. The presence of emission lines from low-ionization species like Na and Mg in the early spectra and subsequent formation of the dust support the predictive property of these lines as indicators of dust formation as proposed by Das et al. (2008). The rising continuum in the spectra taken on 2010 April 11 also shows the dust formation in the nova ejecta.

6. From the low resolution optical spectra various phases of the spectral evolution of V496 Sct have been identified using the Tololo classification system for novae (Williams et al. 1991, 1994). The optical spectra show that the nova is evolved in the $P_{fe}A_O$ spectral sequence.

7. We have also estimated the physical parameters from our optical and IR data. The mass of the dust and gas is estimated 1-5 $\times$ 10^{-10} $M_\odot$ and 2.0 $\pm$ 0.6 $\times 10^{-4} M_\odot$, respectively.

8. The mass of the white dwarf for V496 Sct is estimated to be approximately 0.7 $M_\odot$ and the outburst luminosity is estimated to be 5.1 $\times$ 10^4 $L_\odot$.

6.1.3 Results from the study of KT Eri

1. From the optical light curve, the distance to the nova is estimated to be 6.3 $\pm$ 0.1 kpc. The infrared spectra indicate that the nova is of the He/N type. KT Eri is one of the fast He/N type of novae with t_2 = 5.7 d.

2. KT Eri is one of the very high latitude nova in last few years with galactic latitude (-32 deg) and distance below the galactic plane $z = 3.3 \pm 0.1$ kpc nova in last few years.

3. We have found the evidence for bipolar flow, which shows the presence of two high velocity components at radial velocities of -1530 and 2090 km s^{-1} for Paβ and at -1940 and 1930 km s^{-1} for the Brγ lines, respectively. The central components have full width at half-maximum (FWHM) of 2340 and 1930 km s^{-1} for the Paβ and Brγ lines, respectively.

4. The case B analysis of hydrogen Brackett series lines has been used to estimate the mass of the gas in the ejecta and this lies in the range 2.4-7.4 $\times$ 10^{-5} M$_\odot$.

5. The mass of the white dwarf for KT Eri is estimated to be approximately 1.15 M$_\odot$ and the outburst luminosity is estimated 2.9 $\times$ 10^5 L$_\odot$.

6. We have also discssed the possibility of 15th magnitude star to be the proginator and the evolution of the continuum of the spectra. The temporal evolution of Brγ line does not favour a red giant as the companion star.

6.2 Future work

It would be appropriate to indicate a few suggestions for future work.

It was pointed out that V5579 Sgr is a very fast nova of Fe II class that formed dust as early as $\triangle t = 15$ d after optical maximum. The possible reasons for dust formation in this very fast nova and that too at such an early date will be examined.

A good observational coverage of the less frequently observed pre-maximum risisng phase is presented in the case of V496 Sct. The high resolution optical echelle spectra and the J band near-infrared spectrum soon after the optical maximum will be used to study the mass loss process during the onset of the run away thermonuclear reactions in the accreted layers on the white dwarf leading to the ejection of the nova shell. The work presented in Chapter 4 concentrated only on the Fe II 5018 line to study the absorption system during the early decline phase. This analysis will be extended to other lines. An effort will be made to look for the transient heavy elements absorption systems resulting from the secondary star in V496 Sct system using the echelle spectra. Such absorption system have been reported by Williams et al. (2008).

The intriguing possibility of KT Eri being a recurrent nova makes it an interesting target for future studies. The high velocity bipolar flow seen in KT Eri demonstrates that nova ejecta is not expanding in a spherically symmetric pattern and therefore it is necessary to account for the shape of the nova ejecta with more detailed work. I plane to use $SHAPE$, a morpho-kinematical code that is used to analyse and understand the 3D geometry and kinematical structure of nebulae (Steffen & Lopez 2006; Steffen et al. 2010). SHAPE allows modelling of the structure and kinematics of an object to compare with the observed images and spectra. The Paβ and Brγ line profiles of KT Eri that clearly show bipolar flows will be modelled to determine the inclination of the ejecta and relate it to the orbital axis of the underlying binary system.

As already mentioned a fairly large number of additional novae have been observed as mentioned in Chapter 2, during the course of the studies presented here. The complete analysis of the data on these novae will be taken up and their results should add to further insights into the infrared development of novae as described in this thesis.

Bibliography

[1] Abdo A. A., 2010, Science, 329, 817

[2] Andrea J., Drechsel H. & Starrfield S., 1994, A&A, 291, 869

[3] Anupama G. C., 2002, in American Institute of Physics Conference Series, Vol. 637, Classical Nova Explosions, ed. M. Hernanz & J. Jose, 32

[4] Ashok N. M., Banerjee D. P. K., Varricatt W. P., Kamath U. S., 2006, MNRAS, 368, 592

[5] Balam D., Sarty G., 2009, IAU Circular, 9093, 1

[6] Banerjee D. P. K., Bobra A. D. & Subhedar D. V., 1997, BASI, 25, 555

[7] Banerjee D. P. K., Das R. K., Ashok N. M., 2009, MNRAS, 399, 357

[8] Beardmore A. P., Osborne J. P., Page K. L., Goad M. R., Bode M. F., Starrfield S., 2008, ASP, 401, 296

[9] Beardmore A. P., Balman S., Osborne J. P., Page K. L., Bode M. F., Drake J. J., Ness J.-U., Orio M., 2010, ATel 2423

[10] Benedict W. S., Herman R., Moore G. E. & Silverman S., 1962, ApJ, 135, 277

[11] Bessel M. S., Castelli F. & Plez B., 1998, A&A, 333, 231 (err. 337, 321)

[12] Bode M. F. & Evans A., 2008, editors Classical Novae, 2nd Edition (Cambridge University Press)

[13] Bode M. F., Osborne J. P., Page K. L., Beardmore A. P., Ness J.-U., Walter F. M., Darnley M. J., Evans A., Eyres S. P. S., Krautter J., O'Brien T. J., Schwarz G., Starrfield S., Truran J., 2009, ATel 2025

[14] Bode M. F., Osborne J. P., Page K. L., Beardmore A. P., Walter F. M., Ness J.-U., Schwarz G., Starrfield S., Kuulkers E., O'Brien T. J., Balman S., Darnley M. J., Evans A., Evans P., Eyres S. P. S., Krautter J., 2010, ATel 2392

[15] Boyarchuk A. A. & Antipova L. I., 1990, Lect. Notes Phys., 369, 97

[16] Capaccioli et al. 1990, ApJ, 360, 63

[17] Carrol B. W. & Ostlie D.A., 2007, An introduction to Modern Astrophysics, (2nd edition, San Francisco: Addison-Wesley), 662, 673

[18] Cassisi S., Iben I. J. & Tornambe A., 1998, ApJ, 496, 376

[19] Cheung C. C., Glanzman T., Hill A. B., 2012, ATel, 4284

[20] Cheung et al. 2012, ATel, 4310

[21] Ciardullo R., Tamblyn P., Jacoby G. H., Ford H. C. & Williams R. E., 1990, AJ, 99, 1079

[22] Clayton D. D. & Hoyle F., 1974, ApJ, 187, 101

[23] Clayton D.D., Wickramasinghe N.C.,1976, Ap & SS, 42, 463

[24] Clayton D. D., 1981, ApJ, 244, 97

[25] Cohen J. G., 1985, ApJ, 292, 90

[26] Contini M., Prialnik D., 1997 , ApJ, 475, 803-811

[27] Crawford J. A. & Kraft R. P., 1956, ApJ, 123, 44

[28] Darnley M. J., Bode M. F., Kerins E. J., Newsam A. M., An J., Baillon P., Belokurov V., Calchi Novati S., Carr B. J., Creze M., Evans N. W.,

Giraud-Heraud Y., Gould A., Hewett P., Jetzer Ph., Kaplan J., Paulin-Henriksson S., Smartt S. J., Tsapras Y. & Weston M., 2006, MNRAS, 369, 257

[29] Darnley M. J., Ribeiro V. A. R. M., Bode M. F., Munari U., 2011, A&A, 530, 70

[30] Das R.K., Banerjee D.P.K., Ashok N.M., 2006, ApJ, 653, L141

[31] Das R.K., Banerjee D.P.K., Ashok N.M., Chesneau O., 2008, MNRAS, 391, 1874

[32] Das R.K., Banerjee D.P.K., Ashok N.M., 2009, MNRAS, 398, 375

[33] della Valle M., Bianchini A., Livio M. & Orio M., 1992, A&A, 266, 232

[34] della Valle M. & Livio M., 1995, ApJ, 452, 704

[35] Della Valle M., Pasquini L., Daou D., Williams R. E., 2002, Astronomy and Astrophysics, 390, 155

[36] de Vaucouleurs G., 1978, ApJ, 223, 351

[37] Downes R. A. & Duerbeck H. W., 2000, ApJ, 120, 2007

[38] Drake A.J., Djorgovski S.G., Graham M.J., Mahabal A.A., Williams R., Wils P., Greaves J., Catelan M., Prieto J., Beshore E.C., Larson S.M., Boattini A., Gibbs A., Grauer A., Hill R., Kowalski R., Christensen E., 2009, ATel 2331

[39] Dvorak S., 2008, IAUC 8937

[40] Ederoclite et al., 2006, A&A, 459, 875

[41] Ennis D., Beckwith S., Gatley I., Matthews K., Becklin E. E., Elias J., Neugebauer G., Willner S. P., 1977, ApJ, 214, 478

[42] Evans A., Geballe T. R., Rawlings J. M. C., Scott A. D., 1996, MNRAS, 282, 1049

[43] Evans A. & Rawlings J. M. C., 2008, in Classical Novae, 2nd Edition, eds.: M. F. Bode & A. Evans, (Cambridge Univ. Press: Cambridge)

[44] Eyles et al. 2003, KLUWER, 217, 319

[45] Ferland G. J., Lambert D. L., Netzer H., Hall D. N. B., Ridgway S. T., 1979, ApJ, 227, 489

[46] Fujii M., 2008, IAUC 8937

[47] Gallagher J.S., Starrfield S.G. 1978, Ann. Rev. Astr. Astrophys., 16, 17l

[48] Gehrz R.D., Grasdlen G.L., Hackwell J.A., Ney E.P., 1980, ApJ, 237, 855

[49] Gehrz R.D., 1988, ARA&A, 26, 377

[50] Gehrz R. D., Jones T. J., Woodward C. E., Greenhouse M. A., Wagner R. M., Harrison T. E., Hayward T. L. & Benson J., 1992, ApJ, 400, 671

[51] Gehrz R. D. & Ney E. P., 1992, Icarus, 100, 162

[52] Gehrz R. D., Truran J.W. & Williams R. E., 1993, in Protostars and Planets III, eds. E. H. Levy & J. I. Lunine, Tuscon: Univ. Arizona Press, p. 75

[53] Gehrz R.D., Truran J. W., Williams R. E. & Starrfield S., 1998, PASP, 110, 3

[54] Gehrz R. D., 2002, in Classical Nova Explosions, eds. HernanzM. & Jose J., NewYork: American Institute of Physics, p. 198

[55] Gehrz R.D., 2008, in Classical Novae, Second Edition, eds. Bode M.F. & Evans A., Cambridge University Press, p. 175

[56] Gehrz R.D., 2008, in Classical Novae, ed. M.F. Bode & A. Evans., Cambridge Univ. Press. p. 167

[57] Guido E., Sostero G., 2009, IAUC 9093

[58] Hachisu I., Kato M.,2001, Ap J, 558, 323

[59] Hachisu I., These proceedings, 2002

[60] Hachisu I., Kato M.,2006, Ap JS, 167,59

[61] Hachisu I., Kato M., Luna G. J. M., 2007, ApJL, 659, 153

[62] Hack M., Struve O., 1970, Stellar Spectroscopy of Peculiar Stars, Publ. Trieste Astronomical Observatory

[63] Hajduk M et al., 2005, Science, 308, 231

[64] Henden A., & Munari, U, 2008, IAU Inform. Bull. Var. Stars, 5834, 1

[65] Hernanz, M., & Sala, G. 2002, Science, 298, 393

[66] Hernanz, M., & Sala, G. 2010, Astronomische Nachrichten, 331, 169

[67] Hick P., Buffington A. & Jackson B. V., 2007, Solar Physics and Space Weather Instrumentation II, 6689, 66890C

[68] Hjellming R. M. & Wade C. M., 1970, ApJ, 162, L1

[69] Hjellming R. M., 1974, in Galactic and Extragalactic Radio Astronomy, eds. Vershuur G. L. & Kellermann K. I., New York: Springer, p. 159

[70] Hounsell R., Bode M. F., Hick P. P., Buffington A., Jackson B. V., Clover J. M., Shafter A. W., Darnley M. J., Mawson N. R., Steele I. A., Evans A., Eyres S. P. S. & OBrien T. J. 2010, ApJ, 724, 480

[71] Hounsell R., Bode M. F., Hick P., Buffington A., Jackson B., Clover J., Shafter A. W., Darnley M. J., Evans A., O'Brien T. J., Eyres S. P. S., 2010, ATel 2558

[72] Hubble E., 1929, ApJ, 69, 103

[73] Hyland A.R., McGregor P.J., 1989, in Allamandola L. J., Tielens A. G. G. M., eds, IAU Symp. 135, Interstellar Dust. NASA, Washington, p. 495

[74] Jose J. & Hernanz M., 1998, ApJ, 494, 680

[75] Jurdana-Sepic R. & Munari U., 2008, Information Bulletin on Variable Stars, 5839, 1

[76] Jurana-Sepic et al. 2011, Astronomy & Astrophysics, 534, 17

[77] Jurdana-Sepic et al. 2012, Astronomy & Astrophysics, 537, 34

[78] Kahabka, P., & van den Heuvel, E. P. J. 1997, ARA&A, 35, 69

[79] Kamath U. S., Anupama G. C., Ashok N. M., Chandrasekhar T., 1997, Astronomical Journal, 114, 2671

[80] Kato M., Hachisu I., 1994, ApJ, 437, 802

[81] Kenyon S. J., 1988, in Astrophysics and Space Science Library, Vol. 145, IAU Colloq. 103: The Symbiotic Phenomenon, ed. J. Mikolajewska, M. Friedjung, S. J. Kenyon, & R. Viotti, 11

[82] Knigge C., King A. R. & Patterson J., 2000, A&A, 364, L75

[83] Koornneef J., 1983, A&A, 128, 84

[84] Kuncarayakti H., Kristyowati D., Kunjaya C., 2008, ApSS, 314, 209

[85] Kwok S., 1997, in Astronomical Society of the Pacific Conference Series, Vol. 130, The Third Pacific Rim Conference on Recent Development on Binary Star Research, ed. K.-C. Leung, 163

[86] Lamers H.J.G.L.M., Cassinelli J.P., 1999, Introduction to Stellar Winds, Cambridge Univ.Press, p. 16

[87] Landolt A.U., 1992, AJ, 104, 340

[88] Liller W. & Mayer B., 1987, PASP, 99, 606.

[89] Liller W., Camilleri P., 2008, Cent. Bur. Electron. Telegrams 1344

[90] Livio M., 1992, ApJ, 393, 516

[91] Li Q., Brown J. C., Ignace R., Cassinelli J. P., Oskinova L. M., 2000, A&A ,357,233

[92] Lynch D. K., Rudy R. J., Mazuk S., Puetter R. C., 2000, ApJ, 541, 791

[93] Lynch D.K., Rossano G.S., Rudy R.J., Puetter R.C, 1995, AJ, 110, 2274

[94] Lynch, D. K., Russel, R. W., Sitko, M. L. 2001, AJ, 122, 3313

[95] Maehara, H.; Arai, A.; Isogai, M., 2009, Central Bureau Electronic Telegrams, 2055

[96] Mason C.G., Gehrz R.D., Woodward C.E., Smilowitz J.B., Greenhouse M.A., Hayward T.L., Houck J.R., 1996, ApJ, 470, 577

[97] mason et al. 2001, AIP Conference Proceedings, 637, 486

[98] Mason E., Brandeker A., Ederoclite A., Della Valle M., Liller W., 2005, IAUC, 8582

[99] Mayo, S. K., Wickramasinghe, D. T., Whelan, J. A. J. 1980, MNRAS, 193, 793

[100] McLaughlin D. B., 1939, Pop. Astr., 47, 410, 481, 538

[101] McLaughlin D. B., 1945, PASP, 57, 69

[102] McLaughlin D. B., 1960, in Stellar Atmospheres, ed. J. L. Greenstein (University of Chicago Press), p. 585

[103] Munari U. & Whitelock P. A., 1989, MNRAS, 239, 273

[104] Munari U., Zwitter T., 1997, A&A, 318, 269

[105] Munari et al., 2008, A&A, 492, 145

[106] Munari U., Henden A., Valentini M., Siviero A., Dallaporta S., Ochner P., Tomasoni S., 2008, MNRAS, 387, 344

[107] Munari U., Siviero A., Moretti S., Tomaselli S., Maitan A., Castellani F., Dallaporta S., Ochner P., 2008, CBET 1352

[108] Munari U., Siviero A., Moretti S., Tomaselli S., Maitan A., Castellani F., Dallaporta S., Ochner P., 2008, CBET 1344

[109] Munari U., Siviero A., Buzzi L., Valisa P., 2009, IAU Circular, 9093, 1

[110] Munari U., Siviero A., Valisa P., Dallaporta S., Baldinelli L., 2009, CBET, 2034, 1

[111] Munari U., Ribeiro V. A. R. M., Bode M. F., Saguner T., 2011, MNRAS, 410, 525

[112] Munari U. & Moretti S., 2012, Baltic Astronomy, 21, 22

[113] Munari U. et al., 2012, Baltic Astronomy, 21, 180

[114] Ness, J.-U., Schwarz, G. J., Retter, A., Starrfield, S., Schmitt, J. H. M. M., Gehrels, N., Burrows, D., & Osborne, J. P. 2007a, ApJ, 663, 505

[115] Naik S., Banerjee D. P. K., Ashok N. M., 2009, MNRAS, 394, 1551

[116] Naito H. et al., 2012, A&A, 543, 86

[117] Nakano S., Nishiyama K., Kabashima F., 2008, IAU Circ. 8937

[118] Nakano S., 2009, IAUC 9093

[119] Neckel Th., Klare G., 1980, A&AS, 42, 251

[120] Nelson T., Orio M., Cassinelli J. P., Still M., Leibowitz E., Mucciarelli P., 2008, ASPC, 401, 287

[121] Nesci R., Mickaelian A., Rossi C., 2009, ATel 2338

[122] Ness J.-U., Starrfield S., Beardmore A., Bode M. F., Drake J.J., Evans A., Gehrz R. D., Goad M. R., Gonzalez-Riestra R., Hauschildt P., Krautter J., O'Brien T. J., Osborne J.P., Page K. L., Schonrich R. A., Woodward C. E., 2007, ApJ, 665, 1334

[123] Ness J.-U., Drake J.J., Starrfield S., Bode M., Page K., Beardmore A., Osborne J.P., Schwarz G., 2010, ATel 2418

[124] Ney E.P., Hatfield B.F., 1978, ApJ, 219, L111

[125] O'Brien T.J., Muxlow T.W.B., Stevens J., Datta A., Roy N., Eyres S.P.S., Bode M.F., 2010, ATel 2434

[126] Orio, M., Covington, J., Ogelman, H. 2001, A&A, 373, 542

[127] Osborne J., Page K., Beardmore A., Goad M., Bode M., O'Brien T., Schwarz G., Starrfield S., Ness J.-U., Krautter J., Drake J., Evans A., Eyres S.P.S., 2006, ATel 770

[128] Osterbrock D. E., 1989, Astrophysics of gaseous nebulae and active galactic nuclei (University Science Book)

[129] Patterson J., Kemp J., Shambrook A., et al. 1998, PASP, 110, 380-395

[130] Pavlenko Y. V., Geballe T. R., Evans A., Smalley B., Eyres S. P. S., Tyne V. H., 2004, A&A, 417, L39 Yakovina LA

[131] Payne-Gaposchkin C. H. P., 1957, Amsterdam, North-Holland Pub. Co.; New York, Interscience Publishers, 1957

[132] Payne-Gaposchkin C., 1964, The Galactic Novae, Dover, New York

[133] Payne-Gaposchkin C. 1977, Astr. J., 82, 665

[134] Pejcha O., Prieto J. L., Denney K., ATel 1825

[135] Pfau W., 1976, A&A, 50, 113

[136] Pojmanski, G., 1997, ACA, 47, 467

[137] Pontefract M. & Rawlings J. M. C., 2004, MNRAS, 347, 1294

[138] Prieto J. L., Denney K., Pejcha O., Wagner R. M., ATel 1835

[139] Ragan E., Brozek T., Suchomska K., Skalbania A., Konorski P., Galan C., Swierczynski E., Tomov T., Mikolajewski M., Wychudzki P., 2009, ATel 2327

[140] Raj A., Ashok N.M., Banerjee D.P.K., 2009, CBET 2069

[141] Raj A., Ashok N.M., Banerjee D.P.K., 2011, MNRAS, 415, 3455

[142] Rieke and Lebofsky, 1985, ApJ, 288, 618

[143] Romano D., Matteucci F., 2003, MNRAS, 342, 185

[144] Rudy R. J., Dimpel W. L., Lynch D. K., Mazuk S., Venturini C. C., Wilson J. C., Puetter R. C., Perry R. B., 2003, ApJ, 596, 1229

[145] Rudy R.J., Lynch D.K., Russell R.W., Crawford K., Kaneshiro B., Woodward C. E., Sitko M., Skinner M., 2008, IAUC, 8952

[146] Rudy R.J., Prater T.R.,Puetter R.C., Perry R.B., 2009, IAUC, 9099

[147] Rudy R. J., Prater T. R., Russell R. W., Puetter R. C., Perry R. B., 2009, CBET, 2055

[148] Russell R.W., Rudy R.J., Lynch D.K., 2008, IAUC, 8948

[149] Russell R.W., Laag A.,Rudy R.J.,Skinner M. A.,Gregory S. A., 2010, IAUC, 9118

[150] Schlegel D. J., Finkbeiner D. P., Davis M., 1998, ApJ, 500, 525

[151] Schmidt Th., 1957, Zeitschrift fur Astrophysik, 41, 182

[152] Schwarz et al. 2009, ATel, 2173

[153] Seaquist E. R. & Bode M. F., 2008, in Classical Novae, Second Edition, eds. Bode M.F. & Evans A., Cambridge University Press

[154] Shafter A.W., 2002, in Classical Nova Explosions, eds.Hernanz M. & Jose J., New York: American Institute of Physics, p. 462

[155] Shara M., Zurek D.R., Williams R.E., et al. 1997, AJ, 114,258-264

[156] Snijders M. A. J., Batt T. J., Seaton M. J., Blades J. C. & Morton D. C., 1984, MNRAS, 211, 7

[157] Snijders M. A. J., Batt T. J., Roche P. F., Seaton M. J., Morton D. C., Spoelstra T. A. T. & Blades J. C., 1987, MNRAS, 228, 329.

[158] Snijders M. A. J., 1990, Lect. Notes Phys., 369, 188

[159] Starrfield S., Truran J. W., Sparks W. M., Kutter G. S., 1972, ApJ, 176, 169

[160] Starrfield S., Sparks W. M., Truran J. W., 1974, ApJ, 192, 647

[161] Starrfield S., Sparks W. M. & Truran J. W., 1985, ApJ, 291, 136

[162] Starrfield S., SparksW. M., & Truran J. W., 1986, ApJ, 303, L5

[163] Starrfield S., Gehrz R. D., Truran J. W., 1997, in Bernatowicz T. J., Zinner E., eds, AIP Conf. Proc. 402, Astrophysical Implications of the Laboratory Study of Presolar Materials. Am. Inst. Phys., New York, p. 203

[164] Starrfield S., Iliadis C. & Hix W. R., 2008, in Classical Novae, 2nd Edition, ed. M. F. Bode & A. Evans (Cambridge University Press), p. 77

[165] Steffen W., Lopez J. A., 2006, RMXAA, 26, 30

[166] Steffen et al. 2010, arXiv:1003.2012

[167] Stickland D. J., Penn C. J., SeatonM. J., SnijdersM.A. J. & Storey P. J., 1981, MNRAS, 197, 107

[168] Storey P. J., Hummer D. G., 1995, MNRAS, 292, 41

[169] Strope R. J.,Schaefer E., Henden A. A., 2010, AJ, 140, 34

[170] Teyssier F., 2009, AAVSO Alert Notice, 412, 1

[171] Tomov T., Mikolajewski M., Ragan E., Swierczynski E., Wychudzki P., 2008, ATel, 1475

[172] Uthas H., Knigge C., Steeghs D., 2010, MNRAS, 409, 237

[173] van den Bergh S., Younger P.F., 1987, A&AS, 70, 125

[174] Wallace P. T., 1994, Astronomical Data Analysis Software and Systems III, A.S.P. Conference Series, 61, 481

[175] Warner B., 1995a, Cataclysmic variable stars (Cambridge University Press)

[176] Warner B., 1995b, Ap&SS, 232, 89

[177] Warner B., 2008, in Classical Novae, 2nd Edition, ed. M. F. Bode & A. Evans (Cambridge University Press), p. 16

[178] Warner B., 2008, in Classical Novae, ed. M. F. Bode & A. Evans, Cambridge Univ. Press, p. 21

[179] Wichmann R., Krautter J., Kawara K., Williams R. E., 1990, Astron. Gesellschaft Abstr. Ser., 5, 17

[180] Wichmann R., Krautter J., Kawara K., Williams R. E., 1991, in "The infrared spectral region of stars", Proceedings of the International Colloquium held in Montpellier, France 1990, eds. C. Jaschek, Y. Andrillat, Cambridge University Press, p. 353

[181] Williams R. E., 1985, in Production and Distribution of CNO Elements, ed. Danziger I. J., ESO, Garching, p. 225.

[182] Williams R. E., 1990, in Lecture Notes in Physics, Berlin Springer Verlag, Vol. 369, IAU Colloq. 122: Physics of Classical Novae, ed. A. Cassatella & R. Viotti, 215

[183] Williams R. E., Hamuy M., Phillips M. M., Heathcote S. R., Wells L., Navarrete M., 1991, ApJ, 376, 721

[184] Williams R. E., 1992, AJ, 104, 725

[185] Williams R. E., Phillips M. M., Hamuy M., 1994, ApJS, 90, 297

[186] Williams R. E., 1994, ApJ, 426, 279

[187] Williams R., Mason E., Della Valle M., Ederoclite A. 2008, ApJ, 685, 451

[188] Williams R., 2012, Astronomical Journal, 144, 98

[189] Woodward C. E., Lawrence G. F., Gehrz R. D., Jones T. J., Kobulnicky H. A., Cole J., Hodge T., Thronson H. A., 1993, ApJ, 408, L37

[190] Yaron O., Prialnik D., Shara M. M., Kovetz A.,2005, ApJ, 623, 398

[191] Yamaoka H., Haseda K. & Fujii M., 2008, CBET, 1344, 1

[192] Yamaoka H., 2009, Cent. Bur. Electron. Telegrams 2050

[193] Zwicky F., 1936, PASP, 48, 284, 191

Publications attached with the thesis

1. **“Nova V5579 Sgr 2008: near-infrared studies during maximum and the early decline phase”**
   Ashish Raj, N. M. Ashok, D. P. K. Banerjee
   2011, MNRAS, 415, 3455

2. **“V496 Scuti: an Fe II nova with dust shell accompanied by CO emission”**
   Ashish Raj, N. M. Ashok, D. P. K. Banerjee, U. Munari, P. Valisa and S. Dallaporta
   2012, MNRAS, 425, 2576